BLIND MODULATION IDENTIFICATION OF QUADRATURE AMPLITUDE MODULATION (QAM) AND PHASE-SHIFT KEYING (PSK) SIGNALS IN DUAL-POLARIZED CHANNELS

by

Daimei Zhu

A dissertation submitted to the faculty of
The University of Utah
in partial fulfillment of the requirements for the degree of

Doctor of Philosophy

Department of Electrical and Computer Engineering

The University of Utah

August 2017

The University of Utah Graduate School

STATEMENT OF DISSERTATION APPROVAL

The dissertation of **Daimei Zhu**

has been approved by the following supervisory committee members:

V John Mathews ,	Chair(s)	**13 March 2017** Date Approved
Behrouz Farhang-Boroujeny ,	Member	**15 March 2017** Date Approved
David H. Detienne ,	Member	**15 March 2017** Date Approved
Rong-Rong Chen ,	Member	**15 March 2017** Date Approved
Neal Patwari ,	Member	**20 March 2017** Date Approved

by **Gianluca Lazzi** , Chair/Dean of

the Department/College/School of **Electrical and Computer Engineering**

and by **David B. Kieda** , Dean of The Graduate School.

ABSTRACT

This dissertation deals with blind modulation identification of quadrature amplitude modulations (QAM) and phase-shift keying (PSK) signals in dual-polarized channels in digital communication systems. The problems addressed in this dissertation are as follows: First, blind modulation identification of QAM and PSK signals in single noisy channels and multipath channels are explored. Second, methods for blind separation of two information streams in a dual-polarized channel and identification of the modulation types of the two information streams are developed.

A likelihood-based blind modulation identification for QAM and PSK signals in a single channel with additive white Gaussian noise (AWGN) is developed first. This algorithm selects the modulation type that maximizes a log-likelihood function based on the known probability distribution associated with the phase or amplitude of the received signals for the candidate modulation types. The approach of this paper does not need prior knowledge of carrier frequency or baud rate. Comparisons of theory and simulation demonstrate good agreement in the probability of successful modulation identification under different signal-to-noise ratios (SNRs). Simulation results show that for the signals in AWGN channels containing 10000 symbols and 20 samples per symbol, the system can identify BPSK, QPSK, 8PSK and QAMs of order 16, 32, 64, 128 and 256 with better than 99% accuracy at 4 dB SNR. Under the same condition, the simulation results indicate the two competing methods available in the literature can only reach at most 85% accuracy even at 20 dB SNR for all the modulation types. The simulation results also suggest that when the symbol length decreases, the system needs higher SNRs in order to get accurate identification results. Simulations using different noisy environments indicate that the algorithm is robust to variations of noise environments from the models assumed for derivation of the algorithm. In addition, the combination of a constant modulus amplitude (CMA) equalizer and the likelihood-based modulation identification algorithm is able to identify the QAM signals in multipath channels in a wide range of SNRs. When compared with

the results for the signals in AWGN channels, the combination of the CMA equalizer and the likelihood-based modulation identification algorithm needs higher SNRs and longer signal lengths in order to obtain accurate identification results.

The second contribution of this dissertation is a new method for blindly identifying PSK and QAM signals in dual-polarized channels. The system combines a likelihood-based adaptive blind source separation (BSS) method and the likelihood-based blind modulation identification method. The BSS algorithm is based on the likelihood functions of the amplitude of the transmitted signals. This system tracks the time-varying polarization coefficients and recovers the input signals to the two channels. The simulation results presented in this paper demonstrate that the likelihood-based adaptive BSS method is able to recover the source signals of different modulation types for a wide range of input SNRs. Comparisons with a natural gradient-based BSS algorithm indicate that the likelihood-based method results in smaller symbol error rates. When a modulation identification algorithm is applied to the separated signals, the overall system is able to identify different PSK and QAM signals with high accuracy at sufficiently high SNRs. For example, with 20,000 symbols, the system identified BPSK and 16-QAM signals with better than 99% accuracy when the input SNR was 8dB and the polarization coefficients rotated with a rate of 1.3 ms. Higher SNRs are needed to obtain similar levels of accuracy when the polarization changes faster or when the number of input symbols is shorter. When compared with the identification results for signals in AWGN channels, the system needs higher SNRs and longer signal length to obtain accurate results for signals in dual-polarized channels.

CONTENTS

LIST OF FIGURES

LIST OF TABLES

ACKNOWLEDGEMENTS

I would like to give my immense gratitude to my supervisor, Professor V John Mathews. His patience, guidance and pearls of wisdom have been the biggest inspiration and support to me. I would also like to thank Raytheon Applied Signal Technology for their funding of this challenging project. I want to thank Dr. David. H. Detienne for his support and insights, which have been a great inspiration for me during this challenging project.

Special thanks to all my colleagues in the Information Processing Groups at both Utah and Oregon. I enjoy every moment working with each of them, whom I respect so much for their work ethics and attitudes. I have not only learned greatly from their commitment and perseverance on research, but also their positive attitude towards goals, aspirations and life.

I also would like to thank my friends in both China and the United States who have been taking care of me during my Ph.D. studies. Their unconditional support has kept me going through some of the long and lonely hours when I needed help and encouragement.

Last but not least, I want to thank my family - Mother, Father, Sister and Brother. Their endless love was the guiding light throughout this journey.

CHAPTER 1

INTRODUCTION

In this chapter, the background of this dissertation is introduced first. Then, the methods that have been developed before for modulation identification and cross-polarization cancellation are reviewed. Next, the contributions of this dissertation are presented. Finally, the organization of this dissertation is described.

1.1 Background

In many RF communication systems, information is transmitted through two polarizations to improve transmission rates. For example, dual polarization in mobile communication, which were vertical and horizontal polarizations, increases the system capacity without changing the size of the system [5] [9] [18]. In most practical systems, the received signals may not maintain the relative separation of the polarization angles due to rotation of the polarizations and other distortions. In such situations, the two information-bearing signals reconstructed at the receiver may be a mixture of the source signals. Additional processing is required to recover the original signals before they can be demodulated.

Automatic modulation identification is needed for surveillance, electronic warfare and other applications [47]. The modulation types of the received signals may vary with different transmitters under multiple channel environments. Blind modulation identification, i.e., modulation identification without *a priori* knowledge of the carrier frequency, symbol rate and other parameters of signal transmission, plays a significant role in detecting the signal characteristics. Furthermore, blind modulation identification has been implemented on commercial systems performing spectrum management, interference detection and so on. Blind modulation identification is applied to develop smarter, more efficient and reliable receivers by decreasing the number of symbols needed under higher noisy environments.

Increasing the capacity of electronic communication transmitters is one approach with

the growing demand for the channel spectrum. Dual polarization increases the system capacity without changing the size of the transmitters. Blind modulation identification methods can help the system capture the signal information and determine the modulation types in current spectrum. Therefore, the ability to blindly identify the modulation types of signals in dual-polarized channels will build more powerful communication receivers. Furthermore, more efficient receivers require that the system identify the modulation types faster and more accurately under various channel impairments.

1.2 Problem Statement

A dual polarization system is shown in Figure 1.1. Ideally, the two polarizations are in vertical and horizontal directions. However, cross-polarization between the two polarizations will make the two received signals possibly time-varying mixtures of the two input signals. The channel impairments considered in this dissertation are Gaussian noise and multipath. The channel and signal parameters are assumed to be unknown.

The goal of this research is to identify the modulation types of the input signals in dual-polarized channels accurately with no prior knowledge about the characteristics of the signal and channel such as carrier frequency, baud rate, noise variance, etc. There are two problems addressed in this dissertation. First, the blind modulation identification for phase-shift keying (PSK) and quadrature amplitude modulation (QAM) signals in single channel with additive white Gaussian noise (AWGN) is explored. In addition, the blind modulation identification of the signals in multipath channels is considered. The second problem is to blindly separate the received signals and identify the modulation types of

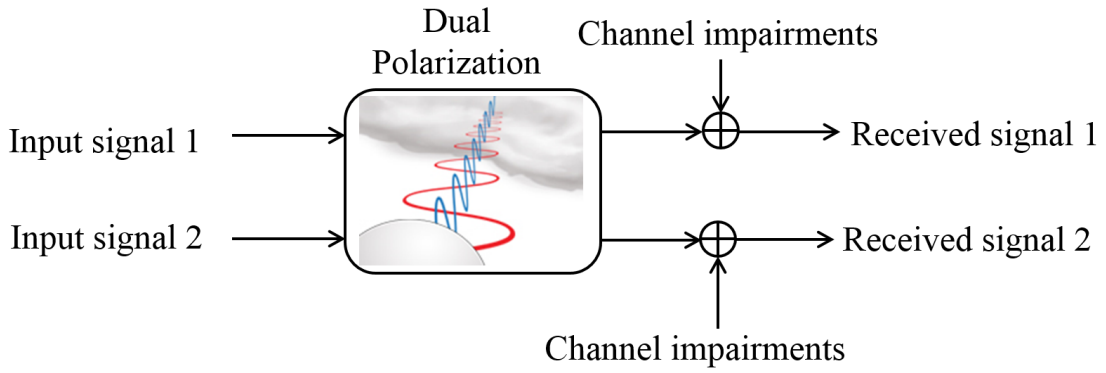

Figure 1.1: Block diagram of the received signals in a dual-polarized channel.

the received signals after transmission through dual-polarized channels. This includes blind separation of the mixtures of the received signals. The modulation types of interest in this dissertation are BPSK, QPSK, 8-PSK, 16-QAM, 32-QAM, 64-QAM, 128-QAM and 256-QAM.

1.3 State of the Art

As far as the author knows, there are no available articles in the literature for blind modulation identification for dual-polarized signals. The available literature deals with blind modulation identification of signals transmitted in single AWGN or multipath channels. A few papers focusing on recovering the signal from dual polarized channels and demodulating the signals assuming known modulation types are also available in the literature. This section provides a review of the previous methods in these three categories.

1.3.1 Cross-polarization Cancellation for Signals Transmitting in Dual-polarized Channels

Cross-polarization cancellation for signals in dual-polarized RF and optical transmitters has been studied since the 1980s. Most of those methods assumed known signal parameters such as the modulation types, carrier frequency, symbol rate, etc. These methods can be divided into two broad classes: the first class is based on the least-mean-square (LMS) algorithm and the second class is based on the statistical characteristics of the signal.

1.3.1.1 LMS-based Algorithms

In [6], the authors developed an LMS algorithm to update the channel coefficients. They assumed that the symbols transmitted through each channel were known. In this paper, the authors estimated the coefficients of the assumed equalizer corresponding to the dual polarized channel by minimizing the mean-square-error (MSE) between the transmitted symbols and the recovered symbols after equalization in both channels.

Similarly, a cross-polarization interference canceler for mobile communications using a recursive least-squares filter was implemented in [14]. The authors also assumed known training signals from the transmitters.

A joint constant modulus amplitude (CMA) and decision-directed LMS algorithm were introduced in [60]. The authors also assumed known transmitted symbols. Their goal

was to minimize the joint cost function based on the error functions of CMA and LMS algorithm. This joint function was a convex combination of the two error functions with the desired source symbols.

1.3.1.2 Statistical Characteristic-based Algorithms

The bootstrapping algorithm for the cross-polarization cancellation was introduced in [5], [9] and [18]. This method was designed to minimize the power or correlations based on the relationship between the received signals and the source signals. The authors assumed that the signals were in baseband.

In [51], the author developed a decision-directed algorithm to estimate the dual polarized channel coefficients. This method also was based on the statistical relationship between the estimated signal and the output signal under the assumption that the input symbols at the transmitter are independently and identically distributed (i.i.d.). The author used the correlation matrix between the estimated signal and the output signal to update the channel coefficients.

A blind equalizer based on the Soft Constraint Satisfaction (SCS) was developed in [63]. Different from the other equalizers which were to minimize the error between the estimated signal and source signal, this method minimized the error between adjacent channel coefficients during the adaption under the constraints that the estimated signal satisfied the constant modulus features. However, the authors assumed that the source signals before transmitting through dual polarization were baseband signals.

1.3.2 Blind Modulation Identification of Signals in Noisy Channel

The automatic modulation identification for PSK and QAM signals in single channels with Gaussian noise has attracted the attention from scientists since the 1990s. The main algorithms developed were based on likelihood functions, cyclic cumulants, wavelet transformation and clustering of the received signals.

1.3.2.1 Likelihood Function-based Algorithm

A method for QAM modulation identification based on computation of the likelihood function of the signal amplitudes was presented in [26]. This approach does not need

prior knowledge of the carrier frequency and the symbol rate. Since QAM signals with different orders have different amplitude distributions, the likelihood functions based on the probability density functions (PDFs) of the signal amplitude were distinct for different QAMs. The PDF of the signal amplitude for QAM signals was derived based on the amplitude distribution of a sinusoid perturbed by a white Gaussian noise. However, the authors did not consider pulse shaping in their signal models, and direct application of the method on pulse shaped signals results in poor performance. Another method implementing the maximization of the likelihood functions of the amplitude for QAM signals were demonstrated in [13] and [30]. Different from the PDF of the amplitude in [26], the authors assumed that the PDF of the amplitudes satisfied Gaussian distribution. They also assumed known signal parameters such as baud rate and carrier frequency.

In [28], the author introduced the modulation identification algorithm of PSK signals in AWGN channels based on the maximization of the likelihood functions of phase. The PDF of the phase was assumed to be Gaussian distribution. The author also assumed known signal parameters. The quasi average likelihood ratio test (ALRT) algorithm for the modulation identification of PSK signals in AWGN channels were developed in [7], [15], [17] and [39]. In addition, the hybrid likelihood ratio test (HLRT) algorithm for PSK signals in AWGN channels were developed in [16], [31] and [32]. The likelihood ratio test implemented the ratio between the likelihood functions under different hypothesized modulation types. By setting the threshold of the ratio for different PSKs, the modulation types can be identified. The authors also assumed known signal parameters such as baud rate and carrier frequency. The results in these papers indicated that the likelihood-based modulation classifiers can identify BPSK, QPSK and 8-PSK accurately at relatively low SNRs. For example, the ALRT algorithm in [17] can identify between BPSK and QPSK signals with 99% accuracy at signal-to-noise ratio (SNR) equal to -7.8 dB with 1024 symbols.

1.3.2.2 Cyclic Cumulants-based Algorithm

A different approach to QAM and PSK modulation identification that employed cyclic cumulants of the received signals was described in [10], [22], [23], [24], [34], [36], [38], [40], [41] and [59]. The cumulants are defined as the higher-order moments of the received signals. The cumulants of different QAM and PSK symbols have different characteristics.

This algorithm identifies different modulation types by setting a threshold based on the value of the cumulants with different orders. For example, the authors selected the fourth order cumulants to identify between 16-QAM and 32-QAM. Some of the authors selected higher-order such as sixth and eighth order cumulants to identify different PSK or QAM signals. But the method required knowledge of the symbol rate for good performance. Also, both numerical considerations and simulation results have shown that they have poor discrimination capabilities within the subset of commonly used non-square QAMs (for example, 32 and 128-QAM) and square QAMs (such as 16, 64 and 256-QAM).

1.3.2.3 Clustering-based Algorithm

A blind recognition algorithm combining Hilbert transform and clustering algorithms for identifying QAM signals was developed in [52]. This approach did not need the prior information of the carrier frequency and the symbol rate. For different QAM symbols, the symbol groups in the constellation maps are distinct. By clustering the symbols in the constellation maps into different groups, the modulation types can be identified as the corresponding QAM types. Results presented in [52] indicated that this method can identify 16-QAM with 100% accuracy at SNR as low as 9 dB with 1000 symbols when the signal was corrupted by white Gaussian noise. A similar method for blind modulation recognition of PSK signals based on constellation reconstruction was presented in [56]. The results showed in the paper indicated that this method can identify BPSK, QPSK and 8-PSK with 100% accuracy at 15 dB SNR with 500 symbols.

1.3.2.4 Wavelet Transformation-based Algorithm

In [29] and [53], the authors presented a modulation identification method based on a likelihood function of phase parameters extracted from the Morlet wavelet transform of the input signal. Simulation results in [53] indicated that this approach identified BPSK, QPSK and 8-PSK with 100% recognition rate with 1000 symbols when the SNR was more than 12 dB.

1.3.3 Blind Modulation Identification of Signals in Multipath Channels

The available literature for modulation identification of signals in multipath channels is mostly based on higher-order statistical characteristics such as moments and cumulants [35], [50] and [55]. Different higher-order moments or cumulants for PSK and QAM signals have different features. Because the symbols are assumed to be i.i.d., the statistical characteristics of signals in multipath channels are functions related to the channel coefficients and can be identified.

Another method combining the constant modulus amplitude(CMA) equalizer and the clustering modulation identification method for identifying the QAM signals in a multipath channel was developed in [58]. The authors implemented the CMA equalizer to eliminate the effect of the multipath channel for the received signal so that the transmitted signal without multipath is recovered. Next the clustering method similar to [52] was applied to identify different QAM types.

As a summary, the comparisons of these methods are shown in Table 1.1. From this table, the blind modulation identification for dual-polarized signals need to be developed. A novel method for blindly identifying both QAM and PSK signals in both AWGN and multipath channels with higher accuracy under lower SNRs should be explored.

Table 1.1: Comparison of different methods for blind modulation identification

Methods	Performance
LMS cross-polarization canceller Decision-directed algorithm [6] [14] [60] [5] [9] [18] [51] [63]	Prior knowledge of transmitted symbols; no modulation identification
Amplitude likelihood functions [26] [13] [30]	No consideration of pulse shaping filter. Assumed known signal parameters
Likelihood ratio test [7] [15], [17] [39] [16] [31] [32] [17]	Prior knowledge of signal parameters, poor performance for higher-order QAMs.
Cyclic cumulants [10] [22] [23] [24] [34], [36] [38] [40] [41] [59] [35] [50] [55]	Poor performance for higher-order QAMs; Channel estimation of multipath channels.
Clustering methods [52] [56] [58]	Poor performance for higher-order QAMs.
Wavelet transform [29] [53]	Need high SNRs for good identification of different PSKs.

1.4 Contributions of This Dissertation

Contributions of this dissertation includes three aspects for blind modulation identification of the signals in various channel conditions.

First, the likelihood-based modulation identification algorithm of the PSK and QAM signals in AWGN channel is presented in this dissertation. This algorithm does not assume any prior knowledge of the signals or channel and is able to obtain accurate identification results for all the modulation types of interest, especially for higher-order QAMs such as 128-QAM and 256-QAM. Results of performance evaluation indicate that this new method is substantially superior to competing methods available in the literature. The method in this dissertation differs from other methods available in the literature in several ways: (1) This algorithm implements the actual PDF of the amplitude or phase to calculate the likelihood functions by eliminating the effect of the pulse shaping filter in the process. In particular, the likelihood function applying the actual PDF of phase is new in this field; (2) This algorithm is robust to variations of the signal characteristics from the signal model assumed in the derivation of the algorithm; and (3) A theoretical analysis of the performance of the algorithm is included in this dissertation.

Second, this dissertation presents a likelihood-based blind source separation (BSS) algorithm to recover the signals in time-varying dual-polarized channels. As far as the author knows, there is no such methods for the signals in dual-polarized channels. The BSS algorithm by maximizing the likelihood functions implementing the actual PDF of the amplitude of the signal is also new in this field. The simulation results indicate that this likelihood-based BSS algorithm outperforms the other BSS algorithm for the separation of the mixture of the received signals. Combining the likelihood-based BSS and the likelihood-based modulation identification algorithm also shows accurate results for PSK and QAM signals in dual-polarized channels.

Third, the blind modulation identification of the signal in multipath channels is explored in this dissertation. Combining the CMA equalizer and the likelihood-based modulation identification algorithm shows more accurate results comparing with other methods available in the literature. This dissertation also includes the preliminary results of a modified likelihood-based identification algorithm by studying the characteristics of signals in multipath channels.

1.5 Organization of This Dissertation

The rest of this dissertation is organized as follows. Chapter 2 introduces the signal and system models for this research, which includes the model for PSK and QAM signals, the system model of signals transmitted through dual-polarized channels and the model for signals in multipath channels. In Chapter 3, a likelihood-based blind modulation identification for PSK and QAM signals in AWGN channels is developed. In this chapter, a method combining the constant modulus amplitude (CMA) equalizer and likelihood-based modulation identification for identifying the modulation types of the signals in multipath channels is also presented. Chapter 4 presents a likelihood-based BSS algorithm for PSK and QAM signals in dual-polarized channels. The combination of the likelihood-based BSS and the likelihood-based modulation identification algorithm is also presented in this chapter. Finally, Chapter 5 concludes this dissertation and lists possible future work.

CHAPTER 2

SYSTEM MODEL

In this chapter, the system model for the QAM and PSK signals transmitted in dual-polarized channels is described. The signal characteristics for different QAM and PSK types with various channel impairments are also introduced.

A block diagram of a digital signal transmitter with the dual-polarized channel is shown in Figure 2.1. In both channels, the information sequences are transmitted in similar ways. In order to transmit information securely, the information sequences are coded into binary bits in the transmitter first. The binary bit sequence is then transformed to corresponding symbols using different modulation formats. Before transmitting through the dual-polarized channel, the input information sequences become two independent band-limited digital signals in both channels. Due to the cross-polarization effect between the two polarizations, the two signals may be mixed after passing through the dual-polarized channel. Also, various channel impairments such as noise and multipath from the outside environment will be added to the signals during transmission.

The organization of this chapter is as follows: The signal characteristics of PSK and QAM signals will be introduced next. The system and signal characteristics of the received signals in multipath channels are described in Section 2.2. Section 2.3 describes the system and signal characteristics of the received signals transmitting through a dual-polarized channel.

2.1 Digital Modulator

Figure 2.2 shows a block diagram of a digital modulator. When transmitting the information bits through the communication systems, the bit sequences are transformed to corresponding symbol sequences according to the bandwidth efficiency of the transmitter.

Multiple bits can be transmitted as one symbol depending on the order of the modulation types chosen in the transmitter. Then, the pulse shaping filter limits the bandwidth of

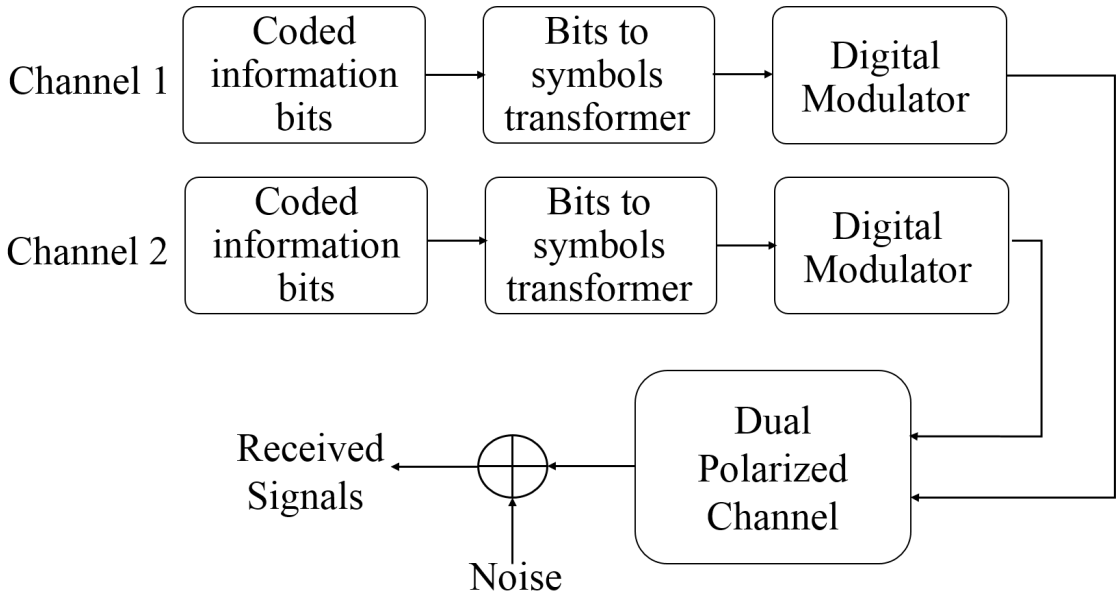

Figure 2.1: Block diagram of a digital signal transmitter with a dual-polarized channel.

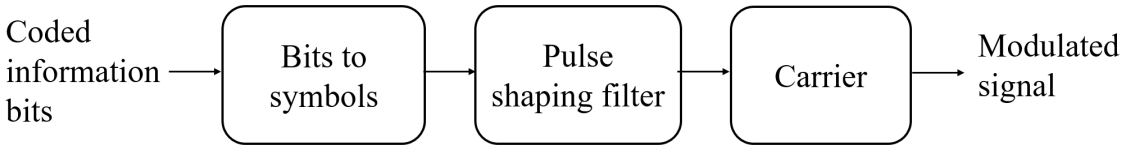

Figure 2.2: Block diagram of a digital modulator.

the symbol sequence so that the symbol sequence can be transmitted through the digital channels. After obtaining the baseband transmitted signal from the pulse shaping filter, the carrier transforms the baseband signal into a bandpass signal around the carrier frequency.

There are several different modulation schemes widely used in the digital communication systems applying different amplitude, phase and frequency characteristics of the symbols. In this dissertation, the PSK modulations and QAM are of interest. Section 2.1.1 and 2.1.2 will introduce these two different modulation schemes.

2.1.1 Signal Characteristics of PSK Signals

Both PSK and QAM signals can have different orders. The higher the order is, the higher number of bits can be transmitted via each symbol. A signal with M-th order modulation type can transmit $log_2(M)$ bits per symbol. The complex symbols for PSKs

with order M can be expressed as

$$s_{PSK} = e^{j\theta_n} \tag{2.1}$$

where θ_n is a vector with length M and is uniformly distributed in $[0, 2\pi]$. The space between adjacent θ_n is $\frac{2\pi}{M}$.

Table 2.1 shows one example of the mapping between the bits and symbols for BPSK, QPSK and 8-PSK.

A constellation map, which represents the distribution of the symbols, is used to display different modulation types. Figure 2.3 shows the constellation maps for BPSK, QPSK and 8-PSK symbols based on the mapping rule in Table 2.1. The number of symbols is 10000. We can see that the PSK symbols with different orders have constant amplitude but different phase groups. For example, BPSK symbols have 2 different phase groups, QPSK symbols have 4 phase groups and 8PSK have 8 phase groups.

When noise is presented in the channel, the phase groups of PSKs signals will change based on the noise level added to the symbols. The phase groups of PSK symbols will not have the "distinct" phase groups but will satisfy some distribution based on the noise type. In this dissertation, the noise is considered to be additive white Gaussian noise.

Figure 2.4, 2.5 and 2.6 show the constellation maps and histograms of the phase difference between adjacent symbols for different PSK signals with different noise levels. In these figures, the noise is directly added to the symbols. From these figures, we can observe that the distribution of the phase difference between adjacent symbols changes with the noise levels. For different PSK signals, the distribution of the phase difference

Table 2.1: Bits to symbols mapping for different PSKs

PSK types	BPSK		QPSK		8PSK	
Mapping	Bits	Symbols	Bits	Symbols	Bits	Symbols
	0	1	(0 0)	$\frac{1+1j}{\sqrt{2}}$	(0 0 0)	1
					(0 0 1)	$\frac{1+1j}{\sqrt{2}}$
			(0 1)	$\frac{1-1j}{\sqrt{2}}$	(0 1 1)	1j
	1	-1	(1 1)	$\frac{-1-1j}{\sqrt{2}}$	(0 1 0)	$\frac{1-1j}{\sqrt{2}}$
			(1 0)	$\frac{-1+1j}{\sqrt{2}}$	(1 1 0)	-1
					(1 1 1)	$\frac{-1-1j}{\sqrt{2}}$
					(1 0 1)	-j
					(1 0 0)	$\frac{-1+1j}{\sqrt{2}}$

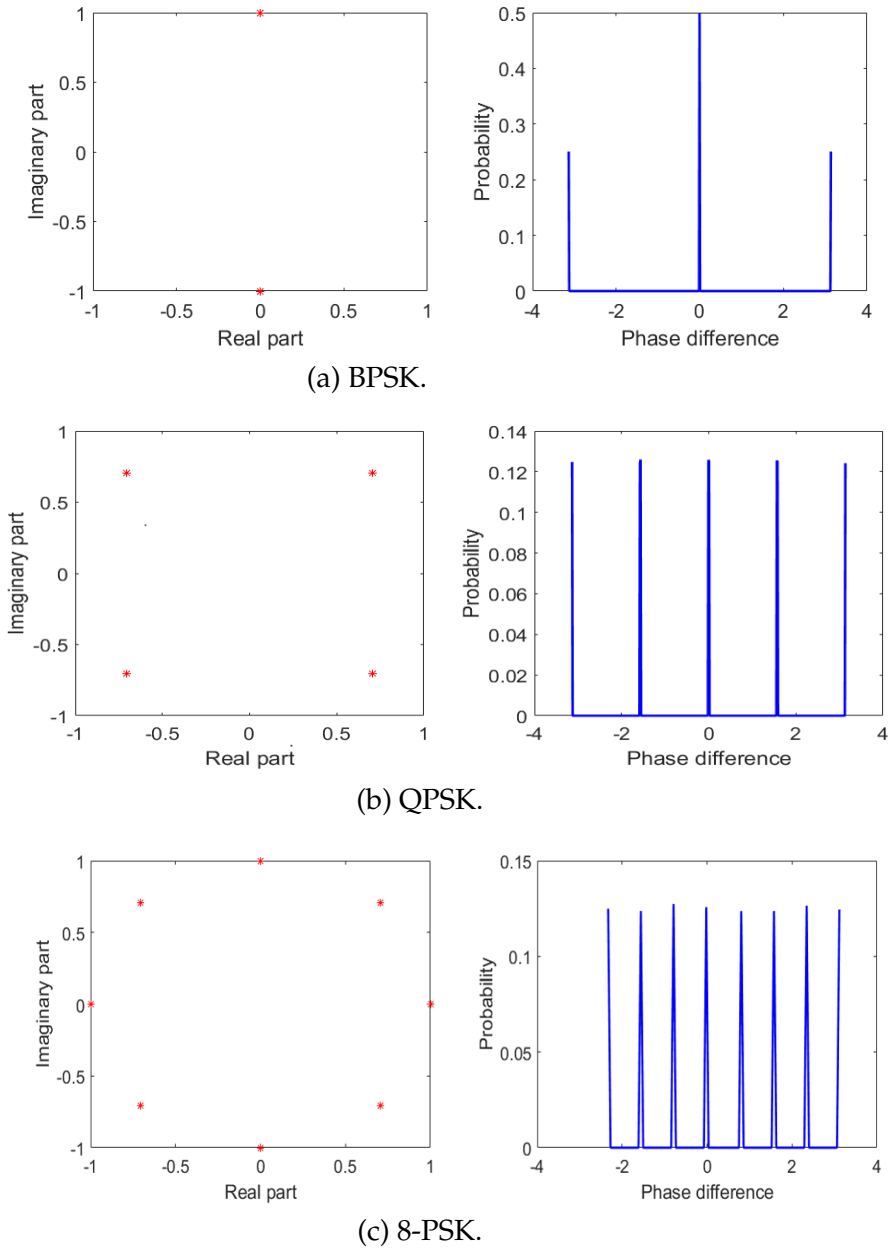

Figure 2.3: Constellation maps of symbols and histograms of the phase difference of the symbols for different PSK types without noise: Number of symbols: 10000.

between adjacent symbols displays different features. For example, at sufficiently high SNRs, 2 peaks for BPSK signal, 4 peaks for QPSK signal and 8 peaks for 8-PSK signal can be observed from the phase distribution. At lower SNRs, the corresponding peaks cannot be observed, but the phase distribution for different PSKs still presents distinguishable features.

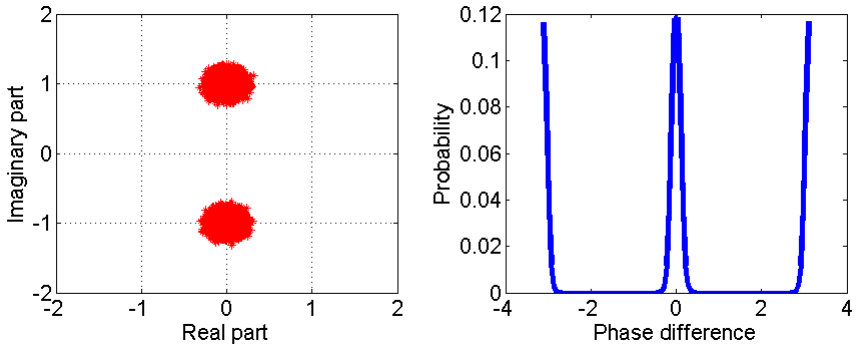

(a) 20 dB.

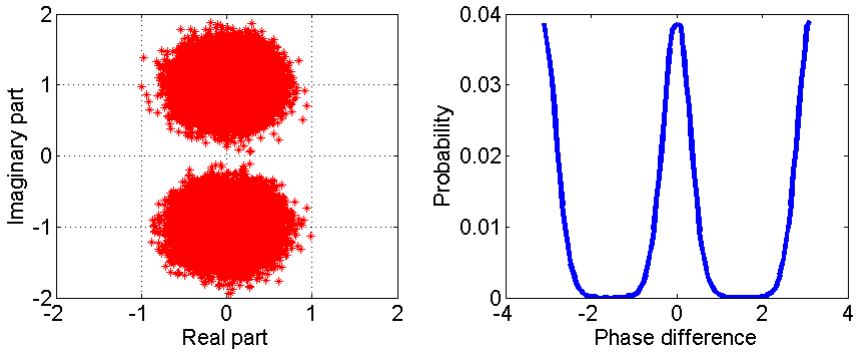

(b) 10 dB.

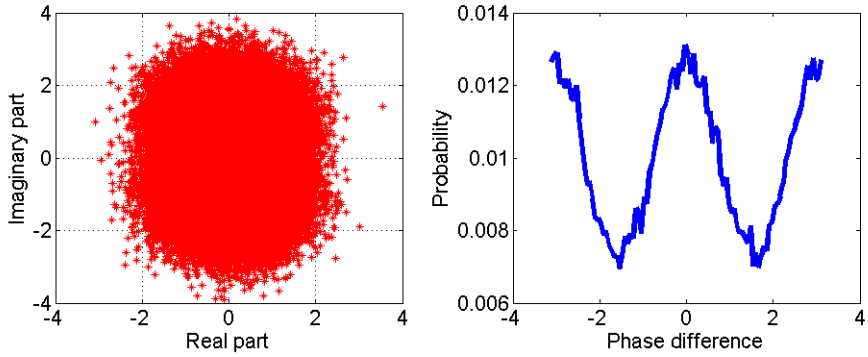

(c) 0 dB.

Figure 2.4: Constellation maps of symbols for BPSK with Gaussian noise of various levels: Number of symbols: 10000.

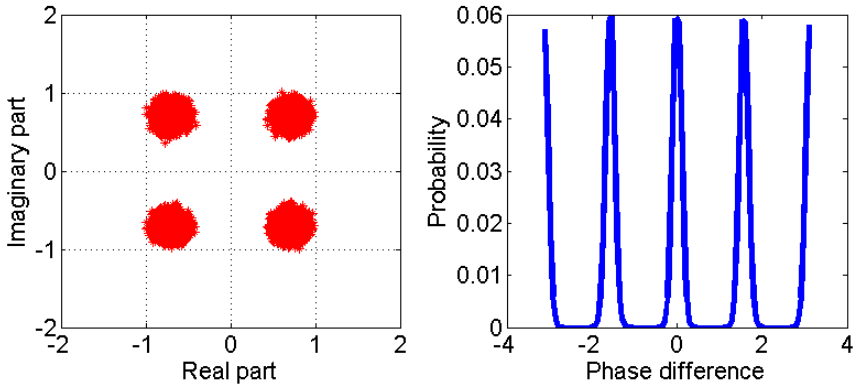

(a) 20 dB.

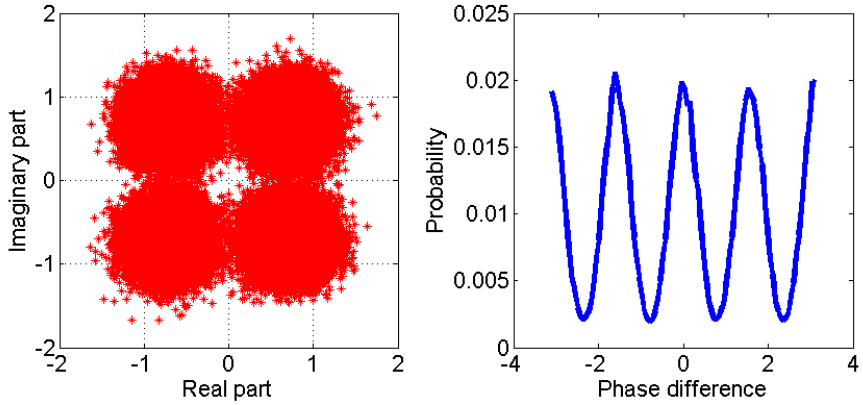

(b) 10 dB.

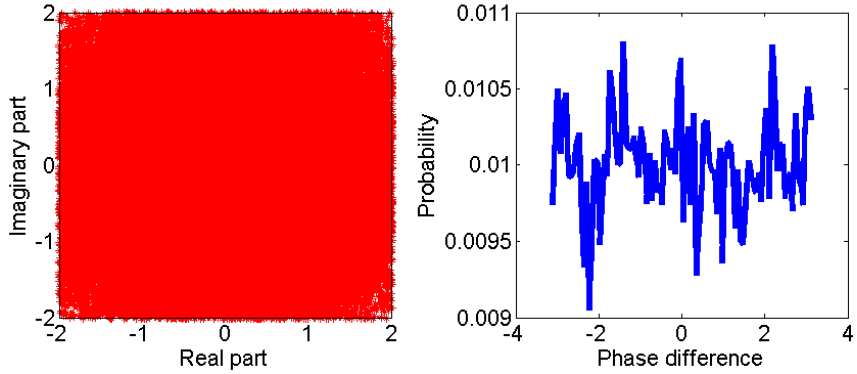

(c) 0 dB.

Figure 2.5: Constellation maps of symbols for QPSK with Gaussian noise of various levels: Number of symbols: 10000.

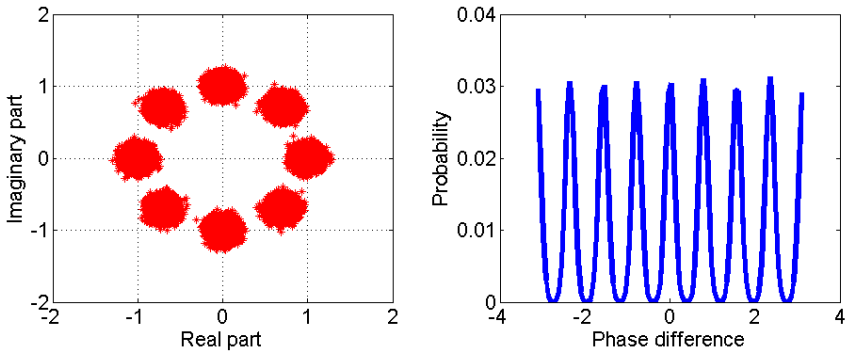

(a) 20 dB.

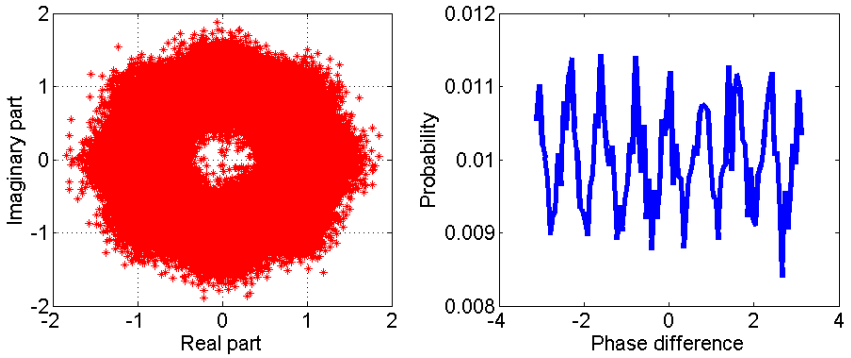

(b) 10 dB.

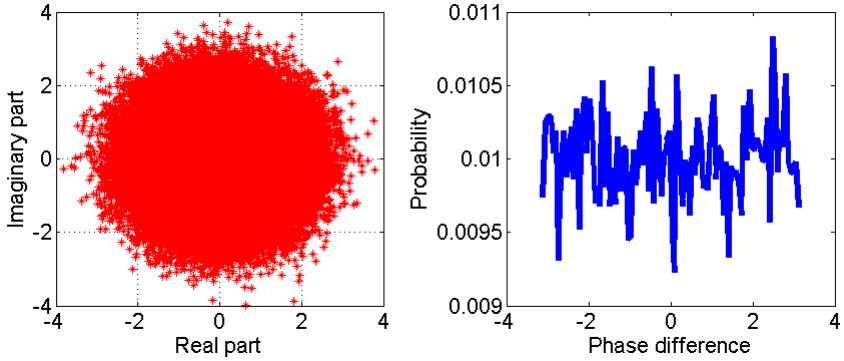

(c) 0 dB.

Figure 2.6: Constellation maps of symbols for 8PSK with Gaussian noise of various levels: Number of symbols: 10000.

2.1.2 Signal Characteristics of QAM Signals

QAM signals can transfer more information with more complicated constellation maps compared to PSK signals. Different from PSK symbols, QAM symbols with different orders have different amplitude and phase values. In this dissertation, the QAM types of interest are 16-QAM, 32-QAM, 64-QAM, 128-QAM and 256-QAM. Among these modulation types, 16-QAM, 64-QAM and 256-QAM are square QAMs while 32-QAM and 128-QAM are non-square QAMs. They can be easily distinguished by the constellation map.

The symbols of a square QAM type with order M can be expressed as

$$s_{QAM} = s_R(n) + js_I(n), n = 0, 1, 2, ... \log_2(M) - 1 \tag{2.2}$$

where $s_R(n)$ and $s_I(n)$ are uniformly distributed among $[-\log_2(M)+1, -\log_2(M)+3, ..., -1, 1, ..., \log_2(M)-1]$. There are many ways to generate the symbols for the non-square QAMs. In this dissertation, the symbols of the non-square QAMs are selected in the following way. The symbols with $\log_2(M) \times \log_2(M)$ values are computed using the formula in (2.2) first. Then, the corresponding number of symbols at the four corners are removed for the non-square QAMs. For example, for 32-QAM symbols, 36 symbols are computed first. Then, the four symbols at each corner of the constellation maps are selected to be removed for 32-QAM symbols.

Figure 2.7 shows the constellation maps and histograms of the amplitude for 16-QAM and 32-QAM symbols when there is no noise added to the symbols. The number of symbols was 10000. The constellation map for 16-QAM is squarely distributed while the constellation map for 32-QAM is non-squarely distributed. In addition, the 3 and 5 amplitude values correspond to 16-QAM and 32-QAM symbols can be seen from the histogram of the amplitudes in the figure.

Figure 2.8 and 2.9 show the distribution of the amplitude of 16-QAM symbols and 32-QAM symbols in the white Gaussian noise of various levels. Different QAM signals show different amplitude distributions. For example, the 3 and 5 amplitude peaks can be observed from the histogram of amplitude for 16-QAM and 32-QAM symbols at SNR = 20 dB. When noise level increases, the difference between the amplitude distributions decreases.

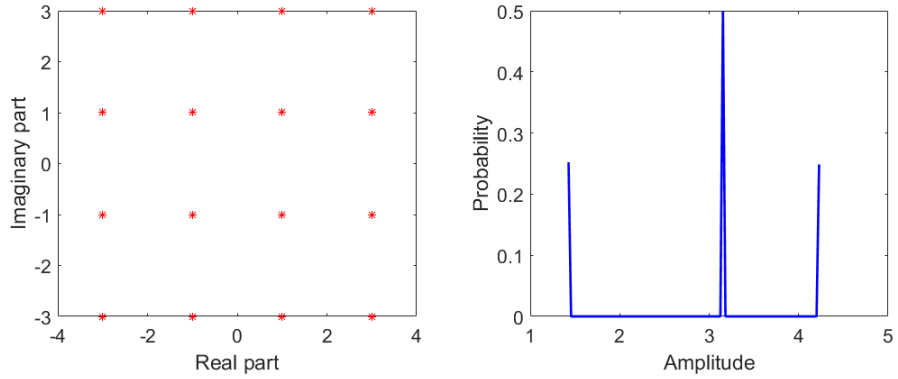

(a) 16-QAM.

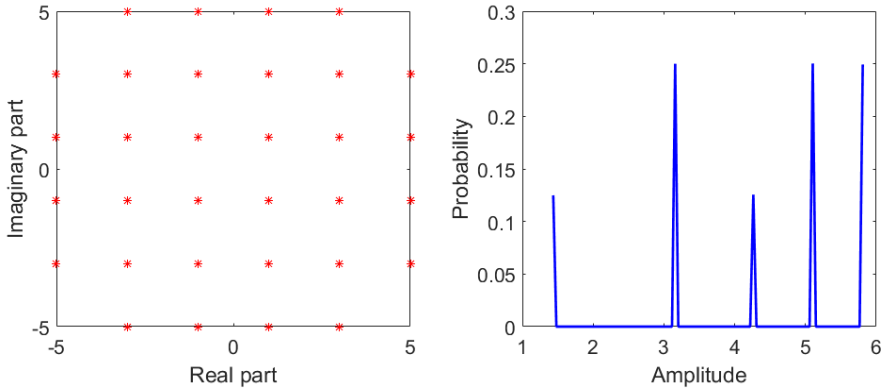

(b) 32-QAM.

Figure 2.7: Constellation maps and histograms of amplitude of symbols for different QAM types without noise: (a) 16-QAM; (b) 32-QAM; Number of symbols: 10000.

2.2 Multipath

Multipath occurs when the signal arriving at the receiver suffers from the propagation with different directions, for example, the reflections of the signal from other obstacles. Figure 2.10 shows an example of a signal transmitted through a multipath environment. During the transmission of the signal, the signal direction will be changed when it encounters different objects from the environment. The signal can be absorbed, attenuated, refracted and reflected. The receiver will receive a mixture of all the paths of the original transmitted signal. Thus, the mixed signals cannot be identified accurately using the modulation identification algorithm for the signals in noisy environment without multipath. The signal model for the signals in multipath channels will be presented in detail in Chapter 3.

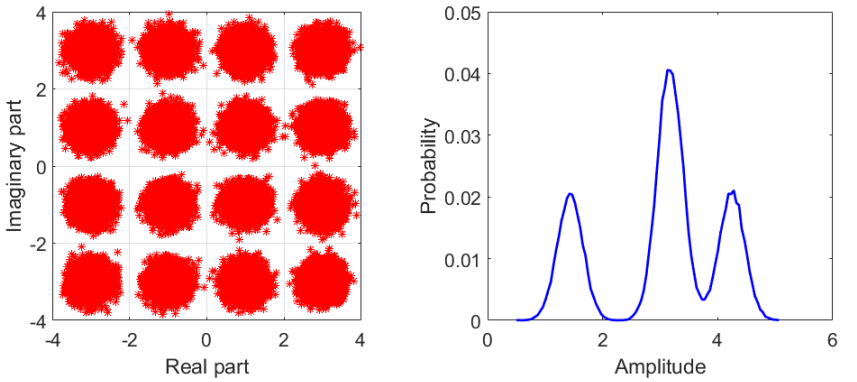

(a) 20 dB.

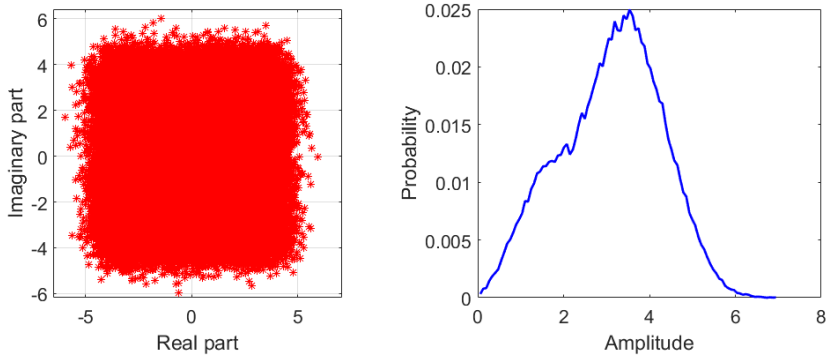

(b) 10 dB.

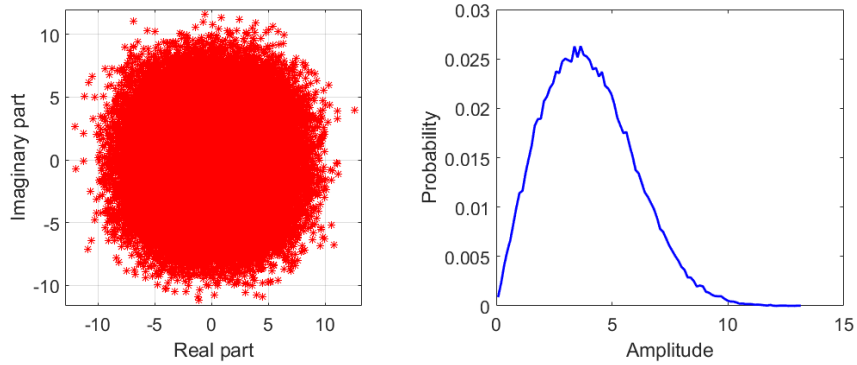

(c) 0 dB.

Figure 2.8: Constellation maps and histograms of amplitude of symbols for 16-QAM with Gaussian noise of various levels: Number of symbols: 10000.

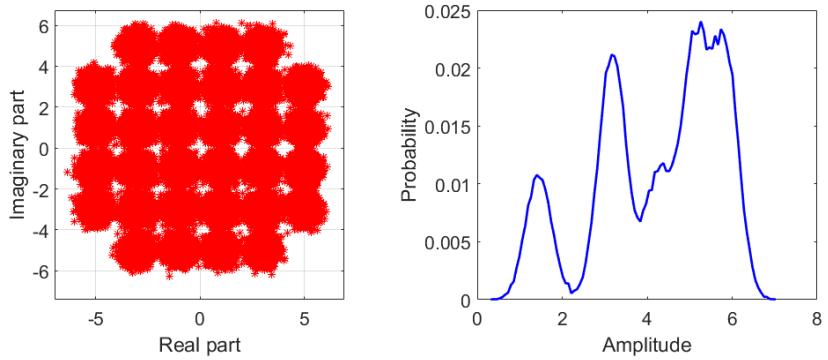

(a) 20 dB.

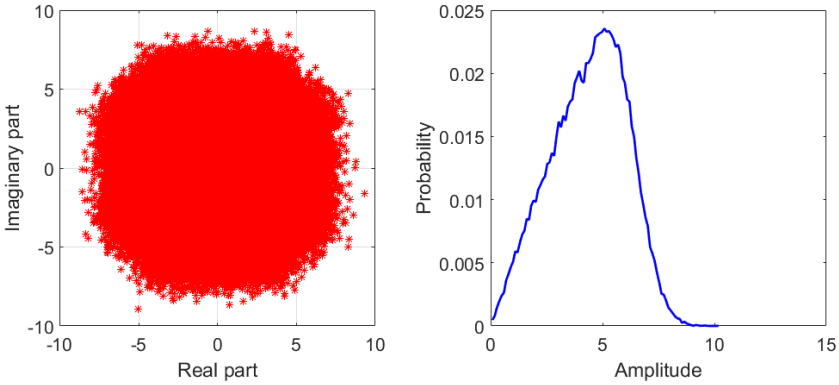

(b) 10 dB.

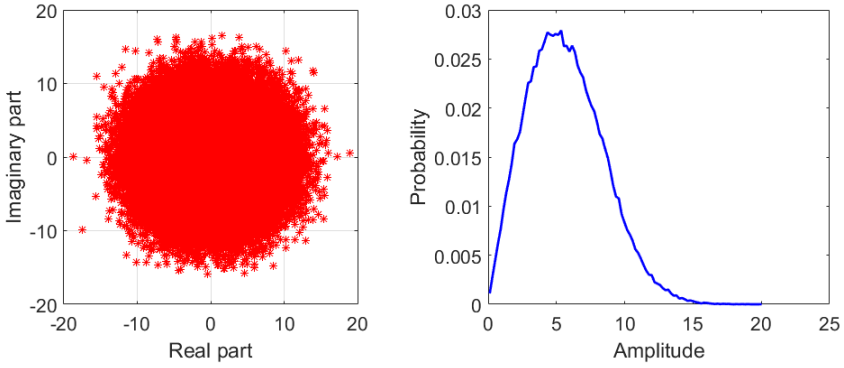

(c) 0 dB.

Figure 2.9: Constellation maps and histograms of amplitude of symbols for 32-QAM with Gaussian noise of various levels: Number of symbols: 10000.

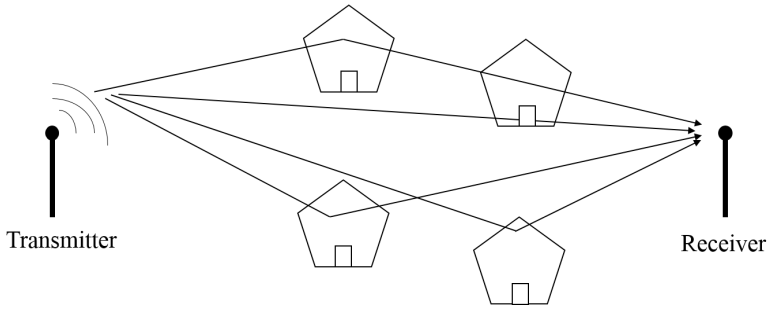

Figure 2.10: Block diagram of the signals with multipath.

Figure 2.11 shows one example of the constellation maps and histograms of phase difference for the QPSK signal after transmitting through a multipath channel. Figure 2.12 shows one example of the constellation maps and histograms of amplitude for the 16-QAM signal after transmitting through a multipath channel.

In these examples, there is only one reflection in the channel. The number of symbols was 20000.

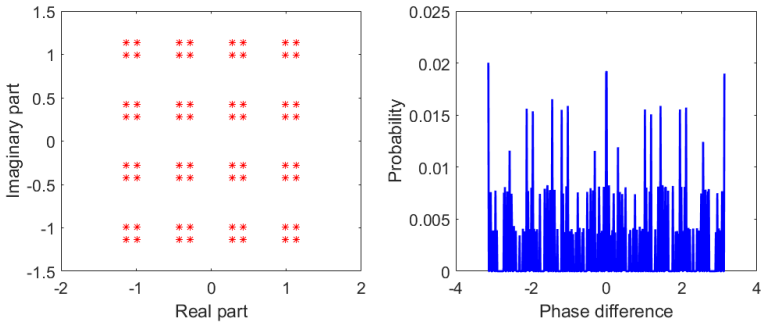

(a) No noise.

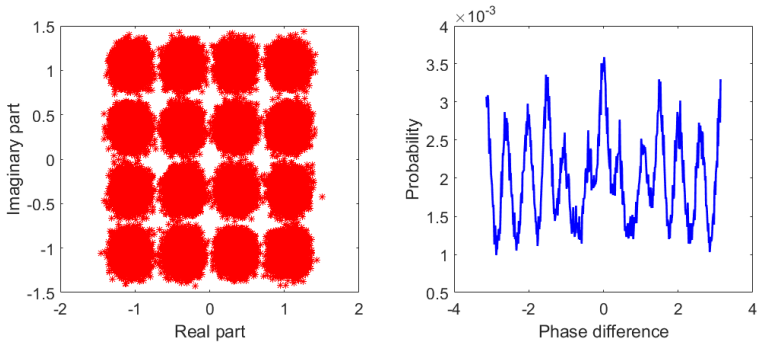

(b) 20 dB.

Figure 2.11: Constellation maps and histograms of phase difference of symbols for QPSK signal in multipath channels: Number of symbols: 20000.

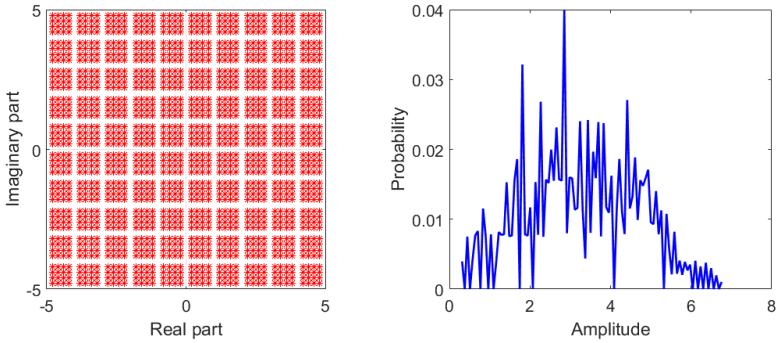

(a) No noise.

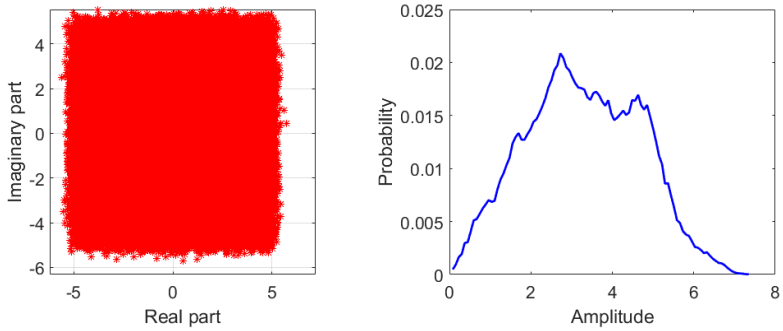

(b) 20 dB.

Figure 2.12: Constellation maps and histograms of amplitude of symbols for 16QAM signal in multipath channels: Number of symbols: 20000.

We can observe from the figures that the phase distributions of QPSK signal and amplitude distributions of 16-QAM signal after transmitting through the multipath channel do not contain the feature for the corresponding symbols.

Similar distortion happens for other PSK and QAM signals in the multipath channels, which gives the system more difficulty identifying among different PSK and QAM signals. Additional methods for channel estimation and equalization of the signals with multipath in order to eliminate the distortion of the signals need to be developed.

2.3 Dual Polarization

In typical communication systems, signals are transmitted through one polarization direction. Transmitting signals at the same time through two polarizations is a means to double the transmission data rates. This is realized by sending two independent modulated signals into two orthogonal polarizations. Generally, these two orthogonal polar-

izations are in vertical and horizontal directions. Ideally, the receiver can receive the two independent signals in the two channels without interference. However, due to the interference during transmission or the misalignment between the antennas of the transmitter or receivers, the cross-polarization interference between these two polarizations will mix the signals in the two channels. A block diagram of the signals transmitted through a dual-polarized channel is shown in Figure 2.13.

Figure 2.14 shows one example of the signals transmitting through a dual-polarized channel with cross-polarization interference. In this example, the two input signals are 16-QAM and 32-QAM signals. The number of symbols was 20000. The signal model for the dual-polarized signals will be presented in detail in Chapter 4. The constellation maps were obtained by demodulating the signals with known signal parameters such as carrier frequency and baud rate. From these figures, the corresponding symbol patterns cannot be detected from the constellation after trying to demodulate the received signals. Also, the statistical properties, which are the amplitude distributions shown in these figures, are not distinct for the 16-QAM and 32-QAM signals. As a result, additional signal separation needs to be done before identifying the modulation types of the received signals in the dual-polarized channels without knowing any information of the channels.

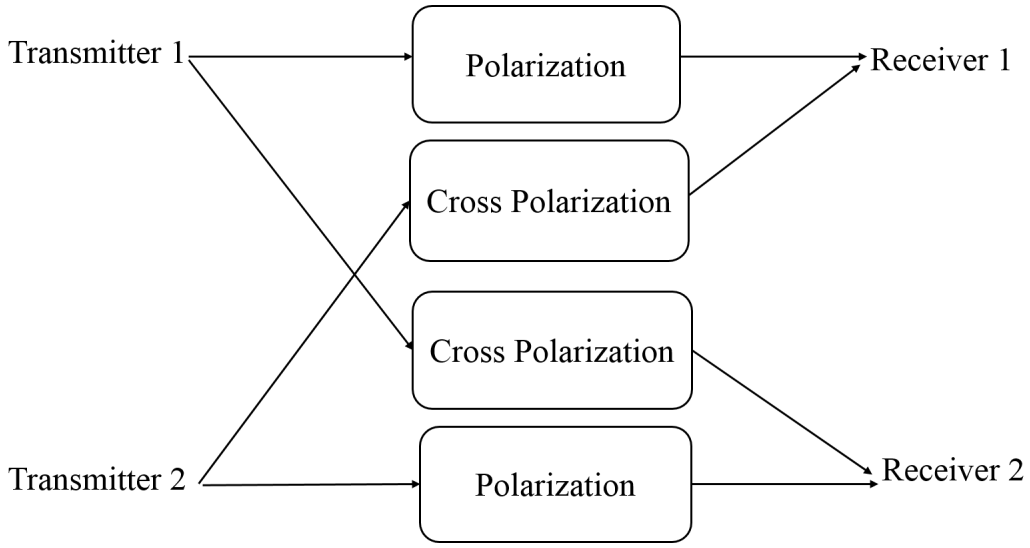

Figure 2.13: Block diagram of signals transmitting through a dual-polarized channel.

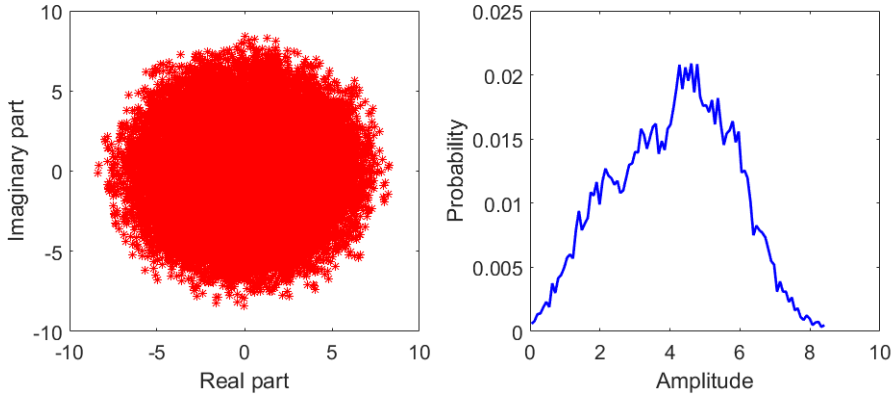

(a) Channel 1.

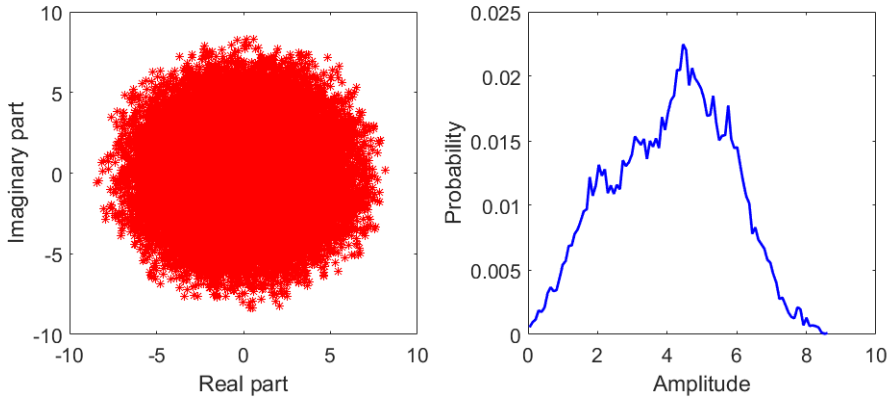

(b) Channel 2.

Figure 2.14: Constellation maps and histograms of amplitude of symbols for 16-QAM and 32-QAM signals after transmitting through dual-polarized channels with Gaussian noise: SNR=20 dB; Number of symbols: 10000.

CHAPTER 3

A LIKELIHOOD-BASED ALGORITHM FOR BLIND IDENTIFICATION OF QAM AND PSK SIGNALS

This chapter introduces a novel method for identifying PSK and QAM signals transmitted in an AWGN channel first. From Chapter 2, we knew that PSK and QAM symbols with different order have different phase and amplitude values. This feature is applied to identify different PSK and QAM signals in this chapter. In information theory, the information of a signal can be represented as the entropy of the signal, which is related to the probability density function(PDF) of the signal. Since different PSK and QAM signals obtain distinct PDFs of phase and amplitudes, the information contained in different signals will be different. Based on this, this chapter developed a likelihood-based algorithm using the PDFs of phase and amplitudes to identify PSK and QAM signals.

In addition, this chapter also implements a combination of a blind equalizer algorithm and the likelihood-based modulation identification method for signals in multipath channels. As shown in Chapter 2, the PDF of the amplitude or phase of the signals in multipath channels changes due to the effect from the additional paths. The blind equalizer mitigates the effect of the multipath so that the likelihood-based modulation identification algorithm will be able to get accurate identification results for PSK and QAM signals in multipath channels. The blind equalizer algorithm used in this chapter is the Constant Modulus Amplitude (CMA) equalizer.

The rest of the chapter is organized as follows: The algorithm derivation for the likelihood-based modulation identification for signals in AWGN channels is described in the next section. It presents the amplitude and phase likelihood-based identification algorithms. A theoretical analysis of the performance of the algorithm is also given in Section 3.2. Section 3.3 contains a comparison of theoretical performance with simulation results and a

performance comparison with two other methods available in the literature. This section also presents simulation results demonstrating the probability of successful modulation identification under different SNR conditions and under several noise environments. In Section 3.4, the combination of the CMA equalizer and the modified likelihood-based modulation identification method is presented. This section also includes the performance evaluation of PSK and QAM signals in multipath channels. Finally, Section 3.5 contains the concluding remarks.

3.1 The Likelihood-based Modulation Identification Algorithm

3.1.1 Signal Model

We assume an additive band-limited white Gaussian channel under which the general model for the received signal [57] is

$$y(t) = Re\{\sum_k (s_k g_T(t - kT_b))e^{j2\pi f_c t} + N_0(t)\} \tag{3.1}$$

where s_k is a complex-valued independent and identically distributed (i.i.d.) symbol sequence with $s_k = a_k + jb_k$, where a_k and b_k are, respectively, the real and imaginary parts of the symbol s_k, T_b is the symbol period, $g_T(t)$ is a square-root raised-cosine pulse shape filter with unknown roll-off factor, f_c is the carrier frequency, and N_0 is the additive band limited white Gaussian noise. We assume that N_0 is such that the sampled version of the noise is i.i.d. Gaussian signals with zero-mean value and variance σ^2. Applying Hilbert transformation to the received signals, the output will become

$$y(t) = \sum_k (s_k g_T(t - kT_b))e^{j2\pi f_c t} + N_0(t) \tag{3.2}$$

In our derivations, a sampled version of this signal is given by

$$y(n) = \sum_k (s_k g_T(nT_s - kT_b))e^{j2\pi f_c nT_s} + N_0(nT_s) \tag{3.3}$$

where T_s is the sampling period and $N_0(nT_s)$ is a band-limited white Gaussian noise with flat spectrum.

In order to decrease the inter-symbol interference (ISI) between adjacent symbols, a matched filter is applied. For a square-root raised-cosine pulse shape filter, the matched filter is the same as itself. The signal after matched filtering is

$$y(n) = \sum_k (s_k g(nT_s - kT_b))e^{j2\pi f_c nT_s} + \eta(nT_s) \tag{3.4}$$

where $g(n) = \sum_l g_T(l)g_T(n-l)$ and $\eta(n) = \sum_l N_0(l)g_T(n-l)$.

Using the Nyquist criterion, the interference between adjacent symbols is negligible at the midpoint of each baud [48]. Let $y(m)$ represent the midpoint of the mth symbol, which can be modeled as

$$y(m) = s_m g_T(0) e^{j2\pi f_c m T_b} + \eta(m) \tag{3.5}$$

where $\eta_0(m)$ is the noise sample at the midpoint of the m^{th} symbol.

3.1.2 System Overview

A schematic block diagram of the blind likelihood-based identification method is given in Figure 3.1. The system first estimates several characteristics of the received signal including the baud rate, parameters of the pulse shaping filter and the noise variance. This information is used to design a matched filter. Then, a phase likelihood-based algorithm is implemented to determine if the modulation type is BPSK. If the modulation type is not BPSK, the system applies an amplitude likelihood-based algorithm to classify the signal as QAM or higher-order PSK (QPSK and 8PSK). This stage can also identify different QAM types. If the QAM identification block determines that the signal is PSK, the system employs the phase likelihood-based algorithm to determine if the modulation type of the signal is QPSK or 8-PSK.

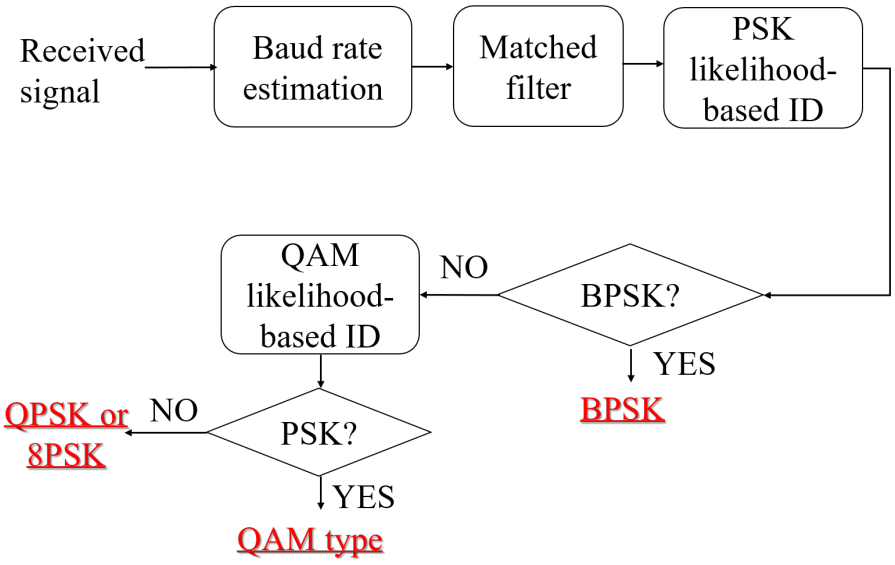

Figure 3.1: Block diagram of the modulation identification system.

3.1.3 Estimation of Signal Characteristics

Based on the signal model in (3.3), the signal spectrum can be expressed as

$$S_{yy}(f) = P_s \|G_T(f)\|^2 + \sigma^2 \tag{3.6}$$

where P_s is the symbol power, $||G_T(f)||^2$ is the squared magnitude of the frequency response of the pulse shaping filter and σ^2 is the noise variance. The bandwidth of the received signal without noise is the same as the bandwidth of the pulse shaping filter. The parameterized model for $G_T(f)$ of a root-raised-cosine filter with roll-off factor α and symbol duration T_b is given by

$$G_T(f) = \begin{cases} T_b; & |f| \leq \frac{1-\alpha}{2T_b} \\ \frac{T_b}{2}\{1 + cos[\frac{\pi T_b}{\alpha}(|f| - \frac{1-\alpha}{2T_b})]\}; & \frac{1-\alpha}{2T_b} \leq |f| \leq \frac{1+\alpha}{2T_b} \\ 0; & \text{otherwise} \end{cases} \tag{3.7}$$

From (3.7), the double-sided bandwidth of the signal spectrum is $\frac{1+\alpha}{T_b}$. The noise variance is estimated as the average of the estimated power spectrum outside the bandwidth.

Because the received signal is band-limited, the difference between the edge of the passband and the maximum value in the spectrum will ideally be the maximum. Based on this, the signal bandwidth is estimated using a four-step process. First, we estimate the signal spectrum $\hat{S}_{yy}(f)$ using Welch's method [3]. Secondly, the maximum value and the corresponding point in the spectrum, denoted as point A in Figure 3.2, are obtained. Thirdly, for each frequency point (for example, point B in Figure 3.2) in the spectrum, the "area" of the difference between the estimated spectrum and the straight line connecting point A and B is calculated. Finally, the left and right edges of the signal spectrum are estimated as the frequencies that have the maximum values of the "area" on the left and right of the peak frequency. Let f_{right} and f_{left} represent the edge of the passband. The bandwidth of the signal is

$$BW = f_{right} - f_{left} \tag{3.8}$$

After estimating the bandwidth, the noise variance is estimated as

$$\hat{\sigma}^2 = \int_{f=0}^{f_{left}} \hat{S}_{yy}(f)df + \int_{f=f_{right}}^{f_{N_f}} \hat{S}_{yy}(f)df \tag{3.9}$$

where N_f is the length of the spectrum. Because, $\int_f |G_T(f)|^2 = 1$, the symbol power P_s is estimated as

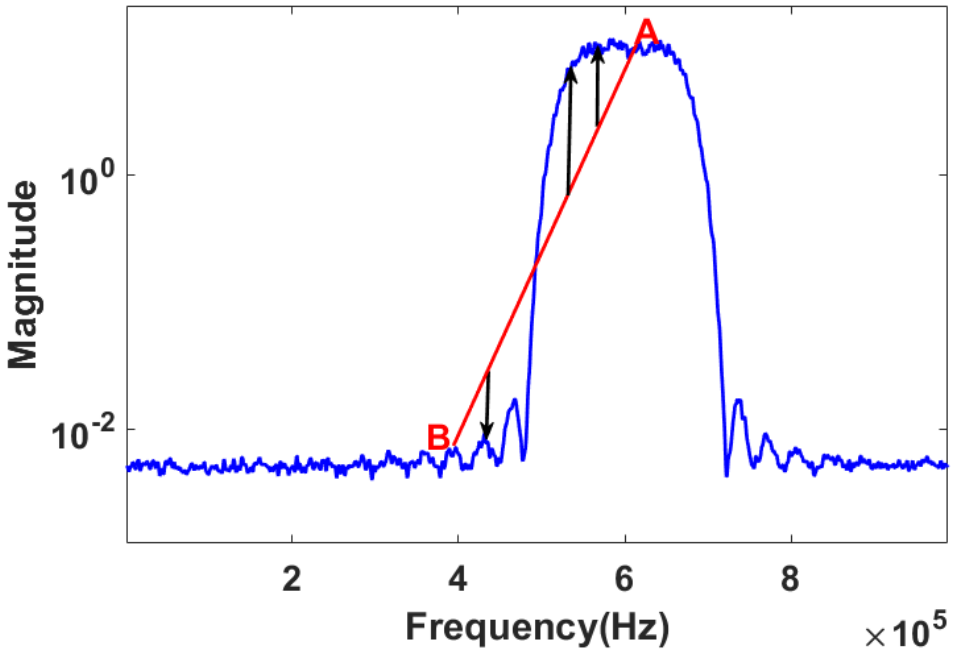

Figure 3.2: Estimation of the bandwidth of the spectrum.

$$\hat{P}_s = \int_{f=0}^{f_{N_f}} \hat{S}_{yy}(f)df - \hat{\sigma}^2 \tag{3.10}$$

Subtracting the estimated noise variance from the estimated spectrum, the squared-frequency response of the root-raised-cosine filter is estimated as

$$\hat{G}_T(f) = \frac{\hat{S}_{yy}(f) - \hat{\sigma}^2}{\hat{P}_s} \tag{3.11}$$

For a square-root raised cosine pulse shape, T_b and α satisfy

$$\frac{1+\alpha}{T_b} = BW \tag{3.12}$$

A least-square fit is applied to $\hat{G}_T(f)$ to estimate T_b and α. T_b and α are estimated by minimizing the cost function given by

$$\{\hat{T}_b, \hat{\alpha}\} = \arg\min_{T_b,\alpha}\{\int_f \|\hat{G}_T(f) - G_T(f)\|^2 df\} \tag{3.13}$$

3.1.4 Matched Filter

In order to decrease the inter-symbol interference (ISI) between adjacent symbols, we apply a matched filter before the subsampling process. The convolution of two matched square-root raised-cosine filters satisfies the Nyquist criterion

$$p(nT_b) = \begin{cases} 1; & n = 0 \\ 0; & \text{otherwise} \end{cases} \tag{3.14}$$

where $p(t)$ is a Nyquist pulse-shape resulting from the matched filtering operation. Ideally, we can eliminate ISI from adjacent symbols by sampling the signals after matched filtering at the right timing phase.

Assuming that the pulse shaping filter is a root raised-cosine filter, the matched filter is designed to have the same magnitude response as the estimated pulse shaping filter estimated as in (3.11).

3.1.5 Phase Likelihood-based Identification Algorithm for PSK Signals

Figure 3.3 shows the block diagram of the phase likelihood-based identification algorithm for different PSK signals. The system first implements a uniform subsampling method to mitigate the effect of higher sampling rate. After that, the likelihood functions of the phase difference between adjacent samples using different hypothesized modulation types are calculated. By finding the maximum value among these likelihood functions, the modulation type of the received signals corresponding to the hypothesis is identified.

3.1.5.1 Uniform Subsampling

For the signal model described in (3.3) with high sampling rates, nearby samples most often correspond to the same symbol, and the phase difference between nearby samples

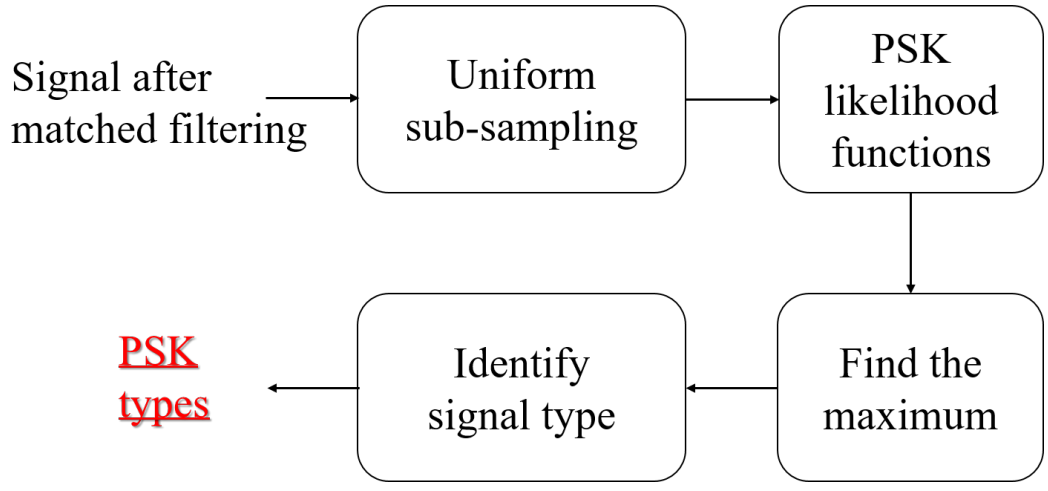

Figure 3.3: Block diagram of the phase likelihood-based PSK identification algorithm.

will be dominated by a fixed value contributed by the carrier frequency. This can be avoided by subsampling the received signals as shown in (3.5), such that the nearby symbols almost always come from different bauds. We perform uniform subsampling here in order to maintain a constant phase contributed by the carrier frequency. For the sampled signals, the number of samples per symbol $T = T_b/T_s$ is used to perform the subsampling process. The subsampling rate T corresponds to the closest integer to the estimated baud rate (in number of samples).

Starting from an arbitrary sample at the beginning of the signal (we chose the first sample in our simulation), subsequent samples are uniformly sampled at a period of the subsampling rate T. Because the phase values in each symbol duration are mostly the same, we can obtain additional samples by choosing different starting points for the subsampling process in one baud. After subsampling the received signal uniformly with the first starting sample, we select an adjacent sample of the first starting sample as a new starting point and pick the samples uniformly as previously described. Because of possible inter-symbol interferences, the number of the starting samples selected is restricted to approximately half of the estimated symbol duration around the first starting sample. The likelihood function is calculated based on the phase difference between adjacent samples of all the subsampling sequences.

Figure 3.4 and 3.5 show the effects of the subsampling process on the phase difference sequences with different number of samples per symbol. In the two figures, the top-left panel displays the scatter plot of the samples of the received signal. The top-right panel shows the histogram of the phase difference between the adjacent samples. The impact of the carrier frequency is clear in both figures. The effect of the pulse shaping is also seen in the top left panel. The corresponding results after subsampling by the estimated symbol duration are shown in the bottom panels. The four distinct values of the phase differences for QPSK symbols can be observed after the subsampling process. Consequently, we can apply the likelihood functions derived for signals without pulse shaping to identify pulse shaped signals after the subsampling process.

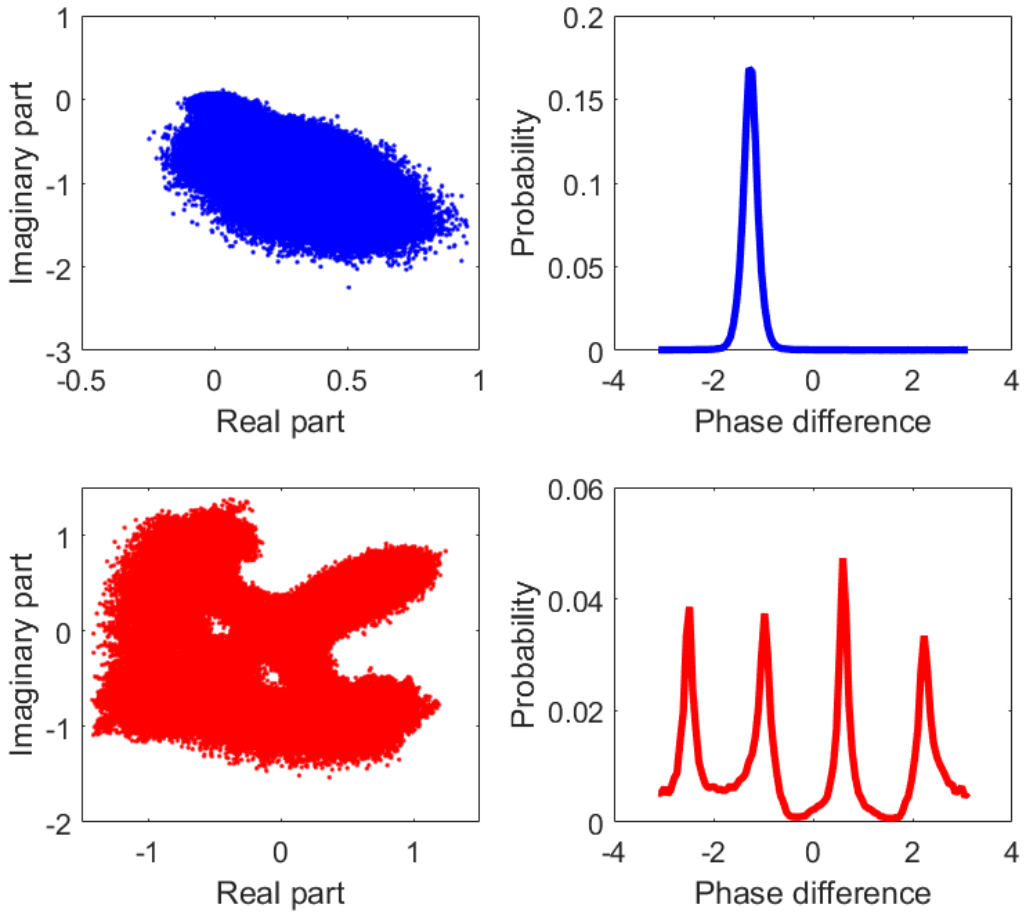

Figure 3.4: Constellation maps and distribution of the phase differences for a received QPSK signal before and after subsampling: SNR=20 dB, number of symbols: 10000, number of samples per symbol: 13.25. Top left: constellation maps for received signal, top right: histogram of phase differences for received signal; bottom left: constellation maps for signal after matched filter and subsampling; bottom right: histogram of phase differences for signal after matched filter and subsampling

3.1.5.2 Phase Likelihood Function

For two continuous sinusoids with the same frequency and initial phase that are independently perturbed by white Gaussian noise with variance σ^2 and zero mean value, the probability density function (PDF) of the phase difference ϕ between them [2] is given by

$$P(\phi) = \frac{1}{2\pi}\int_0^{\frac{\pi}{2}} \{\sin 2\beta[1 + \frac{S}{2}(1 + \cos\phi \sin 2\beta)]e^{-\frac{1}{2}S(1-\cos\phi\sin 2\beta)}\}d\beta \tag{3.15}$$

where S is SNR.

As mentioned in Section 3.1.1, the signal with pulse shaping after subsampling can

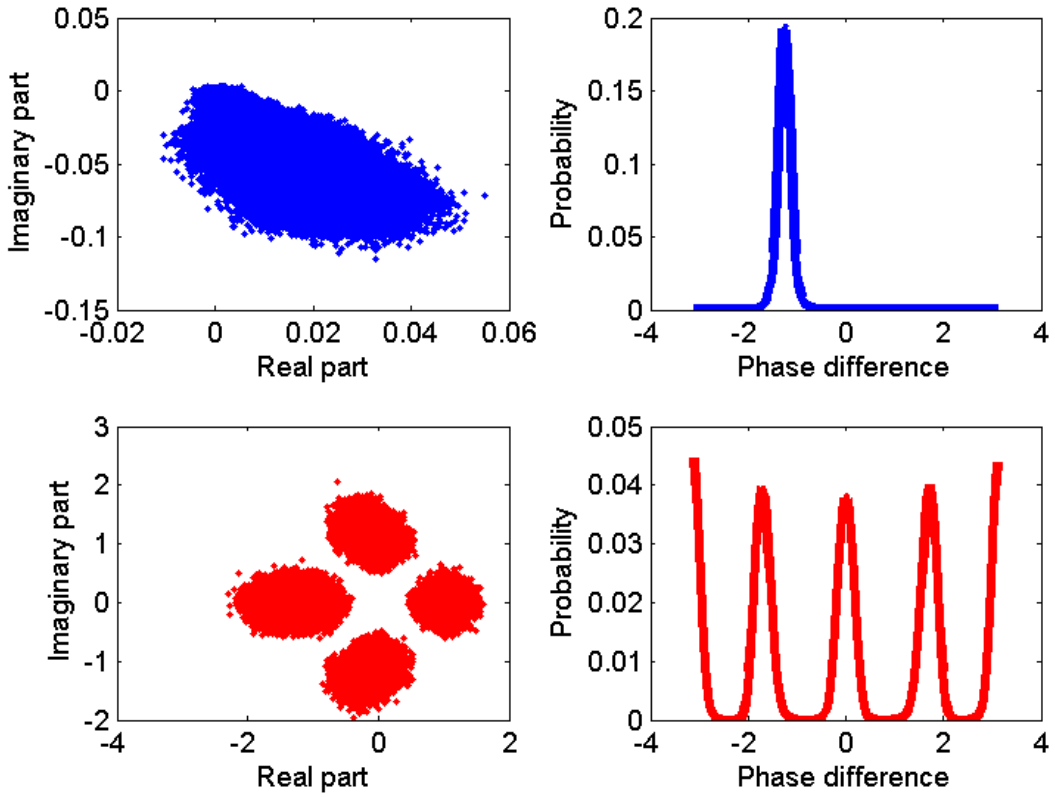

Figure 3.5: Constellation maps and distribution of phase difference for a received QPSK signal before and after subsampling: SNR=20 dB, number of symbols: 10000, number of samples per symbol: 20. Top left: constellation maps for received signal, top right: histogram of phase difference for received signal; bottom left: constellation maps for signal after matched filter and subsampling; bottom right: histogram of phase difference for signal after matched filter and subsampling

be regarded as a sinusoid that is modeled as 3.3. The phase difference between nearby samples after subsampling the received signals can be derived as follows.

The contribution to the phase of $y(m)$ from the carrier frequency changes with different time lag m. Obtaining the phase difference between nearby samples of subsampling signal can avoid this variability. In order to calculate the phase the difference between nearby samples, let

$$\begin{aligned} y_d(m) &= y(m)y^*(m-d) \\ &= \{s_m g(0)e^{j2\pi f_c m T_b} + \eta(mT_b)\}\{s^*_{m-d} g^*(0)e^{-j2\pi f_c (m-d)T_b} + \eta^*((m-d)T_b)\} \\ &= s_m s^*_{m-d} g^2(0)e^{j2\pi f_c d T_b} + \eta(mT_b)\eta^*((m-d)T_b) \end{aligned} \tag{3.16}$$

where d is an appropriately selected lag value.

The phase of $y_d(m)$ is

$$\theta_d(m) = \theta_s + \theta_c + \phi \tag{3.17}$$

where $\theta_c = 2\pi f_c d T_b$ is a fixed value contributed by the carrier frequency f_c, θ_s is the phase difference between the symbols and ϕ is the phase difference contributed by noise. In all the simulations in this paper, we selected d to be 1.

We can see from the above that the phase difference between $y(m)$ and $y(m-d)$ will have a similar distribution (within a constant shift contributed by the carrier frequency) as the phase difference of the original symbol sequence. The phase difference between symbols can take one of a finite number of values depending on the modulation order. Furthermore, assuming that the symbols sequence is independent and identically-distributed, the probability of these phase difference values can be predetermined for each PSK type.

Based on (3.15), the distribution of phase difference θ_d in (3.17) is

$$\begin{aligned} P(\theta_d) = \frac{1}{2\pi} \int_0^{\frac{\pi}{2}} \{ & \sin 2\beta [1 + \frac{S}{2}(1 + \cos(\theta_d - \theta_s - \theta_c) \sin 2\beta)] \\ & e^{-\frac{1}{2}S(1-\cos(\theta_d - \theta_s - \theta_c)\sin 2\beta)} \} d\beta \end{aligned} \tag{3.18}$$

Figure 3.6 shows two examples of the comparison between the theoretical PDF derived as (3.18) and the histogram of the phase difference of QPSK signals after matched filtering and uniform subsampling in the simulation. The number of symbols used in the simulation is 10000. Number of samples per symbol is 20. We can see that the two matched reasonably well. As a result, we should be able to use the theoretical PDF expression of the phase difference in the modulation identification and get good results.

Let there be N_p distinct phase difference values θ_s between symbols for the Mth modulation type. Let the set $\{\theta_s(M,i); i = 1, 2, \cdots, N_p\}$ represent these values and let $w_M[i]$ be the probability of the ith phase difference value for the Mth modulation type. The PDF for the phase difference θ between adjacent samples is given by [2]

$$\begin{aligned} P(\theta_d | H_M) &= \sum_{i=1}^{N_p} P(\theta_d | \theta_s(M,i) w_M[i], -\pi \le \theta \le \pi, \\ &= \sum_{i=1}^{N_p} \int_0^{\frac{\pi}{2}} \{ [1 + \frac{S}{2}(1 + \cos(\theta_d - \theta_s(M,i) - \theta_c) \sin 2\beta)] \\ &\quad \sin 2\beta e^{-\frac{1}{2}S(1-\cos(\theta_d - \theta_s(M,i) - \theta_c)\sin 2\beta)} \} \frac{w_M[i]}{2\pi} d\beta \end{aligned} \tag{3.19}$$

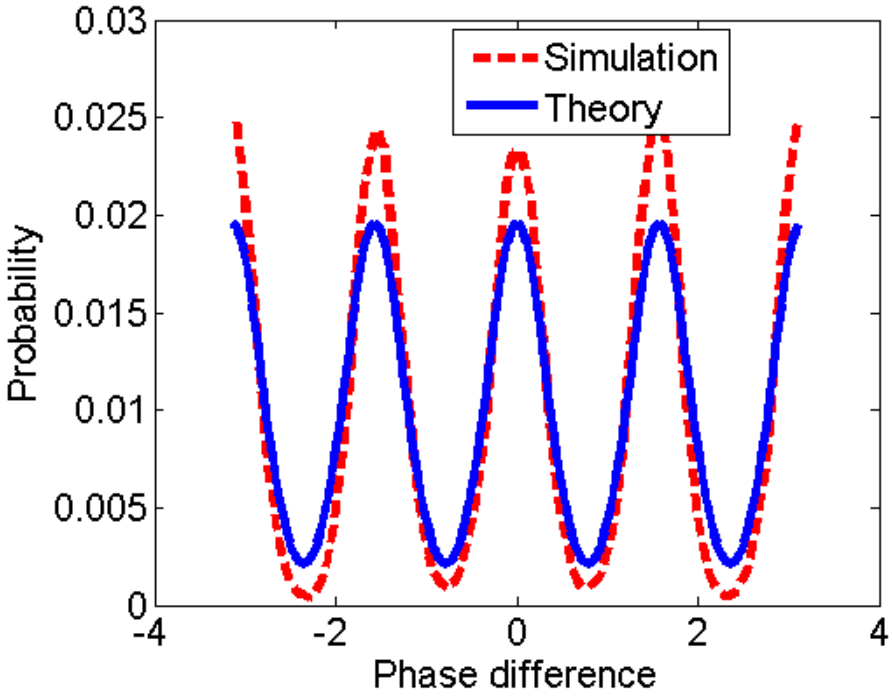

(a) SNR = 0 dB

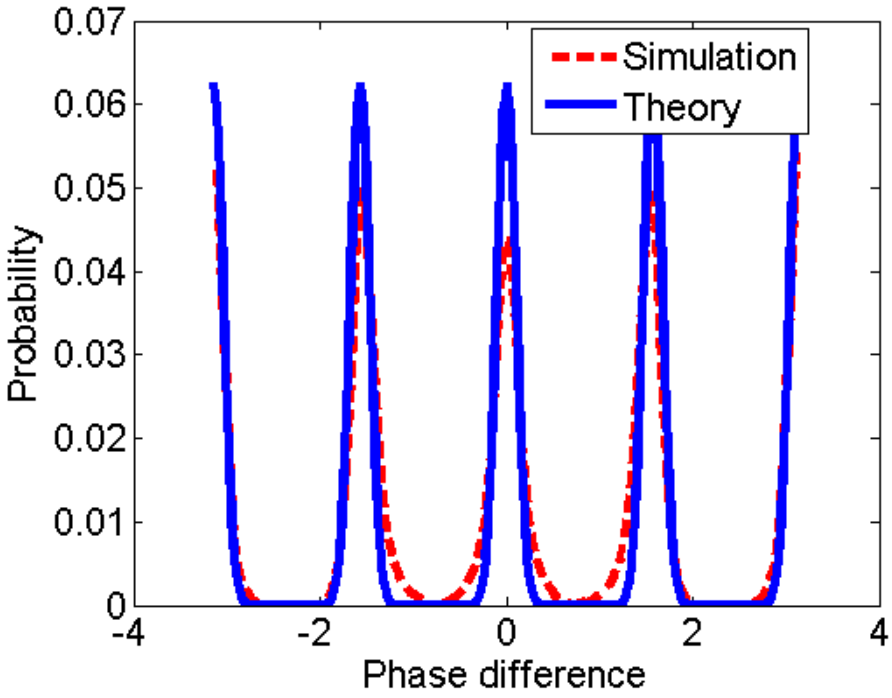

(b) SNR = 10 dB

Figure 3.6: Comparison between the theoretical PDF of phase and the histogram of the phase difference of signals after matched filtering and uniform subsampling in the simulation: QPSK signals; number of samples per symbol: 20, number of symbols: 20000.

Given N independent phase difference values $\theta_1, \theta_2, \ldots, \theta_N$ of the received signals, the PSK likelihood function for H_M can be derived as

$$p(\theta_1, \theta_2, \ldots, \theta_N | H_M) = \prod_{j=1}^{N} \sum_{i=1}^{N_p} \int_0^{\frac{\pi}{2}} \{[1 + \frac{S}{2}(1 + \cos(\theta_j - \theta_s(M,i) - \theta_c) \sin 2\beta)] \sin 2\beta e^{-\frac{1}{2}S(1-\cos(\theta_j - \theta_s(M,i) - \theta_c) \sin 2\beta)}\} \frac{w_M[i]}{2\pi} d\beta \quad (3.20)$$

Let $L_{p_M}(\theta_j) = \ln(P(\theta_j | H_M))$, the PSK log-likelihood function for determining the modulation types is given by

$$l_M = \sum_{j=1}^{N} L_{p_M}(\theta_j) = \sum_{j=1}^{N} \ln(P(\theta_j | H_M)) \quad (3.21)$$

After computing the log-likelihood functions in (3.21) under different hypotheses about the PSK, we identify the PSK type of the received signals as the hypothesis that corresponds to the maximum of the log-likelihood functions.

3.1.5.3 Estimation of the Constant Phase from Carrier Frequency

In the implementation of the phase likelihood functions, we need to estimate the constant phase θ_c contributed by carrier frequency. This parameter is estimated from the histogram of the phase difference between adjacent samples after subsampling.

In the absence of the carrier frequency and assuming phase is i.i.d., the phase difference between symbols for different PSKs is identically distributed in a finite set X in the interval $[0, 2\pi)$, and '0' phase is always a member of this set. The constant phase contributed by the carrier frequency will shift the value of each element in the set X. The distribution of phase difference remains identical in the shifted set Y. Since the phase difference values for different PSK signals are equally-spaced samples in $[0, 2\pi)$, substracting any value in the shifted set Y from the entries of Y will result in the same set X for each modulation type. Therefore, the constant phase is estimated as the phase corresponding to the maximum value of the histogram for the phase differences of adjacent samples after subsampling. Although the estimated constant may be off by an integer multiple of $\frac{2\pi}{N_p}$, the resulting set will be an estimation of the set X for each modulation type.

3.1.6 Amplitude Likelihood-based Identification Algorithm for QAM Signals

Figure 3.7 shows the block diagram of the amplitude likelihood-based identification algorithm. Different from that of the phase likelihood-based identification algorithm, the system applies a nonuniformly subsampling method to mitigate the pulse shaping filter and higher sampling rate. Then similarly, the amplitude likelihood functions of different hypothesized modulation types of the received signal are calculated. The modulation type of the received signal is identified as the corresponding hypothesis with the maximum value among these likelihood functions.

3.1.6.1 Nonuniform Subsampling

Different from the effect of the pulse shaping filter on the phase, the amplitude of the samples in one baud will be different in different locations of the pulse shaping filter. In order to obtain a similar amplitude distribution of the signal as that of the transmitted symbols, the nonuniform subsampling process attempts to detect the midpoint of each baud and sample the received signal at that location. The approach implemented in our algorithm is based on a timing recovery method typically employed in communication receivers [57].

Given the signal model in (3.2), the ensemble average power of $y(t)$ is

$$\rho(t) = E|y(t)|^2 = P_s \sum_k |g(t - kT_b)|^2 \tag{3.22}$$

Since the number of samples per symbol T for a received signal with unknown baud rate is not always an integer, the ensemble power is calculated as follows. First, we interpolate the received signal to a higher sampling rate. Then, for each time instant n, we estimated ρ as

$$\hat{\rho}(n) = \frac{1}{2N_\rho + 1} \sum_{k=-N_\rho}^{N_\rho} |y(nT_s + kT_b)|^2 \tag{3.23}$$

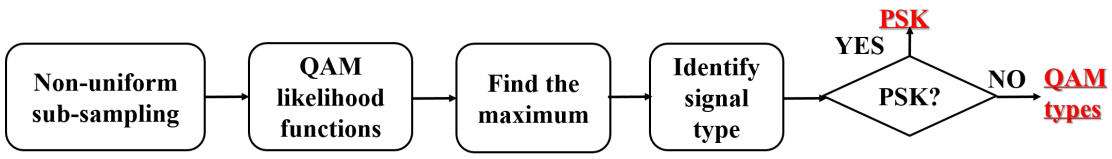

Figure 3.7: Block diagram of amplitude likelihood-based QAM identification algorithm.

where N_ρ is the number of bauds to approximate the ensemble power.

The ensemble power in (3.22) is periodic with period T_b, that is

$$\rho(n + T_b) = \rho(n) \tag{3.24}$$

For typical pulse shapes (for example, root raised cosine filter), $\rho(n)$ will have the maximum value when t corresponds to the right timing phase. Since the number of samples per symbol T for a received signal with unknown baud rate is not always an integer, we employ a nonuniform sampling technique to approximately pick the timing phase of each baud.

The nonuniform subsampling is performed in the following way: we start with an arbitrary sample (the first sample in all our simulations); the next sample is selected as the sample with the peak value of the estimated ensemble average power of the signal when we search over a small interval around the middle point of the next baud based on the last selected sample. In all our simulations described in Section 3.3, we chose the small interval to be the smallest integer larger than or equal to one-fourth of the estimated number of samples per baud. We note that the subsampling process described above is nonuniform since the peak values may not be equally spaced from each other.

Figure 3.8 and 3.9 demonstrate the effects of the matched filtering and the nonuniform subsampling process with different number of samples per symbol. Shown in the figure is one example of the amplitude distribution of the received signals before and after the matched filtering and nonuniform subsampling process for a 16-QAM signal. The top-left panel shows the constellation map of the received signal. The histogram of the signal amplitude is shown in the top-right panel. The corresponding results after matched filtering and subsampling are shown in the bottom panels. The three distinct amplitude values of the 16-QAM signals can be observed clearly after the matched filtering and the nonuniform subsampling process, but not in the received signal prior to this step. Consequently, we can apply the likelihood functions derived for modulation identification of signals without pulse shaping to identify pulse shaped signals after the subsampling.

3.1.6.2 Amplitude Likelihood Function

For a continuous sinusoid with amplitude S that is perturbed by a white Gaussian noise with variance σ^2 and zero mean value, the probability distribution function (PDF) of

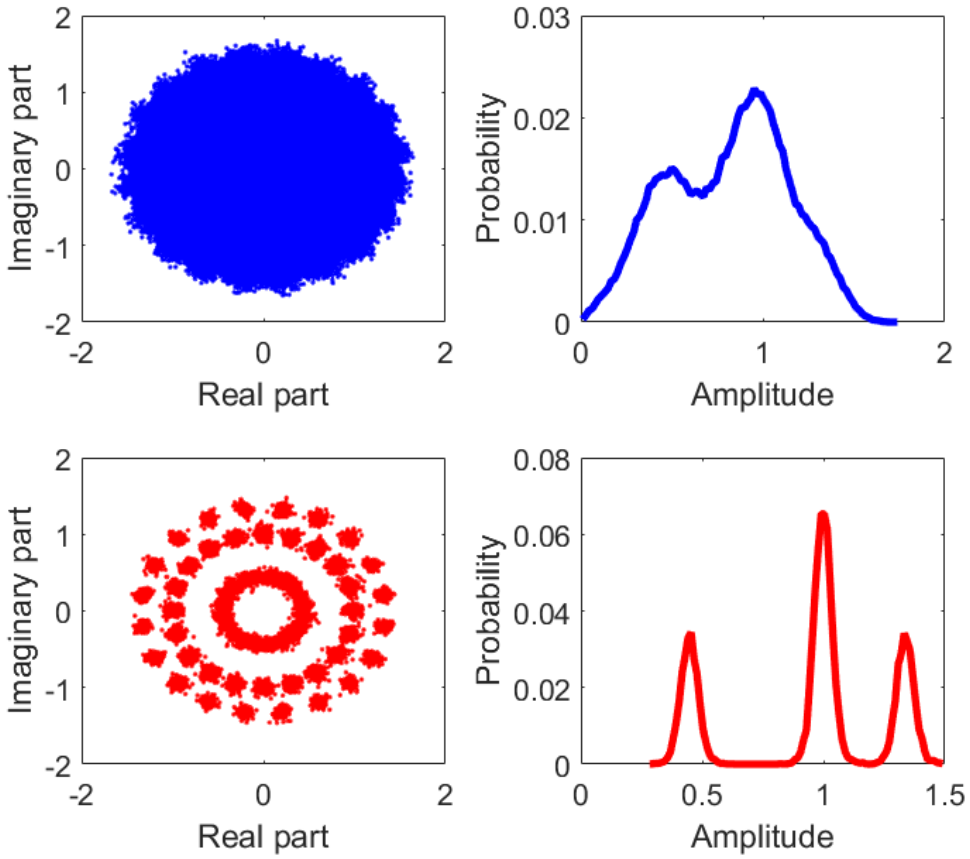

Figure 3.8: Constellation maps and amplitude distribution of the received 16-QAM signals before and after subsampling: SNR = 20 dB, number of symbols: 10000, number of samples per symbol: 13.25. Top left: constellation of the received signal with pulse shaping; right: histogram of amplitude value of the received signal with pulse shaping; bottom left: constellation of the signal after matched filter and subsampling; bottom right: histogram of amplitude of the signal after matched filter and subsampling.

its amplitude R is the Rice distribution given by

$$P(R) = \frac{R}{\sigma^2} e^{-(R^2+S^2)/2\sigma^2} I_0(\frac{RS}{\sigma^2}), R \geq 0 \tag{3.25}$$

where $I_0(\cdot)$ is the zero-order Bessel function of the first kind [1].

For the signal model in Section 3.1.1 with no pulse shaping, the amplitude at any time may be thought of as a noisy sinusoid whose amplitude can take one of a finite number of values depending on the modulation order. Furthermore, assuming that the symbols sequence is independent, identically-distributed, the probability of these amplitude values can be predetermined for each QAM type. Therefore, the distribution of the signal

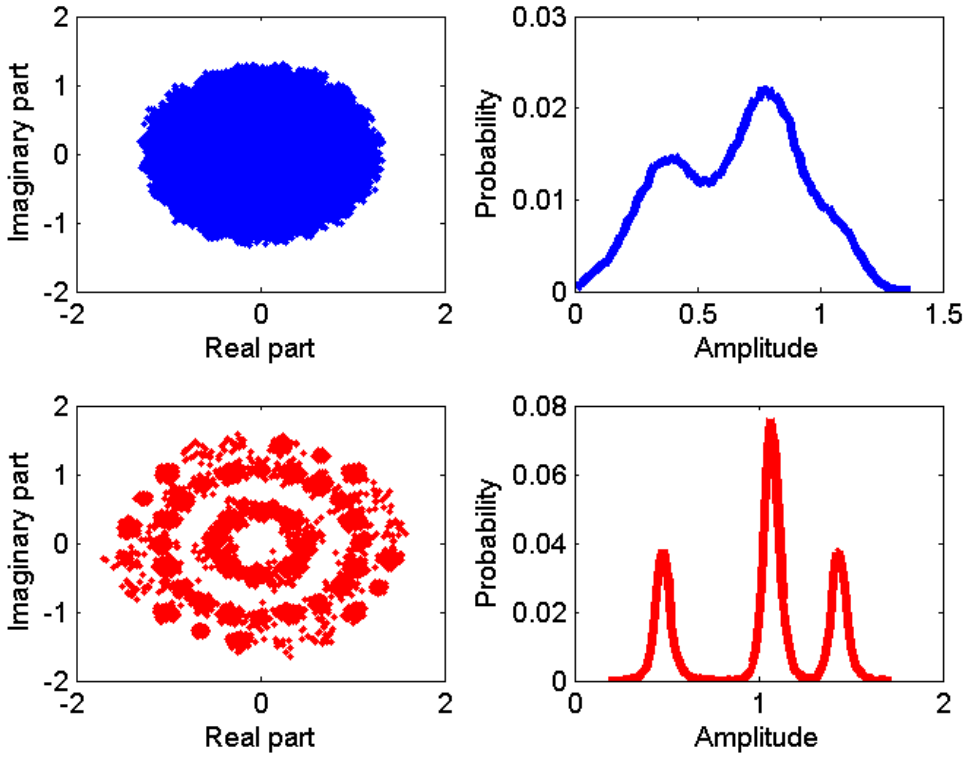

Figure 3.9: Constellation maps and amplitude distribution of received 16-QAM signals before and after subsampling: SNR = 20 dB, number of symbols: 10000, number of samples per symbol: 20. Top left: constellation of the received signal with pulse shaping; right: histogram of amplitude value of the received signal with pulse shaping; bottom left: constellation of the signal after matched filter and subsampling; bottom right: histogram of amplitude of the signal after matched filter and subsampling.

amplitude will be a weighted sum of the Rice distributions corresponding to the different amplitude values.

The amplitude of received signal after subsampling considering the noise is

$$|y(l)|^2 = |s_l g(0)|^2 + n_0(l) \tag{3.26}$$

where $n_0(l) = 2\Re\{s_l g(0) e^{j2\pi f_c l T_b} \eta^*(l)\} + |\eta(l)|^2$ is the component of the received signal amplitude contributed by noise.

From the above, we can see that the amplitude of received signals with pulse shaping after subsampling as above will have the same distribution (within a scaling factor) as the amplitude of signals without pulse shaping.

Let there be N_a distinct amplitude values for the Mth modulation type and let H_M

represent the hypothesis that the Mth modulation type is the actual modulation type of the received signal. Let the set $\{S_{M,i}; i = 1, 2, \cdots, N_a\}$ represent these values and let $w_M[i]$ be the probability of the ith amplitude value for the Mth modulation type. The PDF for the signal amplitude R is [1]

$$\begin{aligned} P(R|H_M) &= \sum_{i=1}^{N_a} \big(P(R|S_{M,i})w_M[i]\big), R \geq 0, \\ &= \sum_{i=1}^{N_a} w_M[i] \frac{R}{\sigma^2} e^{-(R^2+S_{M,i}^2)/2\sigma^2} I_0(\frac{RS_{M,i}}{\sigma^2}) \end{aligned} \tag{3.27}$$

In the above equation, $P(R|S_{M,i})$ is the conditional PDF of the signal amplitude with Mth modulation type and $I_0(\cdot)$ is the zero-order modified Bessel function of the first kind.

Figure 3.10 shows two examples of the comparison between the theoretical PDF derived as (3.27) and the histograms of the amplitude of signals after matched filtering and nonuniform subsampling. We can see the two matched very well, which indicates that the theoretical PDF expression of the amplitude can be used reliably in the system.

Given N amplitude values $R_1, R_2, \ldots, R_N$ of the received signals under the assumption that the samples are independent of each other, the conditional probability that H_M is true is given under the assumption that the samples are independent of each other by

$$p(R_1, R_2, \ldots, R_N|H_M) = \prod_{i=1}^{N} P(R_i|H_M) \tag{3.28}$$

Combining (3.28) with (3.27), the log-likelihood function for the hypothesis H_M can be expressed as

$$l_M = \sum_{i=1}^{N} L_{p_M}(R_i) = \sum_{i=1}^{N} \ln\big(\sum_{i=1}^{N_a} w_M[i] \frac{R_i}{\sigma^2} e^{\frac{-(R_i^2+S_{M,i}^2)}{2\sigma^2}} I_0(\frac{R_i S_{M,i}}{\sigma^2})\big) \tag{3.29}$$

The amplitude likelihood-based identification algorithm identifies the signal modulation type as the hypothesis modulation type that maximizes the log-likelihood function in (3.29). The class of PSK signals is included in this formulation since all PSK symbols have one amplitude value.

3.1.6.3 Non QAM Likelihood Function

In order to identify the situation when the signal does not belong to any of the modulation types of interest, we added two more modulation types in our algorithm. One case assumes that the signal has 50 uniformly distributed amplitude groups. The other case assumes that the signal is the white Gaussian noise.

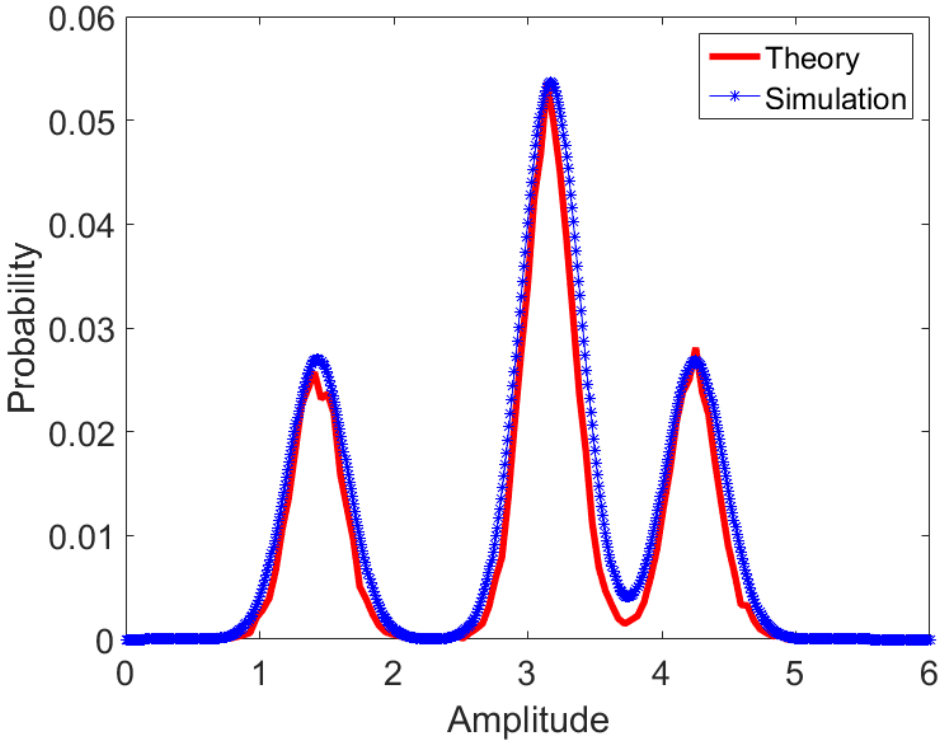

(a) SNR = 20 dB

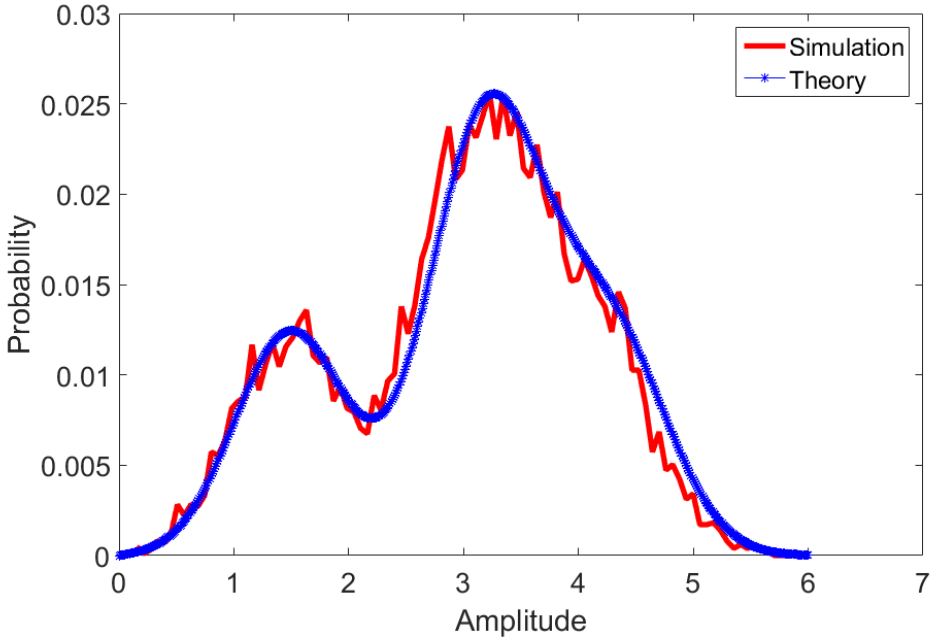

(b) SNR = 10 dB

Figure 3.10: Comparison between the theoretical PDF for amplitude and the histogram of the amplitude of signals after nonuniform subsampling: 16-QAM signals; number of samples per symbol: 20, number of symbols: 20000.

3.1.7 Implementation of the Likelihood-based Modulation Identification Algorithm

In summary, the details of implementing the likelihood-based algorithm for identifying different PSK and QAM types of a received signal are presented in Tables 3.1 and 3.2. The algorithm estimates the baud rate, noise variance and roll-off factor applying the four-step method of the estimated signal spectrum first. Next the matched filtering, estimated as the square root of the signal spectrum subtracting from noise, is applied to the received signal. The phase likelihood-based algorithm is implemented after that. If this algorithm does not identify the modulation type as BPSK, the amplitude likelihood-based algorithm is implemented. In this stage, the samples are chosen nonuniformly as described in Section 3.1.6.1. Then the amplitude likelihood functions are calculated to identify the QAM type. As we discussed before, PSK is treated as a special QAM here. If this algorithm identifies the modulation type as PSK, the QPSK or 8PSK of the received signal can be identified based on the first stage when applying the phase likelihood-based algorithm.

Table 3.1: Definition of variables in the likelihood-based modulation identification algorithm

$y(n)$: received signal
$\hat{S}_{yy}(f)$: estimated spectrum of received signal
f_{left} and f_{right}: the left and right edge of the bandwidth of the estimated spectrum
$\hat{\sigma}^2$: estimated noise variance
$\hat{\beta}$: estimated roll-off factor of the pulse shaping filter
$\hat{T}$: estimated number of samples per baud
$\hat{P}_s$: estimated power of symbol sequence
$\hat{G}_T(f)$: estimated frequency response of the pulse shaping filter
$\hat{g}_t(n)$: estimated pulse shaping filter
$\rho(n)$: ensemble average signal power
N_ρ: number of samples used for calculating $\rho(n)$
$start_j$: the j th starting point for subsampling process
Z_j: selected samples using the j th starting point for phase likelihood functions
y_2: selected samples for phase likelihood functions
θ_y: phase between the adjacent selected samples
$\hat{\theta}_c$: estimated phase contributed by carrier frequency
l_P: log phase likelihood functions algorithm
idx_t: the index for the correct samples in each baud
y_4: selected samples for amplitude likelihood functions
l_A: log amplitude likelihood functions

Table 3.2: The likelihood-based modulation identification algorithm

1. Inputs: $y(n)$;

2. Estimate the spectrum $\hat{S}_{yy}(f)$ of received signal using Welch's method; Estimate the edge of the spectrum using the four-step method: f_{left} and f_{right};

$BW = f_{right} - f_{left}$
Estimate the noise variance:

$\hat{\sigma}^2 = \int_{f=0}^{f_{left}} \hat{S}_{yy}(f)df + \int_{f=f_{right}}^{f_{N_f}} \hat{S}_{yy}(f)df$

Estimate symbol power P_s:

$\hat{P}_s = \int_f \hat{S}_{yy}(f)df - \hat{\sigma}^2$

Estimate the squared frequency response of the root-raised-cosine filter:

$\hat{G}_T(f) = \frac{\hat{S}_{yy}(f) - \hat{\sigma}^2}{\hat{P}_s}$

Estimate $\hat{\beta}$ and $\hat{T}$ using LS fit algorithm:

$\{\hat{T}, \hat{\beta}\} = \arg\min_{T,\beta}\{||\hat{G}_T(f) - G_T(f)||^2\}$
where $\frac{1+\beta}{T} = BW$.

3. Matched filtering:

$\hat{G}_T(f) = \sqrt{\hat{S}_{yy}(f) - \hat{\sigma}^2}$,
when $||\hat{G}_T(f)||^2 < 0, \hat{G}_T(f) = 0$;
$y_1(n) = \hat{g}_T(n) * y(n))$;

'*' denotes convolution operation.

4. Phase likelihood-based algorithm:

$\hat{\rho}(n) = \frac{1}{2N_\rho+1} \sum_{k=-N_\rho}^{N_\rho} |y_1(n+kT)|^2$;
$st_0 = \arg\max_{k_1}(\rho(k_1)); k_1 = 1, 2, ..., 4T$;
$st_j = st_0 - \lfloor \frac{T}{4} \rfloor + j$;
$j = 1, 2, ..., \lfloor \frac{T}{2} \rfloor$;
where $\lfloor a \rfloor$ rounds a to the nearest integers towards minus infinity;

$Z_j(k_2) = y_1(st_j + k_2 T); k_2 = 1, 2, ...$;
$y_2 = [Z_1; Z_2; ....Z_{\lfloor T/2 \rfloor}]$;
$\hat{y}_2(n) = y_2(n-1)$;
$y_3 = y_2\hat{y}_2^H$; 'H' denotes conjugate operator.
$\theta_y = \angle(y_3)$;
$\theta_c = \arg\max_{\theta}(hist(\theta_y))$;
$type_p = [0, 1, 2, 3]$; '0' represents the modulation type with one phase group,
'1' is BPSK, '2' is QPSK, '3' is 8PSK .

$$l_P(k_3) = \sum_{j=1}^{N_p} \ln(P(\theta_y(j)|type_p(k_3))); \quad (3.21)$$

$k_p = \arg\max_{k_3}(l_P)$;
if {type1 $\neq$ BPSK}
  5. Amplitude likelihood-based algorithm:
  $ix_1 = st_0$;
  $ix_t = \arg\max_{k_4}(\rho(ix_{j-1} + T - \lfloor \frac{T}{4} \rfloor + k_4))$;
  $k_4 = 0, 1, ..., \lfloor \frac{T}{2} \rfloor$;
  $ix_j = ix_{j-1} + T - \lfloor T/4 \rfloor + ix_{temp}$;
  $y_4(j) = y_1(ix_{j+1})$;
  $R_y = |y_4|$;
  $type_a = [0, 16, 32, 64, 128, 256, 500]$;
  '0' here represents the PSK type,
  '16' is 16-QAM, '32' is 32-QAM, etc.

$$l_A(k_5) = \sum_{j=1}^{N_a} \ln(P(R_y(j)|type_a(k_5))); \quad (3.29)$$

  $k_a = \arg\max_{k_5}(l_A)$;
  $type = type_a(k_a)$;
  if {type = PSK}
    type=type1.
  endif
else
  type=type1.
endif

3.2 Performance Analysis

A theoretical analysis of the performance of QAM likelihood-based modulation identification algorithm was developed in [26]. No such results exists for the PSK likelihood-based modulation identification algorithm. The analysis in [26] derived the theoretical results for the case when the algorithm attempted to distinguish between only two different modulation types. This section presents a theoretical analysis for the performance of the likelihood-based modulation identification algorithm. This analysis applies to the case of modulation identification from an arbitrary number of choices and can be easily generalized for the complete system for identifying PSK and QAM signals.

The objective is to derive the probability of successful identification for each modulation type as a function of the signal parameters such as SNR. Successful identification for modulation M is the case when the likelihood function under the hypothesis of modulation M is larger than that under all the other hypotheses. Let $p(success|H_M)$ represent the probability of successful identification for modulation M, which can be expressed as

$$p(success|H_M) = p(\bigcap_{m \neq M} l_M > l_m | H_M) \tag{3.30}$$

The probability of successful identification of the algorithm is then written as

$$p(success) = \sum_M p(success|H_M)p(H_M) \tag{3.31}$$

where the summation is over all hypotheses under consideration.

3.2.1 Theoretical Calculation of the Probability of Successful Identification

In order to calculate $p(success|H_M)$, we need to find the PDF of the likelihood function l_M. Because of the complexity of (3.21) and (3.29), the statistics of l_M is difficult to derive. Instead, we utilize the assumption that the signal samples are i.i.d. and use the central limit theorem to model l_M as a Gaussian distributed variable when the number of samples used to calculate l_M is large. This Gaussian distribution can be specified by calculating the mean and variance of l_M.

Let $\Delta_{l_{Mm}} = l_M - l_m$ as the difference of two likelihood functions under different hypothesized modulation type m when the input signal modulation is M. Defining $\Delta_{L_{p_{Mm}}}(s_i) = \{L_{p_M}(s_i) - L_{p_m}(s_i)\}$, $\Delta_{l_{Mm}}$ can be written as

$$\Delta_{l_{Mm}} = \sum_i \Delta_{L_{p_{Mm}}}(s_i) = \sum_i \{L_{p_M}(s_i) - L_{p_m}(s_i)\} \tag{3.32}$$

where s_i is the ith signal sample. For amplitude likelihood functions, s is the amplitude of the signal. Similarly in phase likelihood functions, s is the phase difference of adjacent signal samples. Then,

$$p(\bigcap_{m \neq M} l_M > l_m | H_M) = p(\bigcap_{m \neq M} \Delta_{l_{Mm}} > 0 | H_M) \tag{3.33}$$

Let $\mu_{l_{Mm}}$ represent the mean of $\Delta_{l_{Mm}}$ and $\Omega_{l_{Mm}}$ represent the variance of $\Delta_{l_{Mm}}$. The mean value is given by

$$\begin{aligned} \mu_{l_{Mm}} &= \int_{s_1}\int_{s_2}...\int_{s_{N_s}} \Delta_{l_{Mm}} p(s_1, s_2, ..., s_{N_s}|H_M) ds_1 ds_2 ...ds_{N_s} \\ &= N_s \int_s \Delta_{L_{p_{Mm}}}(s) P(s|H_M) ds \end{aligned} \tag{3.34}$$

where N_s is the number of samples. Similarly,

$$\begin{aligned} \Omega_{l_{Mm}} &= \int_{s_1}\int_{s_2}...\int_{s_{N_s}} [(\Delta_{l_{Mm}} - \mu_{l_{Mm}})^2 p(s_1, s_2, ..., s_{N_s}|H_M)] ds_1 ds_2 ...ds_{N_s} \\ &= N_s \int_s [(\Delta_{L_{p_{Mm}}}(s))^2 P(s|H_M)] ds - \frac{\mu_{l_{Mm}}^2}{N_s} \end{aligned} \tag{3.35}$$

The details of the derivation of the mean and variance of $\Delta_{l_{Mm}}$ can be found in Appendix A.

The probability of successfully identifying the modulation type M can now be expressed as

$$\begin{aligned} & p(success|H_M) = p(\bigcap_{m \neq M} \Delta_{l_{Mm}} > 0 | H_M) \\ &= \int_{\Delta_{l_{Mm_1}}>0}\int_{\Delta_{l_{Mm_2}}>0}...\int_{\Delta_{l_{Mm_{N_m}}}>0} \frac{1}{(2\pi\Sigma)^{N_m/2}} \\ & e^{\frac{(\Delta_{l_M} - \mu_\Delta)^T \Sigma^{-1} (\Delta_{l_M} - \mu_\Delta)}{2}} d\Delta_{l_{Mm_1}} d\Delta_{l_{Mm_2}} ...d\Delta_{l_{Mm_{N_m}}} \end{aligned} \tag{3.36}$$

where N_m is the number of modulation types except M, $\Delta_{lM} = \{\Delta_{l_{Mm_1}}, \Delta_{l_{Mm_2}}, ..., \Delta_{l_{Mm_{N_m}}}\}$, μ_Δ is the mean value of the vector Δ_{l_M} and Σ is covariance matrix of Δ_{lM}. Each element in Σ is given by

$$\Omega_{l_{Mm_{ij}}} = N_s \int_s [\Delta_{L_{p_{Mm_i}}}(s) \Delta_{L_{p_{Mm_j}}}(s) P(s|H_M)] ds - \frac{\mu_{l_{Mm_i}} \mu_{l_{Mm_j}}}{N_s} \tag{3.37}$$

The integrals of the multivariate Gaussian variables in (3.36) can be approximated using the numerical method described in [12].

3.2.2 Performance Variation for Likelihood-based Identification Algorithm

In practice, the matched filtering and subsampling change the signal characteristics from those of the signal model used in the theoretical analysis. In the following subsections, we consider the effect of such changes.

3.2.2.1 SNR Difference after Matched Filtering and Subsampling

The SNR of the received signal in (3.2) is given by

$$SNR_{bf} = \frac{P_s}{T_b} \frac{\int_{-\infty}^{\infty} |G_T(f)|^2 df}{\sigma^2} \tag{3.38}$$

where P_s is the power of the symbols, T_b is number of samples per symbol and $G_T(f)$ is the frequency response of the pulse shaping filter. For the signal model described in (3.2), the signal after matched filtering becomes

$$y(t) = \sum_k (s_k g_T(t - kT_b)) e^{j2\pi f_c t} * g_T(t) + N_0(t) * g_T(t) \tag{3.39}$$

where '*' denotes the convolution operation.

In the absence of noise, if we select one sample per baud with matched filtering, the subsampling samples become

$$y_n(t) = s[n]\delta(t - nT_b) * g_T(t) * g_T(t) \tag{3.40}$$

Under the assumption that the matched filtering satisfies the Nyquist Criterion, the subsampling samples at $t = nT_b$ are

$$y_n(nT_b) = s[n] \int_{-\infty}^{\infty} G_T^2(f) df \tag{3.41}$$

The signal power is

$$E\{|y_n(nT_b)|^2\} = P_s | \int_{-\infty}^{\infty} G_T^2(f) df|^2 \tag{3.42}$$

The subsampling process will not change the statistics of the noise. The noise power is

$$E\{|N_0(t) * g_T(t)|^2\} = \sigma^2 \int_{-\infty}^{\infty} G_T^2(f) df = \sigma^2 \tag{3.43}$$

The SNR after matched filtering and subsampling becomes

$$SNR_{af} = \frac{E\{|y_n(nT_b)|^2\}}{E\{|N_0(t) * g(t)|^2\}} = \frac{P_s \int_{-\infty}^{\infty} G_T^2(f) df}{\sigma^2} \tag{3.44}$$

Combining (3.38) and (3.44), the SNR after matched filtering and subsampling is T_b

times the SNR of the received signal.

The SNRs used in the likelihood functions should be the estimated SNR of the received signal plus the SNR difference.

3.2.2.2 Effect of SNR Estimation Error

The nonuniform subsampling process in the amplitude likelihood-based algorithm adds additional noise to the signal. This reduces the SNR from the theoretically-derived results in Section 3.2.2.1. In this subsection, we consider the effect of this SNR variation on the probability of successful identification of QAM signals.

The SNR described in Section 3.2.2.1 assumes that the signal model after matched filtering and subsampling is

$$y(l) = s_l g(0) e^{j2\pi f_c l T_b} + \eta(l) \tag{3.45}$$

where $g(t) = g_T(t) * g_T(t)$ is a raised-cosine filter and $\eta(l)$ is the noise after matched filtering and subsampling. As shown in (3.43), the noise variance of $\eta(l)$ is σ^2.

In our system, the matched filter is estimated from the spectrum of the signal with noise. The estimated matched filter $\hat{g}_T(t)$ can be expressed as

$$\hat{g}_T(t) = g_T(t) + N_e(t) \tag{3.46}$$

where $N_e(t)$ is the estimation error.

Let $\hat{g}(t) = g_T(t) * \hat{g}_T(t)$ and $N_g(t) = N_e(t) * g_T(t)$, the l^{th} sample obtained via nonuniform sampling in our system is

$$\hat{y}(l) = s_l \hat{g}(\Delta l) e^{j2\pi f_c l T_b} e^{j2\pi f_c \Delta l T_b} + \hat{\eta}(l) \tag{3.47}$$

where Δl is selected based on the nonuniform sampling criterion.

Comparing the two models in (3.45) and (3.48) excluding the noise, the difference between the amplitude of these two models is

$$\Delta y(l) = s_l(\hat{g}(\Delta l) - g(0)) \tag{3.48}$$

$\Delta y(l)$ is the additional disturbance term added to the signal after nonuniform subsampling over the model in the theoretical performance analysis. This is treated as an additional noise in the model. Unfortunately, direct theoretical analysis for the statistics of this noise is not available at this time. Instead, we estimate the variance of this component from simulations to characterize the variation caused by this error. Let σ_a^2 represent the

additional variance, the SNR due to the effect of nonuniform subsampling and matched filtering can be written as

$$SNR_a = \frac{1}{1/SNR_{af} + \sigma_a^2/P_s} \tag{3.49}$$

Figure 3.11 shows the comparison of the true SNR shown in (3.44) and SNR calculated based on (3.49) under the corresponding SNRs of the input signal. σ_a^2 is estimated from the simulations. We can observe that the difference between the true SNR and the SNR due to the effect of nonuniform subsampling increases when SNR increases. We can see that the SNR due to the effect of nonuniform subsampling and matched filtering will be smaller than SNR_{af} because of the additional variance.

3.3 Performance Evaluation

In this section, the performance of the likelihood-based blind modulation identification algorithms is first demonstrated via a comparison between theoretical and simulated results of successful modulation identification. We also present a comparison of the performance with two other competing methods in the literature. In addition, this

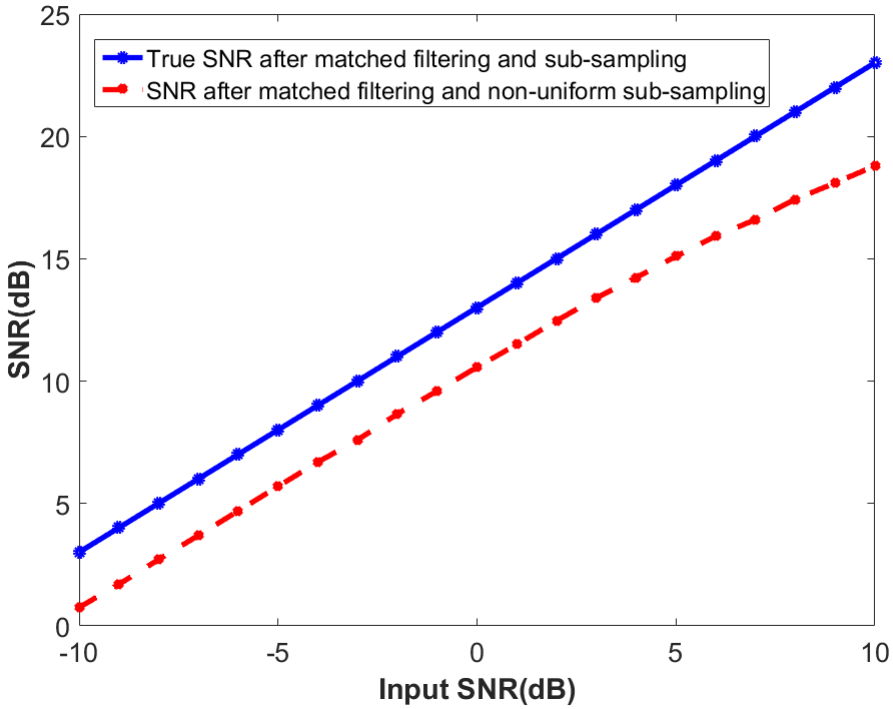

Figure 3.11: Effect of nonuniform subsampling process on the estimation of the SNRs.

section includes simulation results of the likelihood-based blind modulation identification algorithms in noisy environments different from the assumed Gaussian model.

In the simulations of this section, a root-raised cosine filter with parameter $\alpha = 0.5$ was applied to the transmitted symbol sequence and 500 independent data sets were used to calculate the probability of successful identification for each modulation type.

3.3.1 Probability of Successful Identification for Different SNRs

Figure 3.12 (a) and (b) present the comparisons between theory and simulation of the probability of successful identification of the algorithm for the PSK and QAM signals. The number of symbols for the signals was 10,000. The number of samples per symbol were 20 and 8.75. The theoretical results in Figure 3.12 (b) include the effect of the error between the estimated SNRs and true SNRs as described in Section 3.2.2.2.

We can observe from these two figures that the simulation results are close to the theoretical results for the two baud lengths. The probability of successful identification of the received signals varies with the baud length because the SNRs after subsampling and matched filtering are dependent on the number of samples per symbol as shown in (3.44) and (3.49). The loss of the performance between the theory and simulation is mainly due to the estimation errors of the parameters in the simulations.

3.3.2 Comparison with Competing Methods

In this section, we compare the performance of the likelihood-based algorithm in this paper with that of two other modulation identification methods available in the literature, i.e., a method based on the clustering algorithm in [52] [56] and a method based on cumulant-based algorithm in [41] [59]. These methods have reported the best performance among other available methods in the literature.

As mentioned earlier, these two methods assumes the number of samples per symbol is an integer. As a result, the simulations in this section used a baud rate that corresponds to 20 samples per symbol. Figure 3.13 (a) shows the probability that the three methods identify the modulation type as a specific type when the input signal is that modulation type. We can conclude from these results that the method in this paper is superior to the two other methods. Our method identified all the modulation types with 99% accuracy at SNR $\geq$ 4 dB with 10,000 symbols while the two competing methods did not.

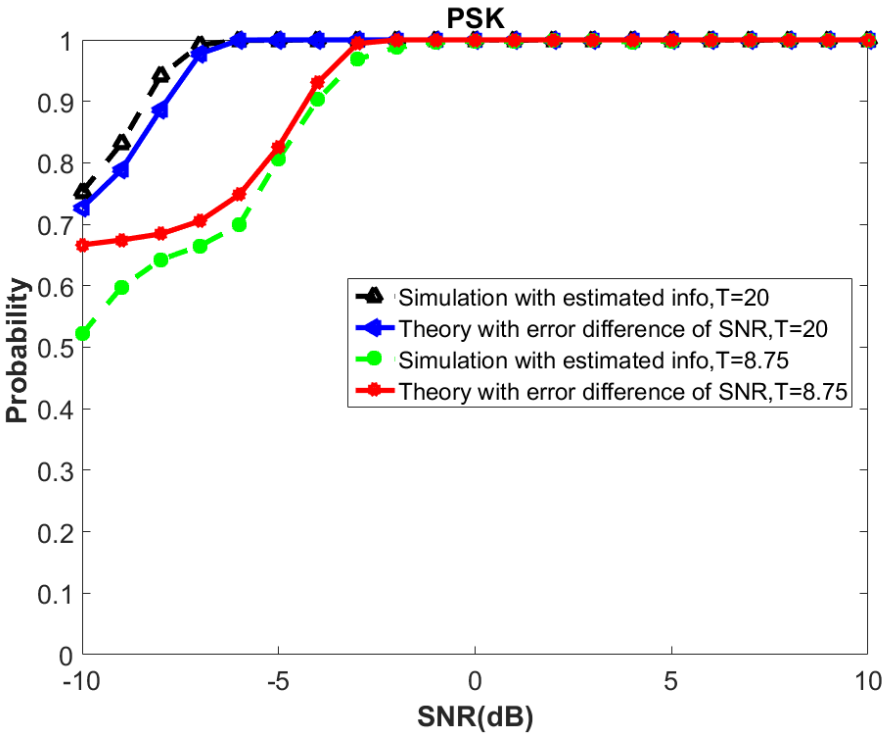

(a) PSK signals

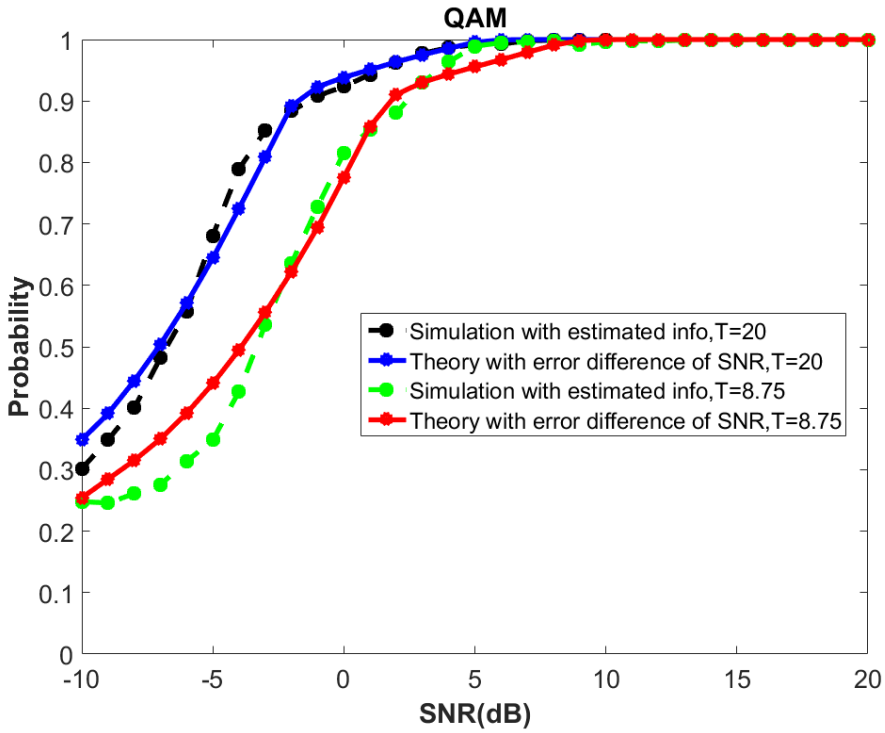

(b) QAM signals

Figure 3.12: Comparison of theoretical identification and simulation results for PSK and QAM signals with different SNRs and different number of samples per baud; number of symbols:10000.

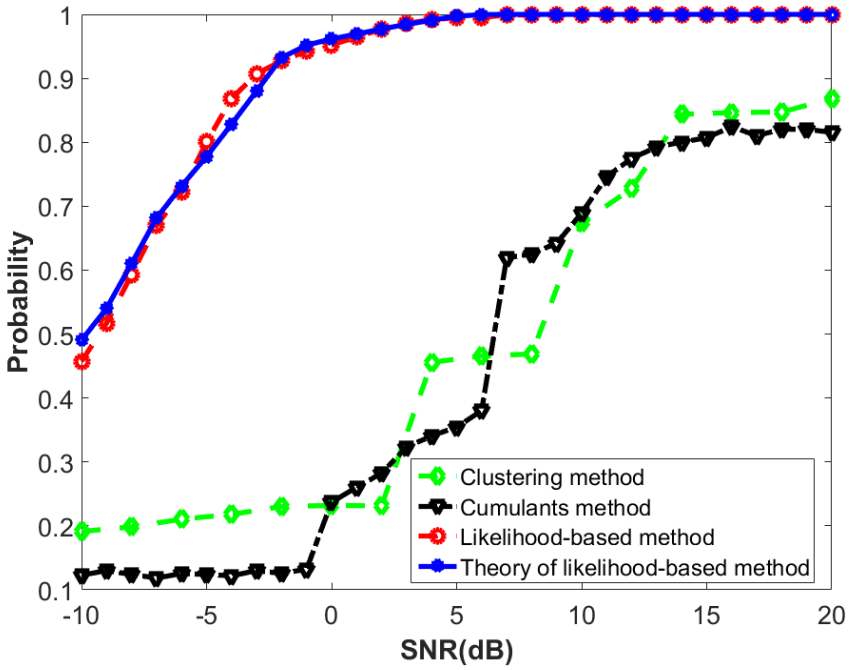

(a)

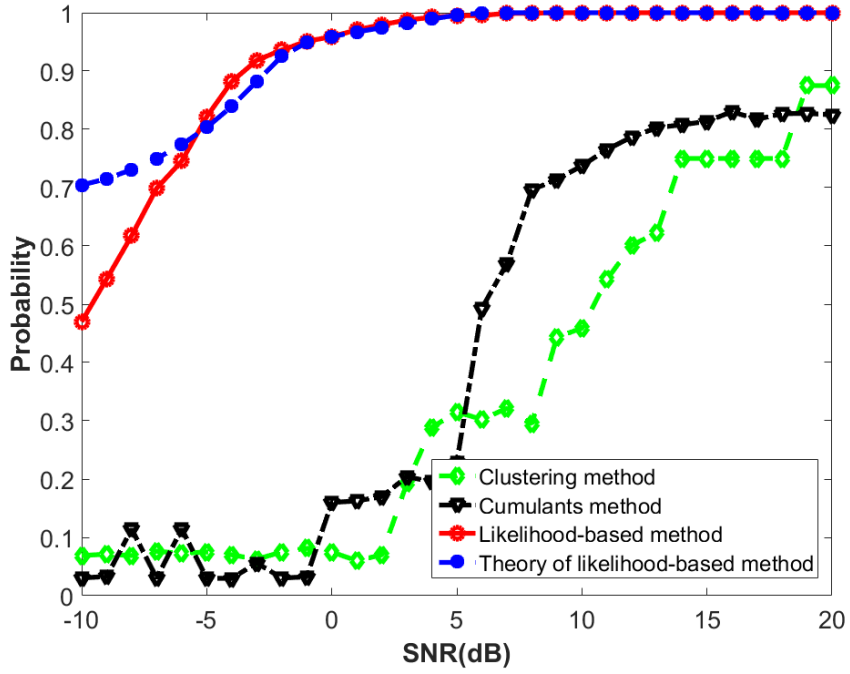

(b)

Figure 3.13: Comparison between the method in this paper, the clustering method and cumulant-based method for identifying PSK and QAM signals; Number of symbols: 10000; Number of samples per symbol: 20; (a). the probability that the system identifies the modulation type as one modulation type when the input signal is that modulation type; (b). the conditional probability that the input signal is one modulation type when the system identifies the input signal as that modulation type.

Another comparison between the three methods is shown in Figure 3.13 (b). This figure shows the conditional probability that the input signal is a specific modulation type when the system identifies the input signal as that modulation type.

Let J_M represent that the input signal is the Mth modulation type and $\hat{J}_M$ denote that the system identifies the input signal as the Mth modulation types. Then, the conditional probability can be expressed as

$$\begin{aligned} p(J_M|\hat{J}_M) &= \frac{p(J_M \bigcap \hat{J}_M)}{p(\hat{J}_M)} \\ &= \frac{p(J_M \bigcap \hat{J}_M)}{\sum_{k=1}^{M_n} p(\hat{J}_M|J_k)p(J_k)} \end{aligned} \tag{3.50}$$

where $p(J_M \bigcap \hat{J}_M) = p(\hat{J}_M|J_M)p(J_M)$, $p(\hat{J}_M|J_M)$ is the probability that the system identifies the modulation type as a specific modulation type when the input signal is that modulation type as shown in Figure 3.13 (a), M_n is the total number of modulation types, $p(\hat{J}_M|J_k)$ is the probability that the system identifies the modulation type as the Mth modulation type when the input signal is the kth modulation type and $p(J_k)$ is the probability that the input signal is kth modulation type.

Assuming equal probability of generating input signals with different modulation types, we obtain $p(J_k) = 1/M_n$. In the theoretical calculation, $p(\hat{J}_M|J_M)$ is the same as $p(success|H_M)$ as derived in Section 3.2.1. The probability $p(\hat{J}_M|J_k)$ is derived by changing the modulation type of the input signal into the kth modulation type.

From the two comparisons in Figure 3.13, we can conclude that, at SNR above 9 dB and with more than 10,000 symbols, the likelihood-based modulation identification method identifies a specific modulation type; the input signal must be that corresponding modulation type. Clearly, the competing methods were not able to perform at this level.

In addition, Figure 3.14 compares the simulation results of probability of successful identification for each PSK and QAM signal. We can observe that, when the order of the modulation types increases, the system needs higher SNRs in order to get above 99% accuracy for the modulation identification.

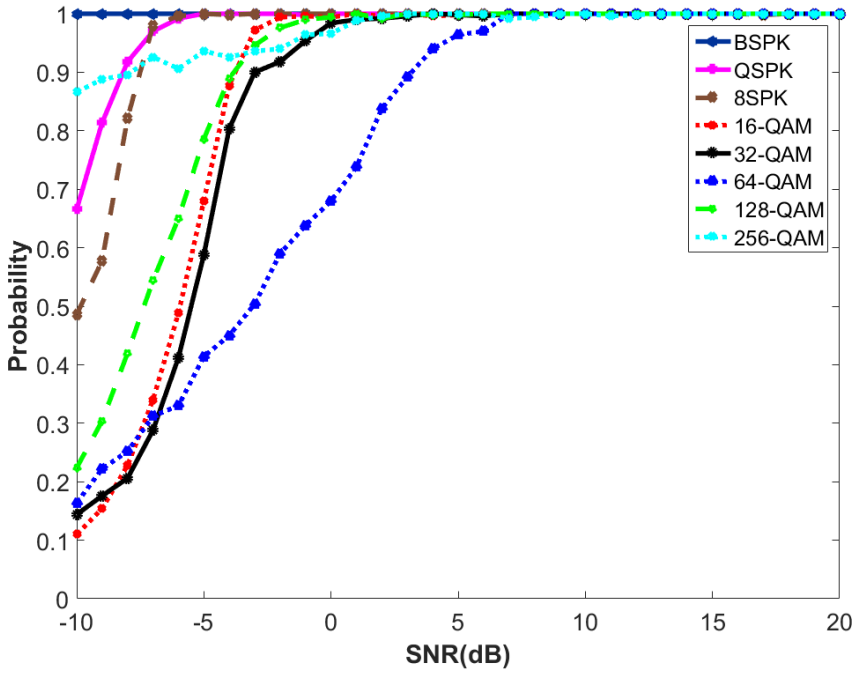

Figure 3.14: Probability of successful identification for different PSK and QAM signals; Number of symbols: 10000; Number of samples per symbol: 20.

3.3.3 Probability of Successful Identification for the Signals with Different Number of Symbols

Figure 3.15 presents the probability of successful identification for the signals with different number of symbols. In all the following examples, the number of samples per symbol was 20. We can see that the number of symbols needed for reaching 100% accuracy of identification decreases when SNR increases. The system is able to identify all the modulation types with 99% accuracy at $SNR = 5$ dB with 8000 symbols. For the signals at $SNR = 10$ dB, the system needs 4000 symbols in order to get 99% accurate identification.

Figure 3.16 compares the theoretical probability of successful identification and simulation results for varying number of input symbols. We observe that the results between theory and simulation show some mismatch for lower number of symbols. This is because that the estimation errors of the parameters such as matched filter, baud rate and noise variance is large when the number of symbols is low. As a result, the difference between the signal model in the simulation and that assumed in the theoretical analysis is large.

In Figure 3.17, the results for the signal with 5000 symbols were presented. We can see that the system will be able to identify all the modulation types with 99% accuracy with

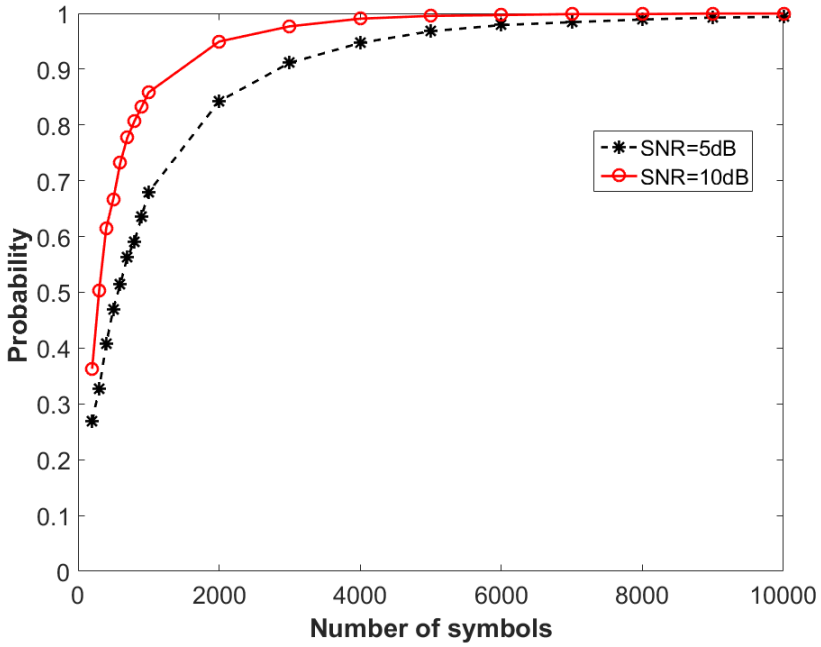

Figure 3.15: Probability of successful identification for PSK and QAM signals with different number of symbols; Number of samples per symbol: 20.

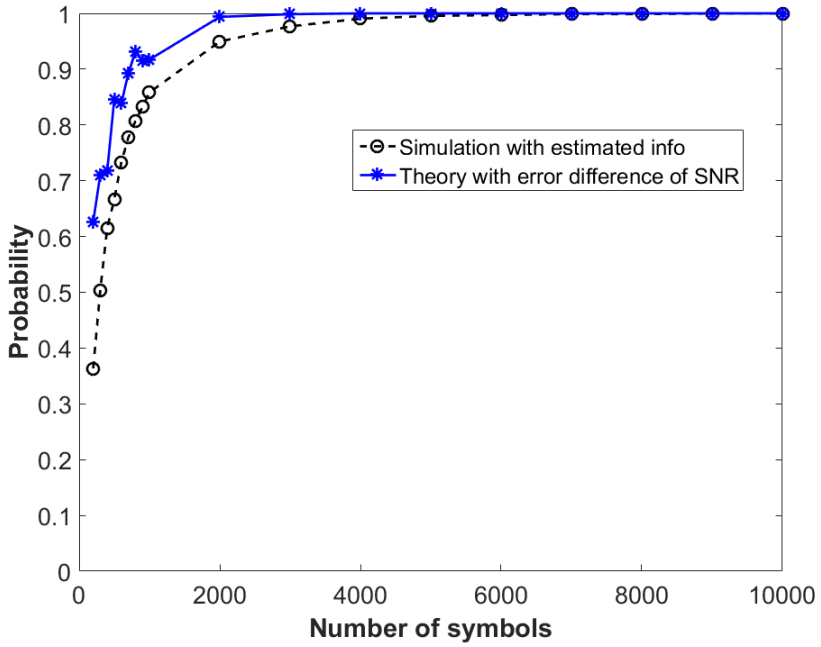

Figure 3.16: Comparison between theoretical identification and simulation results for PSK and QAM signals with different number of symbols; SNR = 10 dB; Number of samples per symbol: 20..

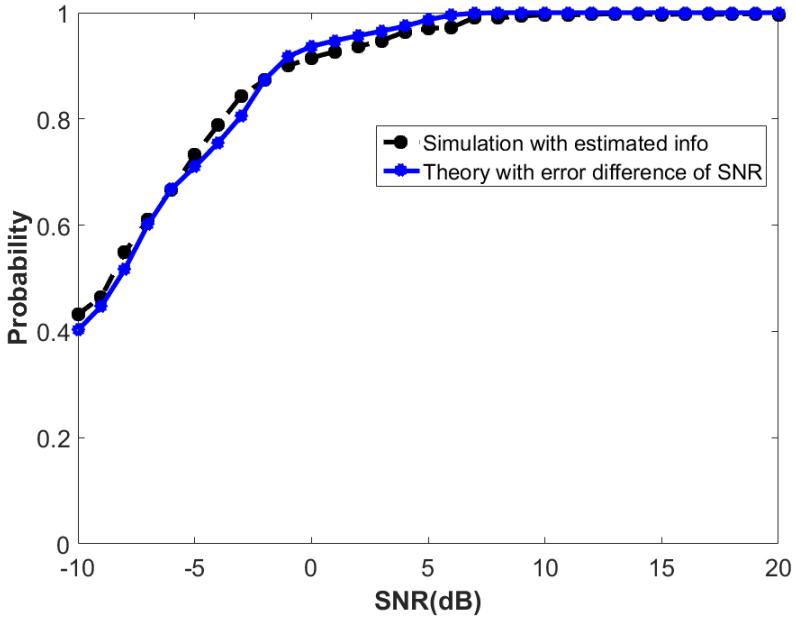

Figure 3.17: Probability of successful identification for PSK and QAM signals; Number of symbols: 5000; Number of samples per symbol: 20.

SNR above 7 dB. The results indicate that the likelihood-based modulation algorithm in this paper is able to identify the PSK and QAM types with high accuracy with shorter signal length at relatively low SNRs.

3.3.4 Identification Results for Different Types of Noise

Figures 3.18 shows the identification results in noise environments different from the assumed Gaussian model. The types of noise were a zero-mean and uniformly distributed noise and a Laplacian noise with zero-mean value. We observe that the performances with uniform noise and Laplacian noise are comparable to the case with Gaussian noise, indicating that the system is robust to variation from the assumed noise model.

3.4 Combination of CMA Equalizer and Modified Likelihood-based Modulation Identification for the Signals in Multipath Channels

In this section, a method identifying the modulation types of the signals in multi-path channels by combining the constant modulus amplitude (CMA) equalizer and the likelihood-based modulation identification method will be described.

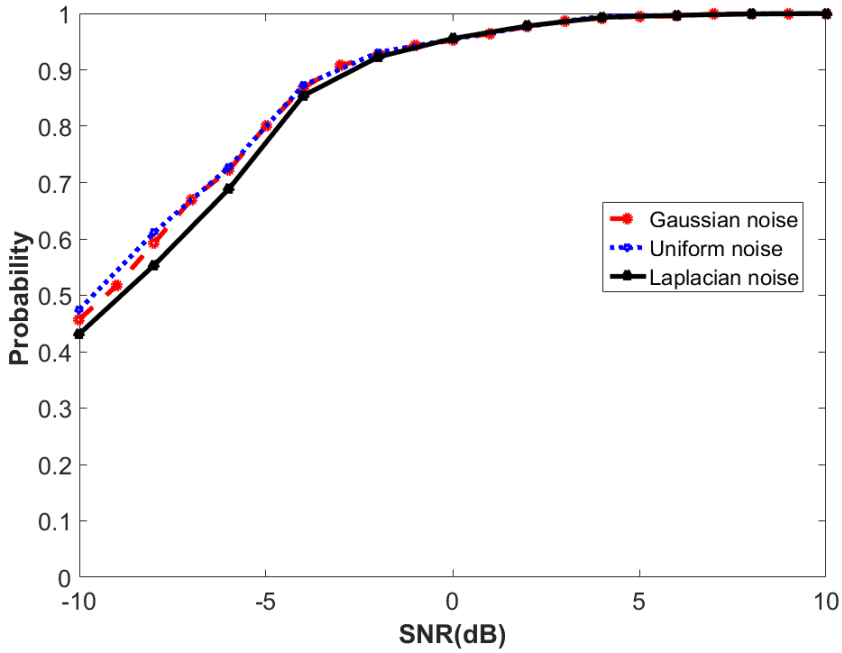

Figure 3.18: Probability of successful modulation identification with different SNRs for signals corrupted by different types of noise; Number of symbols: 10000; Number of samples per symbol: 20.

A block diagram of this method is shown in Figure 3.19. This method first estimates the channel coefficients to mitigate the effect from multipath. Then, the modified likelihood-based modulation identification method is applied to identify the modulation type of the received signal.

The system estimates the baud rate of the received signal first in order to subsample the signal. Then, a blind channel estimation algorithm is applied to the received signal and the equalized signal using the estimated channel coefficients is obtained. The blind equalizer method implemented here is the CMA equalizer. As shown later in this section, the blind equalizer estimates the channel coefficients that corresponds to the combination of the pulse shaping filter and the multipath channel. As a result, the matched filter is not applied before subsampling process. Instead, the system subsamples the signals after the blind equalization directly. Finally, the likelihood functions under different hypothesized modulation types is calculated. The subsampling method and the likelihood functions for the amplitude and phase are the same as shown in Section 3.1. The modulation type corresponding to the maximum likelihood function is the modulation type of the received

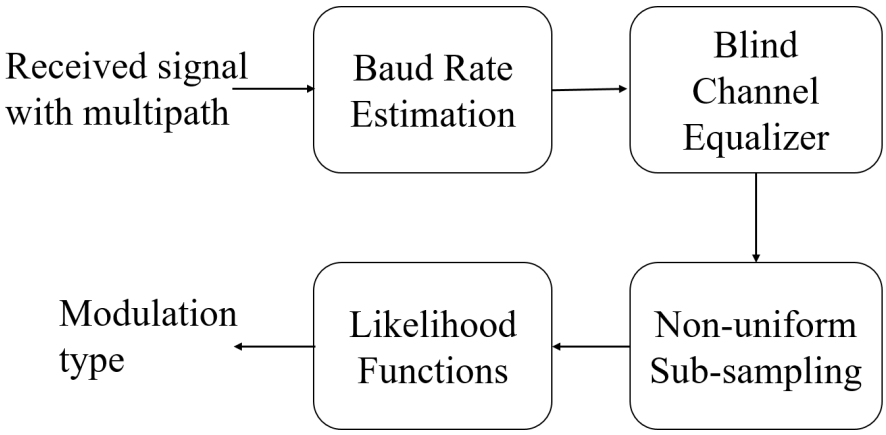

Figure 3.19: Block diagram of combination of blind channel estimation and likelihood-based modulation identification for signals in multipath channels.

signal.

3.4.1 Signal Model of Signals in Multipath Channels

The model of the signals in multipath channels with additive white Gaussian noise can be written as

$$y_c(t) = \int_{t_1} y(t-t_1)h(t_1)dt_1 + N_0(t) \tag{3.51}$$

where $y(t)$ is the signal described in (3.2) without noise, and $h(t)$ represents the impulse response of multipath channels.

The model of the multipath channel $h(t)$ is assumed to be

$$h(t) = \sum_{i=0}^{N_m} \delta(t-\tau_i)a(\tau_i) \tag{3.52}$$

where N_m is the number of path in the channel, τ_i is the delay of each path, $a(\tau_i)$ is the channel coefficient of each path and $\delta(\cdot)$ is the Dirac delta function.

Combining (3.51) with (3.52), the signals in multipath channels are

$$y_c(t) = \sum_i \sum_k (s_k g_T(t-\tau_i-kT_b))e^{j2\pi f_c(t-\tau_i)}a(\tau_i) + N_0(t) \tag{3.53}$$

Changing the order of the two summations in the above equations, the model is modified as

$$y_c(t) = \sum_k s_k \sum_i g_T(t-\tau_i-kT_b)a(\tau_i)e^{j2\pi f_c t}e^{-j2\pi f_c \tau_i} + N_0(t) \tag{3.54}$$

Let $c(t) = \sum_i g_T(t-\tau-i)a(\tau_i)e^{j2\pi f_c(t-\tau_i)}$. Then, the signal model can be expressed as

$$y_c(t) = \sum_k s_k c(t-kT_b) + N_0(t) \tag{3.55}$$

A discrete signal model with the sampling frequency T_s will be

$$y_c(n) = \sum_k s_k c(nT_s - kT_b) + N_0(t) \tag{3.56}$$

3.4.2 Cyclostationarity-based Baud Rate Estimation Algorithm

As described earlier in Chapter 2, the channel characteristics and some of the statistical properties of the signals in a multipath channel will change compared with the signals in an AWGN channel. However, based on the signal model described in Section 3.4.1, the second-order statistical properties of the signal do not change. Thus, the baud rate is estimated using the second-order statistical property of the signals, which is the cyclostationary feature.

Based on the signal model as (3.55), the ensemble power of $y_c(t)$ satisfies

$$\begin{aligned}\rho_{t,\tilde{t}} &= E\{y_c(t)y_c^*(t-\tilde{t})\} \\ &= \sum_k s_k c(t-kT_b) \sum_p s_p^* c^*(t-\tilde{t}-pT_b) + \sigma^2 \\ &= \sum_k \sum_p s_k s_p^* c(t-kT_b)c^*(t-\tilde{t}-pT_b) + \sigma^2\end{aligned} \tag{3.57}$$

where $\tilde{t}$ is the time lag.

Since the symbols are i.i.d, then

$$\rho_{t,\tilde{t}} = P_s \sum_k c(t-kT_b)c^*(t-\tilde{t}-kT_b) + \sigma^2 \tag{3.58}$$

Then, $\rho_{t,\tilde{t}}$ satisfies

$$\rho_{t,\tilde{t}} = \rho_{t+T_b,\tilde{t}} \tag{3.59}$$

Thus $\rho_{t,\tilde{t}}$ is a periodic sequence with the period T_b.

When $\tilde{t} = 0$, further derivation in [57] can be shown that $\rho_{t,\tilde{t}}$ can be expressed as

$$\rho_{t,0} = P_s(\rho_0 + \rho_1 e^{2\pi T_b t} + \rho_{-1} e^{-2\pi T_b t}) + \sigma^2 \tag{3.60}$$

Based on the above equation, we can see that the estimation of baud rate T_b is the same as the estimation of the frequency of a sinusoid. In this dissertation, the baud rate is estimated from the Fourier transform of the ensemble power $\rho_{t,0}$.

The Fourier transform of $\rho_{t,0}$ is

$$
\begin{aligned}
R(f) &= \int_{f=-\infty}^{\infty} \rho_{t,0} e^{-2\pi f t} dt \\
&= P_s \int_{f=-\infty}^{\infty} (\rho_0 + \rho_1 e^{2\pi T_b t} + \rho_{-1} e^{-2\pi T_b t}) e^{-2\pi f t} dt + \sigma^2 \int e^{-2\pi f t} dt \\
&= (P_s \rho_0 + \sigma^2)\delta(f) + \rho_1 \delta(f - T_b) + \rho_{-1} \delta(f + T_b)
\end{aligned} \tag{3.61}
$$

From the above expression, we can see that there exists three peaks in the Fourier transform of the ensemble power: $f = 0, f = T_b$ and $f = -T_b$. The peak of the Fourier transform of the ensemble power for the received signals is the corresponding baud rate.

Figure 3.20 displays one example of the Fourier transform of $\rho_{t,0}$ for a 16-QAM signal in a multipath channel. In this example, SNR in the channel was 20 dB. The number of symbols was 20000. The number of samples per baud T_b/T_s was 20. The multipath channel is the six-path channel model described in [21] for the typical urban (TU) wireless system. The channel coefficients are described in Table 3.3. We can see that the corresponding three peaks can be observed from the Fourier transform. By finding the peaks in the curves, the baud rate can be estimated. In this example, the first peak is at $f_0/f_s = 0$. The distance between the other two peaks to the first peak are 0.05, which corresponds to the number of samples per baud 20.

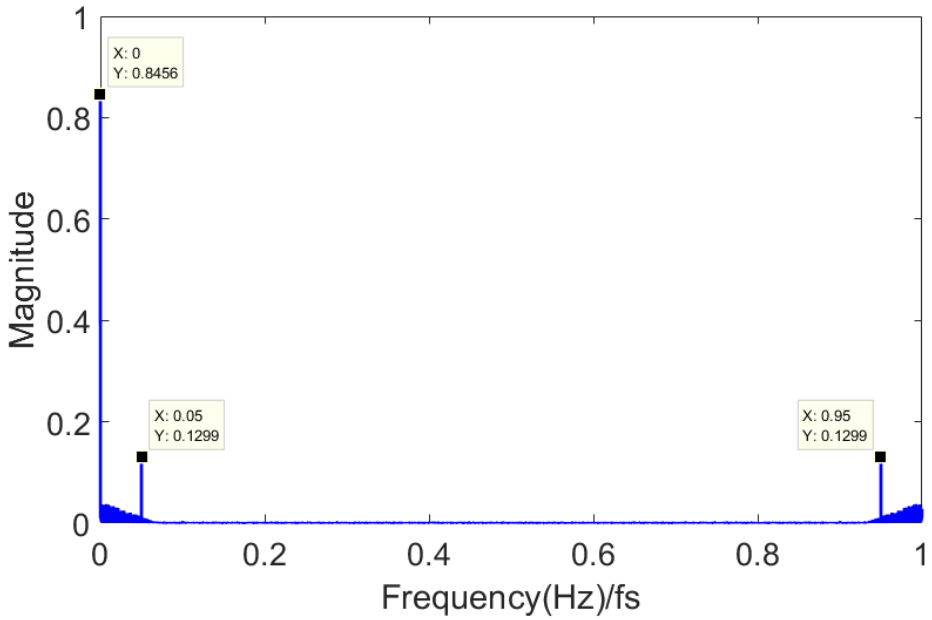

Figure 3.20: Fourier transform of the ensemble power of the received signal in a multipath channel: 16-QAM signal; Number of symbols: 20000; Number of samples per baud: 20; SNR = 20 dB; TU six-path channel.

Table 3.3: TU six-path channel model

Path delay kT_s	Fractional power a
0	0.189
5	0.618
10	0.095
15	0.061
20	0.000
25	0.037

3.4.3 Constant Modulus Amplitude Equalization

The PDF of the amplitude or phase of the signals in multipath channels is different from that of the signals in AWGN channels. Blind equalization to mitigate the effect of the multipath on the signals is implemented before identifying the modulation type of the signals in multipath channels.

From the symbol patterns of the PSK and QAM signals, we know that PSK signals have a constant modulus amplitude for the symbols and QAM signals have a finite number of amplitudes for the symbols. In order to estimate the channel coefficients and eliminate the effect of the multipath, a constant modulus amplitude (CMA) equalizer is implemented.

Let $\hat{s}[n]$ be the estimated symbols after blind equalization and let w be the estimated channel coefficient vector with length L. The goal of the CMA equalizer is to estimate w so that the estimated symbols $\hat{s}[n]$ can match well with the source symbols. They satisfy

$$\hat{s}[n] = \sum_{l=0}^{L-1} w(l) y_c(n-l) \tag{3.62}$$

The criteria of the CMA equalizer is to minimize the error between the estimated amplitude of the signal and the constant modulus amplitude. The cost function of the CMA equalizer is

$$J_{CM} = E\{(|\hat{s}[n]|^2 - r_m)^2\} \tag{3.63}$$

where r_m is the constant modulus.

In general, r_m is a constant defined as

$$r_m = \frac{E\{|s[n]|^4\}}{E\{|s[n]|^2\}^2} \tag{3.64}$$

In this dissertation, r_m is chosen to be 1.

In order to minimize the cost function, the gradient method is used to update the channel coefficients. The channel is updated as

$$w(n+1) = w(n) - \mu_c \frac{\partial J_{CM}}{\partial w(n)}$$
$$= w(n) - \mu_c (y_c(n)^H \hat{s}(n)(|\hat{s}(n)|^2 - 1)) \quad (3.65)$$

where μ_c is the step size.

The CMA equalizer estimates the channel coefficients to recover the symbols by eliminating the channel effects including the pulse shaping filter and the multipath channel. As a result, the estimated symbol sequence after the CMA equalizer will be an up-sampled version of the original source symbols. Thus, direct subsampling process for the estimated symbols will result in an estimate of the input symbols of the transmitted signals.

In addition, the estimated channel coefficients are complex variables based on the channel model described in (3.55). The effect of the phase of the channel coefficients on the PSK signals give the system a difficult time identifying different PSKs. In this section, the system concentrates in identifying different QAM signals in multipath channels.

3.4.4 Performance Evaluation

In this section, the performance of the CMA equalizer is shown by comparing the constellation maps and the histogram of amplitudes between the signals in multipath channels and the signals after CMA equalization first. Next, the probability of successful identification of different QAM signals in multipath channels applying the combination of the CMA equalizer and the likelihood-based modulation identification algorithm is presented. 100 independent data sets were used to calculate the probability of successful identification for each modulation type. In all the simulations in this section, the number of samples per baud in the signal was 20. The number of symbols was 20000. The multipath channel is the six-path channel model and the coefficients are shown in Table 3.3.

3.4.4.1 Comparison of the Histograms of Amplitude of the Signals

In this section, the constellation maps and the histogram of the amplitude of the signals are compared. The SNR in the channel was 20 dB.

Figure 3.21 and 3.22 show the comparisons of the constellation maps and histograms of the amplitude of the source signals, signals with multipath and signals after equalizer. We can see that the equalizer do recover the signal characteristics. The three amplitude

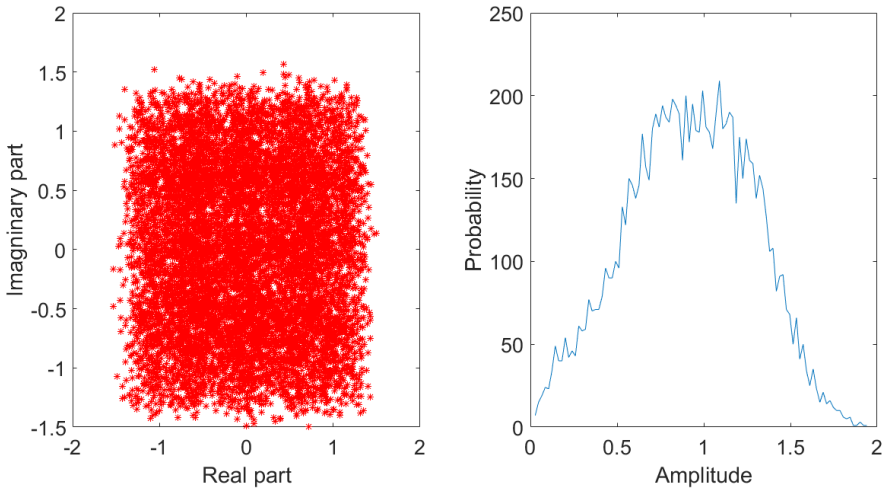

(a) Signal in a multipath channel after subsampling.

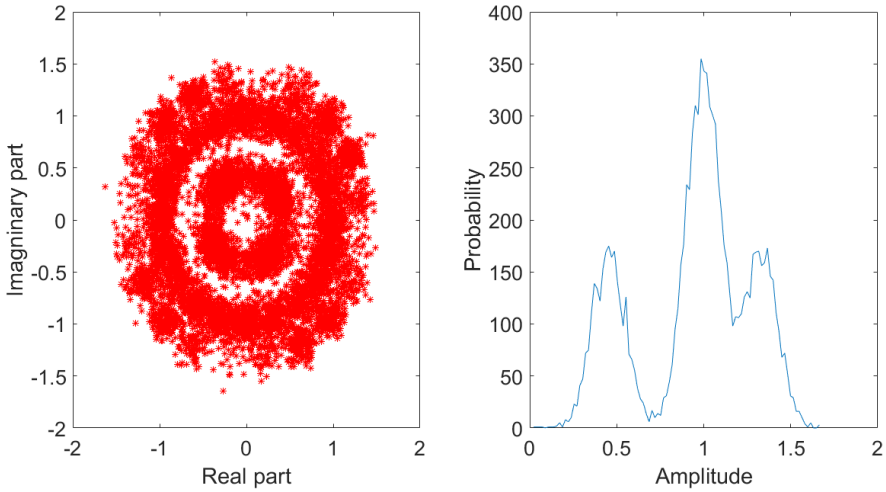

(b) Signal after CMA equalizer and subsampling.

Figure 3.21: Constellation maps and histograms of the amplitude of the signals:16-QAM signal; Number of symbols: 20000; Number of samples per symbol: 20; SNR = 20 dB; TU six-path channel.

values cannot be observed for the 16-QAM signals from the histogram of the amplitude in the multipath channel. However, after the CMA equalizer, the corresponding amplitude distribution for 16-QAM signals can be observed.

Similar performance is also shown for 32-QAM signals. The amplitude distribution corresponding to the five amplitude groups of 32-QAM signals can be observed from the histogram of the amplitude for the signal after blind equalization.

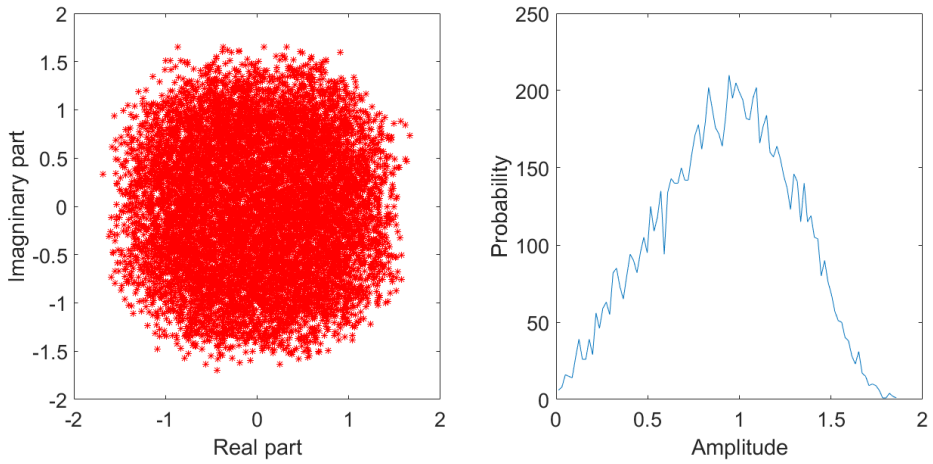

(a) Signal in a multipath channel after subsampling.

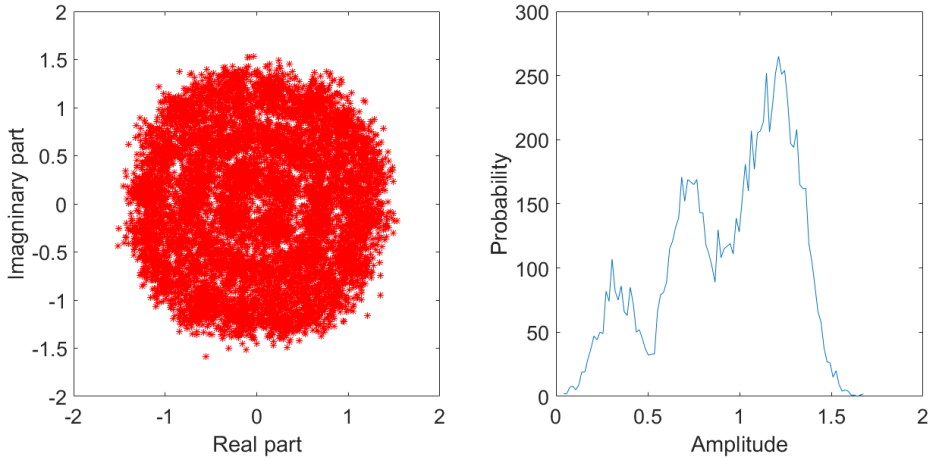

(b) Signal after CMA equalizer and subsampling.

Figure 3.22: Constellation maps and histograms of the amplitude of the signals: 32-QAM signal; Number of symbols: 20000; Number of samples per symbol: 20; SNR = 20 dB; TU six-path channel.

3.4.4.2 The Probability of Successful Identification for QAM Signals in Multipath Channels

Figure 3.23 presents the probability of successful identification for the signals in multipath channels with different modulation types under different SNRs.

We can see that the system can identify different QAM signals in multipath channels with sufficient high SNRs. For example, the system can identify 16-QAM signals with above 99 % accuracy with 7 dB SNR with 20000 symbols. For higher-order QAM signals, the system needs higher SNRs in order to get accurate identification results. For example, for 256-QAM signals, the system can only get above 90% accuracy even at high SNRs. This

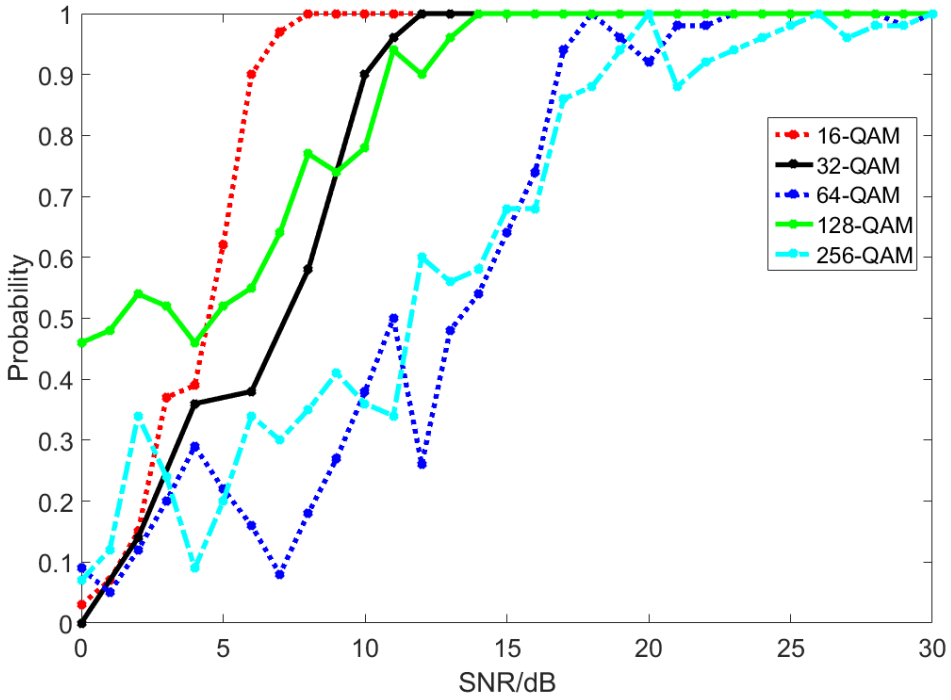

Figure 3.23: Probability of successful identification for different QAM signals in a multipath channel; Number of symbols: 20000; Number of samples per symbol: 20; TU six-path channel.

suggests that error of the blind equalizer using CMA method has a larger influence on the higher-order QAMs than the lower-order QAMs.

Comparing with the results shown in Section 3.3 for the signals in AWGN channels, the combination of CMA equalizer and the likelihood-based modulation identification algorithm needs higher SNRs in order to obtain accurate identification results for different QAM signals. This was expected because the equalization for the signals in multipath channels adds more errors for recovering the source symbols.

3.5 Conclusions

This chapter first developed a novel likelihood-based modulation identification algorithm for different QAM and PSK signals. This method performs well at relatively low SNRs and using relatively short signal durations. The theoretical analysis of the performance of the modulation identification algorithm showed good agreement with simulation results. This analysis provides a reliable prediction about the SNR levels and

signal length needed for the algorithms to identify different modulation types accurately.

The method in this chapter was shown to be superior to two other methods available in the literature. Under the same signal environment, the method in this paper identifies all the modulation types of interest above 99% accuracy at SNR $\geq$ 4 dB using 10,000 symbols while the two other methods could not. In addition, the simulation results indicate that at SNR above 9 dB and with more than 10,000 symbols, when the method in this paper identifies a specific modulation type, the input signal must be that corresponding modulation type. Furthermore, the system is able to identify all the modulation types with shorter symbol length with high accuracy at low SNRs. Finally, the simulation results presented indicated that the performance was robust under different noise environments. The results presented in the paper suggest that the likelihood-based algorithm is a strong alternative to currently available methods for blind modulation identification for PSK and QAM signals.

The combination of the CMA equalizer and the modified likelihood-based modulation identification method is also included in this chapter. The results indicate that the system is able to identify the QAM signals in multipath channels with a wide range of SNRs. For example, the system can identify 16-QAM signals with above 99% accuracy with 7 dB SNR with 20000 symbols. Comparing with the results for the signals in AWGN channels, the combination of CMA equalizer and the likelihood-based modulation identification algorithm needs higher SNRs in order to obtain accurate identification results for different QAM signals.

Additional work on performance evaluation under a variety of impairments as well as algorithm refinements to reduce computational complexity and to further improve performance is underway at this time.

CHAPTER 4

BLIND MODULATION IDENTIFICATION OF QAM AND PSK SIGNALS IN DUAL-POLARIZED CHANNELS

As described in Chapter 2, signals transmitted through dual-polarized channels will be a mixture of the signals in the two channels due to the cross-polarization between the two polarized channels. As a result, the features for the modulation identification of the received signals are not distinct. Modulation identification of the information-bearing signals in dual-polarized channels can be achieved by combining an adaptive blind source separation (BSS) algorithm with the likelihood-based blind modulation identification algorithm.

In this chapter, a system that can separate and identify the modulation types of signals transmitted in dual-polarized channels is developed. A block diagram of the system is shown in Figure 4.1. The system employs the adaptive blind source separation (BSS) algorithm to obtain the source signals from the mixed signals arriving at the receiver. Then, the likelihood-based modulation identification algorithm will be applied to identify the modulation types of the estimated signals after separation.

The rest of the chapter is organized as follows. Section 4.1 introduces the likelihood-based blind separation algorithm. Next, the probability of the correct modulation identification for the signals in dual-polarized channels is presented in Section 4.3. Finally, Section

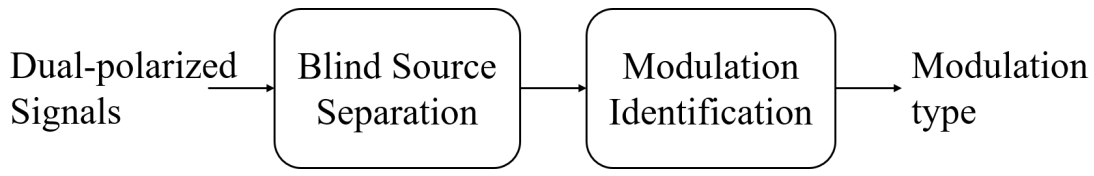

Figure 4.1: Block diagram of the two-step likelihood-based separation and identification method for signals in dual-polarized channels.

4.4 contains the concluding remarks for this chapter.

4.1 Likelihood-based Blind Separation of Signals in Time-varying Dual-polarized Channels

In this section, an adaptive likelihood-based blind source separation method, which implements the likelihood functions of the amplitude of the received signals to estimate the channel coefficients and the source signals, is presented. We assume that the two transmitted signals are independent of each other, but no other information about the communication system is assumed. We also assume that the transmitted signals belong to QAM signals (PSK is a special case of QAM), but no knowledge of the modulation type is assumed. The modulation types of the source signals will not affect the separation performance as long as the two source signals are independent of each other. This method is different from other BSS algorithms available in the literature in the sense that the separation is achieved using a likelihood-based approach that utilizes the probability density function (PDF) of the amplitude of the transmitted signals.

The rest of the section is organized as follows. Section 4.1.1 introduces the signal model for the received signals with dual polarization. In Section 4.1.2, the adaptive likelihood-based BSS algorithm is developed. The performance including the symbol error rate (SER) of recovered signals after applying BSS and the BSS system's capability to track the channel coefficients is presented in Section 4.2.

4.1.1 System Model

Figure 4.2 displays the system model of the signals transmitted through a time-varying dual-polarized channel.

In this figure, $x_1(t)$ and $x_2(t)$ represent the input signals of the two channels correspondingly. They are modulated signals and are generated using the digital modulator described in Chapter 2.

The two signals are transmitted through a time-varying dual-polarized channel. The complex-valued variables $\psi_{11}(t), \psi_{12}(t), \psi_{21}(t)$ and $\psi_{22}(t)$ are the time-varying channel coefficients, and $y_1(t)$ and $y_2(t)$ are the received signals. The noise in the received signals is assumed to be additive white Gaussian noise. The existence of the two polarizations of transmission is explicitly shown here. Let $X(t) = [x_1(t), x_2(t)]$, $Y(t) = [y_1(t), y_2(t)]$ and

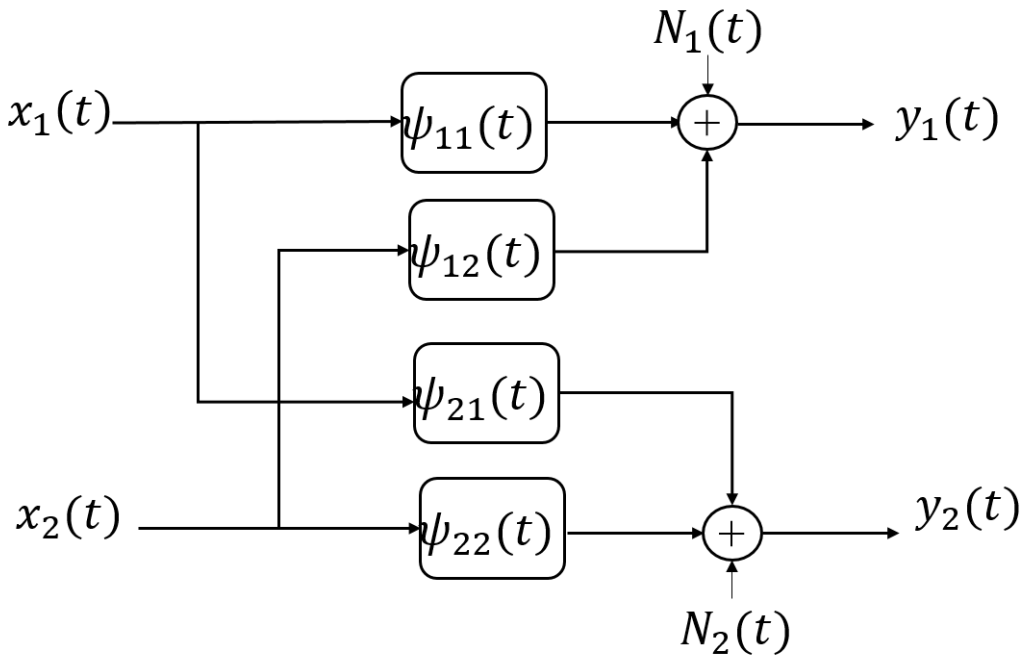

Figure 4.2: Block diagram of a dual-polarized channel.

$N(t) = [N_1(t), N_2(t)]$. Then, the relation between the transmitted and received signals of the channel can be expressed as

$$Y(t) = \Psi(t)X(t) + N(t) \tag{4.1}$$

where $\Psi(t) = \begin{bmatrix} \psi_{11}(t) & \psi_{12}(t) \\ \psi_{21}(t) & \psi_{22}(t) \end{bmatrix}$ is a 2×2 matrix with elements representing the time-varying polarization at time t.

The polarization during transmission of the signals changes because of the variations of the channel. Therefore, the state of polarization of a received signal is not known at the receiver. The unitary Jones matrix shown below describes a common model for a time-varying dual-polarized channel [51].

$$\Psi(t) = \begin{pmatrix} \cos\{\upsilon\pi t\}e^{j\delta\pi t/2} & -\sin\{\upsilon\pi t\}e^{-j\varepsilon\pi t/2} \\ \sin\{\upsilon\pi t\}e^{j\varepsilon\pi t/2} & \cos\{\upsilon\pi t\}e^{-j\delta\pi t/2} \end{pmatrix} \tag{4.2}$$

In the above equation, υ represents the cross-talk between the two polarization modes and δ and ε describe the phase differences introduced by each channel. Based on this model, we observed that each component in $\Psi(t)$ is periodic. In this paper, we call the period of the amplitude of each component as the period of the change of the dual polarization. The period of the amplitude of each components is determined by υ.

4.1.2 A Likelihood-based Adaptive Blind Source Separation Algorithm for Complex Signals

Blind source separation has been widely applied to separate the mixtures of source signals. As shown earlier in this chapter, signals transmitted through dual-polarized channels will be mixtures of the two source signals due to the cross-polarization between the two channels.

We assume that the transmitted symbols of the two source signals are i.i.d. and the two source signals are independent of each other. We also assume that the source signals belong to QAM signals (PSK is a special case of QAM), but no knowledge of the modulation type is assumed. No other information of the communication channels is assumed. The modulation types of the source signals will not affect the separation performance as long as the two source signals are independent of each other. This method is different from other BSS algorithms available in the literature in the sense that the separation is achieved using a likelihood-based approach that utilizes the probability density function (PDF) of the amplitude of the transmitted signals.

The goal of BSS is to find a matrix that de-mixes the dual-polarized signals so that the transmitted signals can be recovered within a scaling factor and a time shift. The problem can be formulated as follows: we wish to find a time-varying matrix $Q(t)$ such that

$$Z(t) = Q(t)Y(t) \tag{4.3}$$

where $Q(t) = \begin{bmatrix} q_{11}(t)\, q_{12}(t) \\ q_{21}(t)\, q_{22}(t) \end{bmatrix}$ is 2×2 matrix at each time and

$Z(t) = \begin{bmatrix} z_1(t) \\ z_2(t) \end{bmatrix} = \begin{bmatrix} q_{11}(t)y_1(t) + q_{12}(t)y_2(t) \\ q_{21}(t)y_1(t) + q_{22}(t)y_2(t) \end{bmatrix}$ is the estimates of the input signals $X(t)$.

One way to achieve a good estimates of the source signals is to maximize the likelihood functions of $Z(t)$ applying the PDF of $X(t)$. Assuming the source signals belong to the PSK or QAM signals, the PDF of the amplitude of different modulation typeS is known as derived in Chapter 3.

Since the signals are sampled at discrete times in practice, sampled signals will be used in the following derivations. The continuous time indices t will be changed to discrete time variables n.

The joint PDF of the amplitude of the two signals can be written as

$$p(|z_1(n)|,|z_2(n)|) = p(|z_1(n)|,|z_2(n)||H_{M_1},H_{M_2})p(H_{M_1},H_{M_2}) \tag{4.4}$$
$$= p(|z_1(n)||H_{M_1})p(|z_2(n)||H_{M_2})p(H_{M_1},H_{M_2})$$

where $p(\cdot)$ is the probability density function (PDF) of the amplitude of input signal $X(n)$ and $p(H_{M_1},H_{M_2})$ is the probability of the assumed modulation types, which is a constant.

Given N independent amplitude values of the received signals at both channels, the cost function for BSS algorithm based on the logarithm of the joint probability density function can be written as

$$C = \sum_{n=1}^{N}\{\log(p(|z_1(n)||H_{M_1})) + \log(p(|z_2(n)||H_{M_2}))\} \tag{4.5}$$

Substituting (3.27) in (4.5), the cost function becomes

$$C = \sum_{n=1}^{N}\log\{\sum_{i=1}^{N_a}\frac{w_{M_1}[i]}{\sigma^2}|z_1(n)|e^{\frac{-(|z_1(n)|^2+S^2_{M_1}[i])}{2\sigma^2}}I_0(\frac{|z_1(n)|S_{M_1}[i]}{\sigma^2})\}$$
$$+\sum_{n=1}^{N}\log\{\sum_{i=1}^{N_a}\frac{w_{M_2}[i]}{\sigma^2}|z_2(n)|e^{\frac{-(|z_2(n)|^2+S^2_{M_2}[i])}{2\sigma^2}}I_0(\frac{|z_2(n)|S_{M_2}[i]}{\sigma^2})\} \tag{4.6}$$

The PDF described in (3.27) belongs to the sub-Gaussian PDF group regardless of the modulation type. This is expected since BSS algorithms employing contrast functions applicable to whole classes of some distributions have been studied before in [27] and [44]. As a result, the derivation in this sections is based on the joint likelihood functions based on the assumed modulation types for two source signals. Later in the section of performance in this chapter, we will show that different modulation types used in the cost function will not affect the performance of the separation.

In order to find the maximum of the likelihood function, the elements of $Q(t)$ are updated by taking the gradient of the cost function in the following manners.

$$Q(n+1) = Q(n) + \mu\frac{\partial C}{\partial Q(n)}$$
$$= Q(n) + \mu\frac{\partial C}{\partial|Z(n)|}\frac{\partial|Z(n)|}{\partial Q(n)} \tag{4.7}$$

where μ is the step size for the adaptation. The gradient $\frac{\partial C}{\partial|Z(n)|}\frac{\partial|Z(n)|}{\partial Q(n)}$will be derived with respect to each element of the matrix $Q(n)$. The update equation is written as

$$\begin{bmatrix} q_{11}(n+1)\, q_{12}(n+1) \\ q_{21}(n+1)\, q_{22}(n+1)\end{bmatrix} = \begin{bmatrix} q_{11}(n)\, q_{12}(n) \\ q_{21}(n)\, q_{22}(n)\end{bmatrix} + \mu\begin{bmatrix} \frac{\partial C}{\partial|z_1(n)|}\frac{\partial|z_1(n)|}{\partial q_{11}(n)} & \frac{\partial C}{\partial|z_1(n)|}\frac{\partial|z_1(n)|}{\partial q_{12}(n)} \\ \frac{\partial C}{\partial|z_2(n)|}\frac{\partial|z_2(n)|}{\partial q_{21}(n)} & \frac{\partial C}{\partial|z_2(n)|}\frac{\partial|z_2(n)|}{\partial q_{22}(n)}\end{bmatrix} \tag{4.8}$$

The four gradients in the above equation are similarly derived. As an example, we

differentiate with respect to q_{11} as shown below

$$\frac{\partial C}{\partial |z_1(n)|}\frac{\partial |z_1(n)|}{\partial q_{11}(n)} = \frac{y_1(n)}{p(|z_1(n)||H_{M_1})}\frac{\partial p(|z_1(n)||H_{M_1})}{\partial |z_1(n)|}\frac{\partial |z_1(n)|}{\partial q_{11}(n)} \tag{4.9}$$

In the above equation, we note firstly that

$$\begin{aligned}
&\frac{\partial p(|z_1(n)||H_{M_1})}{\partial |z_1(n)|} = \frac{\partial p(R)}{\partial R}|_{R=|z_1(n)|} \\
&= \sum_{i=1}^{N_a}\frac{w_{M_1}[i]}{\sigma^2}\frac{\partial R}{\partial R}e^{\frac{-(R^2+S^2_{M_1}[i])}{2\sigma^2}}I_0(\frac{RS_{M_1}[i]}{\sigma^2}) \\
&+ \sum_{i=1}^{N_a}\frac{w_{M_1}[i]}{\sigma^2}R\frac{\partial e^{-(R^2+S^2_{M_1}[i])/2\sigma^2}}{\partial R}I_0(\frac{RS_{M_1}[i]}{\sigma^2}) \\
&+ \sum_{i=1}^{N_a}\frac{w_{M_1}[i]}{\sigma^2}Re^{\frac{-(R^2+S^2_{M_1}[i])}{2\sigma^2}}\frac{\partial I_0(\frac{RS_{M_1}[i]}{\sigma^2})}{\partial R} \\
&= \sum_{i=1}^{N_a}\frac{w_{M_1}[i]}{\sigma^2}e^{\frac{-(R^2+S^2_{M_1}[i])}{2\sigma^2}}[I_0(\frac{RS_{M_1}[i]}{\sigma^2}) \\
&-\frac{R^2}{\sigma^2}I_0(\frac{RS_{M_1}[i]}{\sigma^2}) + \frac{S_{M_1}[i]}{\sigma^2}I_1(\frac{RS_{M_1}[i]}{\sigma^2})]
\end{aligned} \tag{4.10}$$

where $I_1(\cdot)$ is the first-order modified Bessel function of the first kind.

Then, applying the gradient to real and imaginary parts of $q_{11}(n)$ separately, we obtain

$$\frac{\partial |z_1(n)|}{\partial \Re\{q_{11}(n)\}} = \frac{\Re\{z_1(n)\}}{|z_1(n)|}(\Re\{z_1(n)\}\Re\{y_1(n)\} + \Im\{z_1(n)\}\Im\{y_1(n)\}) \tag{4.11}$$

$$\frac{\partial |z_1(n)|}{\partial \Im\{q_{11}(n)\}} = \frac{\Im\{z_1(n)\}}{|z_1(n)|}(-\Re\{z_1(n)\}\Im\{y_1(n)\} + \Im\{z_1(n)\}\Re\{y_1(n)\}) \tag{4.12}$$

Substituting (4.9), (4.10), (4.11) and (4.12) in (4.7), the update equation for q_{11} becomes

$$\begin{aligned}
q_{11}(n+1) &= \Re\{q_{11}(n+1)\} + j\Im\{q_{11}(n+1)\} \\
&= (\Re\{q_{11}(n)\} + \mu\frac{\partial C}{\partial \Re\{q_{11}(n)\}}) + j(\Im\{q_{11}(n)\} + \mu\frac{\partial C}{\partial \Im\{q_{11}(n)\}}) \\
&= \frac{y_1(n)}{p(|z_1(n)||H_{M_1})}\frac{\partial p(|z_1(n)||H_{M_1})}{\partial |z_1(n)|}[\frac{\partial |z_1(n)|}{\partial \Re\{q_{11}(n)\}} + j\partial\frac{|z_1(n)|}{\partial \Im\{q_{11}(n)\}}] \\
&= \frac{y_1(n)}{p(|z_1(n)||H_{M_1})}\frac{\partial p(|z_1(n)||H_{M_1})}{\partial |z_1(n)|}[\frac{\Re\{z_1(n))\}}{|z_1(n)|}y_1^*(t) \\
&+ \frac{\Im\{z_1(n)\}}{|z_1(n)|}(\Im\{y_1(n)\} + j\Re\{y_1(n)\})]
\end{aligned} \tag{4.13}$$

The updating equations for other three elements in $Q(n)$ can be derived similarly as (4.13) and are given by

$$q_{12}(n+1) = \frac{y_2(n)}{p(|z_1(n)||H_{M_1})} \frac{\partial p(|z_1(n)||H_{M_1})}{\partial |z_1(n)|} [\frac{\Re\{z_1(n))\}}{|z_1(n)|} y_2^*(t) + \frac{\Im\{z_1(n)\}}{|z_1(n)|} (\Im\{y_2(n)\} + j\Re\{y_2(n)\})] \quad (4.14)$$

$$q_{21}(n+1) = \frac{y_1(n)}{p(|z_2(n)||H_{M_2})} \frac{\partial p(|z_2(n)||H_{M_2})}{\partial |z_2(n)|} [\frac{\Re\{z_2(n))\}}{|z_2(n)|} y_1^*(t) + \frac{\Im\{z_2(n)\}}{|z_2(n)|} (\Im\{y_1(n)\} + j\Re\{y_1(n)\})] \quad (4.15)$$

$$q_{22}(n+1) = \frac{y_2(n)}{p(|z_2(n)||H_{M_2})} \frac{\partial p(|z_2(n)||H_{M_2})}{\partial |z_2(n)|} [\frac{\Re\{z_2(n))\}}{|z_2(n)|} y_2^*(t) + \frac{\Im\{z_2(n)\}}{|z_2(n)|} (\Im\{y_2(n)\} + j\Re\{y_2(n)\})] \quad (4.16)$$

4.1.3 Implementation of the Likelihood-based BSS Algorithm

The details of implementing the likelihood-based BSS algorithm for the received signals in dual-polarized channels are shown in Table 4.1 and 4.2. The system first initializes the de-mixing matrix, the step size and the estimated signals. At each time, the system updates the de-mixing matrix derived in Section 4.1.2. The estimated signals are obtained using the estimated de-mixing matrix.

4.2 Performance Evaluation

In this section, the results evaluating the ability of the likelihood-based BSS algorithm to track the time-varying coefficients of dual-polarized channels are presented first.

Table 4.1: Defination of variables in the likelihood-based BSS algorithm

$y_1(n)$: received signal at channel 1
$y_2(n)$: received signal at channel 2
$Y(n)$: received signals, a 2×1 matrix = $[y_1(n), y_2(n)]$
$q_{11}(n)$, $q_{12}(n)$, $q_{21}(n)$, $q_{22}(n)$: estimated channel coefficients
$Q(n)$: estimated de-mixing matrix, a 2×2 matrix = $\begin{bmatrix} q_{11}(n) & q_{12}(n) \\ q_{21}(n) & q_{22}(n) \end{bmatrix}$
$z_1(n)$: estimated signal at channel 1
$z_2(n)$: estimated signal at channel 2
$Z(n)$: estimated signals after separation, a 2×1 matrix = $[z_1(n), z_2(n)]$
μ: a constant step size
C: cost function

Table 4.2: The likelihood-based BSS algorithm

Inputs: $Y(n)$;

Initialization:
$Q(0)$; a random 2×2 matrix
μ; a constant step size
$Z(0) = Q(0)Y(0)$;

Adaptation:
for $i = 0 : N - 1$
$\delta_{q_{11}}(n) = \frac{\partial C}{\partial |z_1(n)|} \frac{\partial |z_1(n)|}{\partial q_{11}(n)}$; (4.9), (4.10) and (4.13)
$\delta_{q_{12}}(n) = \frac{\partial C}{\partial |z_1(n)|} \frac{\partial |z_1(n)|}{\partial q_{12}(n)}$; (4.14).
$\delta_{q_{21}}(n) = \frac{\partial C}{\partial |z_2(n)|} \frac{\partial |z_2(n)|}{\partial q_{21}(n)}$; (4.15).
$\delta_{q_{22}}(n) = \frac{\partial C}{\partial |z_2(n)|} \frac{\partial |z_2(n)|}{\partial q_{22}(n)}$; (4.16).
$\delta_{Q(n)} = \begin{bmatrix} \delta_{q_{11}}(n) & \delta_{q_{12}}(n) \\ \delta_{q_{21}}(n) & \delta_{q_{22}}(n) \end{bmatrix}$;
$Q_(n+1) = Q(n) + \mu \delta_{Q(n)}$;
$Z_(n+1) = Q_(n+1) Y_(n+1)$;
end

Next, comparisons between the source signals with the separated signals applying the likelihood-based BSS algorithm are demonstrated. Then, the performance of the likelihood-based BSS algorithm is evaluated using the symbol error rates (SERs) after demodulating the separated signals. The performance is also compared with that of a natural gradient-based BSS algorithm. Finally, simulation results evaluating the probability of successful modulation identification of the signals in time-varying dual-polarized channels obtained using a combination of the likelihood-based BSS algorithm and the likelihood-based modulation identification algorithm are presented.

In all the simulations , a root-raised cosine filter with roll-off factor of 0.5 was applied to the symbol sequence and 100 independent data sets were used to calculate all the results. The number of samples per symbol of the source signals was 20.

The rates of the change of the polarization coefficients, which correspond to the periods of the time-varying coefficients, were adjusted by changing the channel coefficients υ, δ and ε. The parameter values used in the simulations are displayed in Table 4.3.

In the natural gradient-based BSS algorithm, the de-mixing matrix Q is updated as [20]

$$Q(n+1) = Q(n) + \mu F(Q, y) \tag{4.17}$$

Table 4.3: Parameters of the dual-polarized channels in the simulations

Rates of change	υ	δ	ε
1.6 ms	1278	479	639
1.3 ms	1533	575	767
1 ms	2000	750	1000
0.75 ms	2667	999	1333
0.5 ms	4000	1500	2000

where

$$F(Q, y) = [\Lambda - \varphi(y)y^H]Q \tag{4.18}$$

Λ is a diagonal matrix and the operator $(\cdot)^H$ is the conjugate transpose for complex signals.

For the results presented in this chapter, Λ is chosen as the identify matrix. $\varphi(y)$ is selected as

$$\varphi(y) = y^3 \tag{4.19}$$

4.2.1 Tracking of the Channel Coefficients

Figure 4.3 and 4.4 show the tracking ability of the channel coefficients of the likelihood-based BSS algorithm and the natural gradient-based BSS algorithm. Here the two input signals were a 16-QAM signal and a 32-QAM signal. The SNR was 20 dB. The number of symbols was 20000. The rate of the change of the dual-polarized channel was 1.3 ms.

Figure 4.3 presents the comparison between the estimated coefficients and the inverse of the dual polarization matrix. We can see that the two different BSS algorithms track the channel coefficients well with a scaling factor on the amplitude. Both algorithms cannot track the phase of the coefficients well.

Figure 4.4 shows the product of $\Psi(t)$ and the estimated $\hat{Q}(t)$. Ideally, the product would be an identity matrix or a scaled identity matrix. We can see that the amplitudes of two diagonal elements of the matrix for the product are nearly constant and the two off-diagonal elements are close to 0. The phase of the two diagonal elements is linear. This means that the separated signals after the likelihood-based BSS algorithm will be the source signals with constant scaled amplitudes and constant phase shifts. This is as expected for the adaptive source separation algorithms. The constant scaling factor on amplitude and the linear phase shift will not change the characteristics of the source signals.

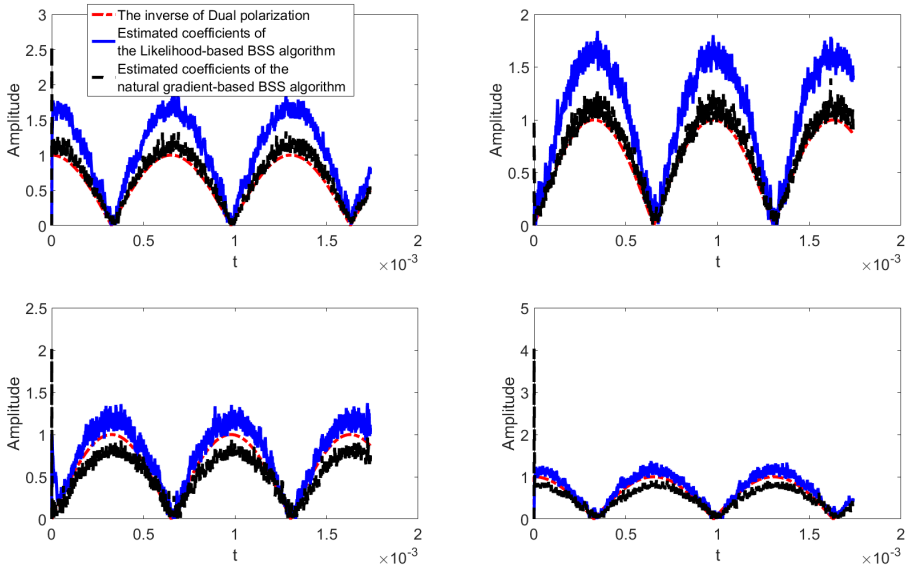

(a) Amplitudes of the coefficients at each time.

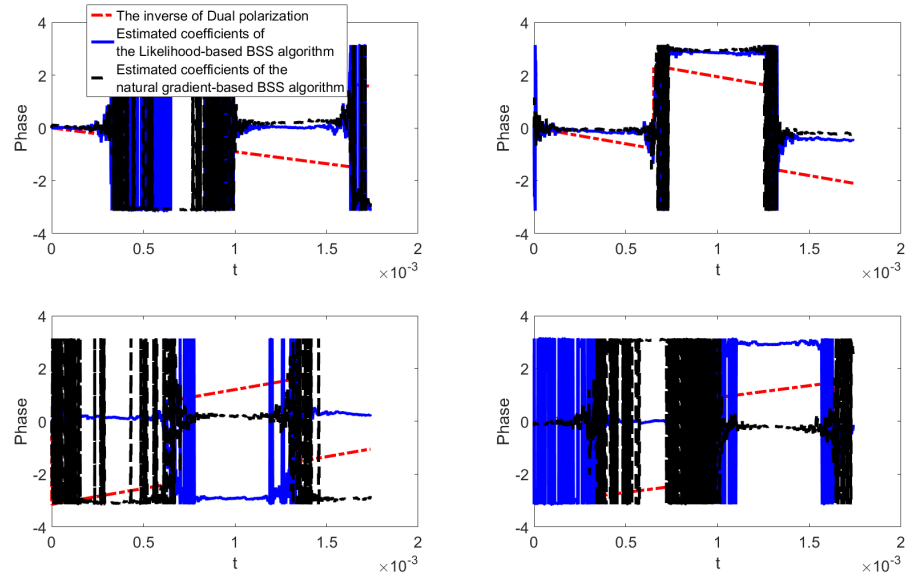

(b) Phase of the coefficients at each time.

Figure 4.3: Comparison of estimated coefficients with actual coefficients at each time: 16-QAM and 32-QAM; Rate of the change of dual-polarized channel: 1.3 ms; Number of symbols: 20000; Red curve: inverse of dual polarization matrix; Blue curve: estimated channel using the likelihood functions of 16-QAM and 32-QAM; Black curve: estimated channel using the likelihood functions of 16-QAM.

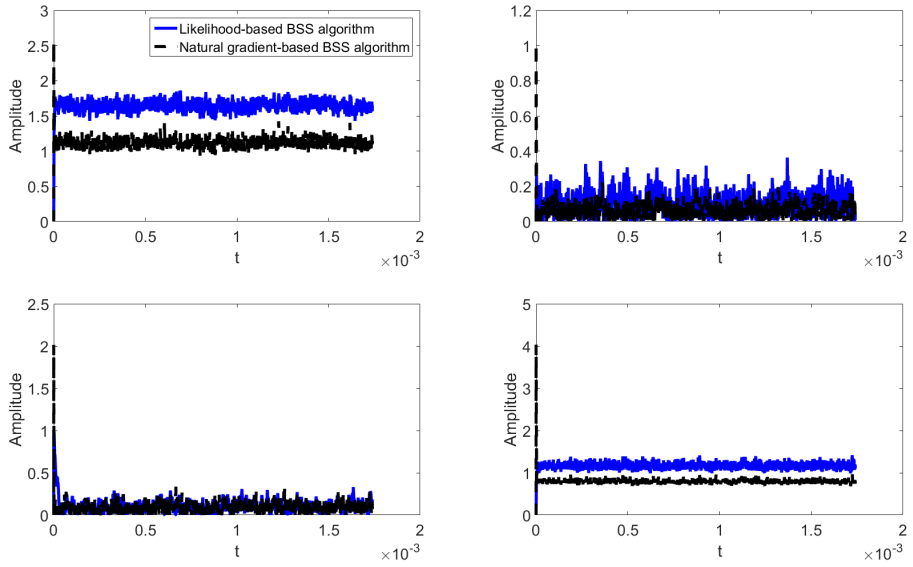

(a) Amplitudes of the coefficients at each time.

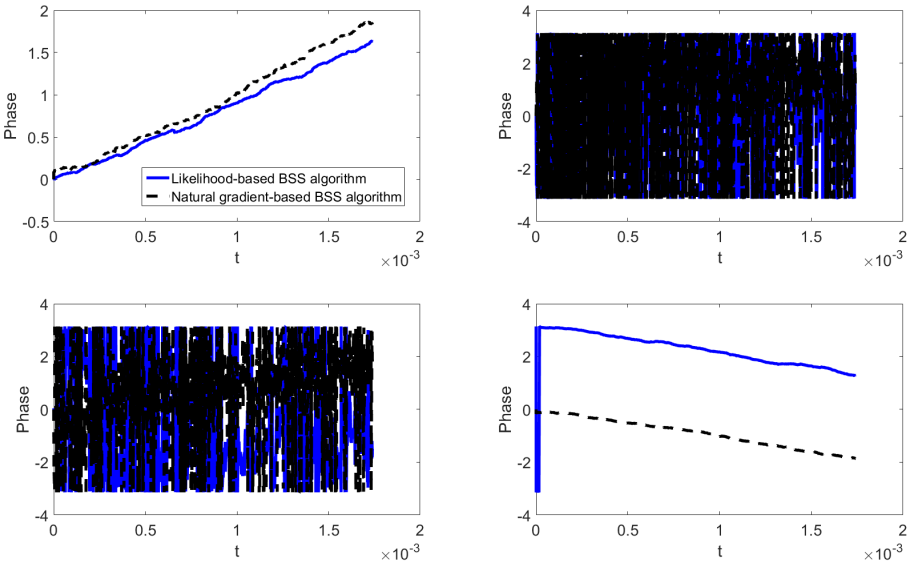

(b) Phase of the coefficients at each time.

Figure 4.4: Product of the dual polarization and estimated coefficients at each time: 16-QAM and 32-QAM; Rate of the change of dual-polarized channel: 1.3 ms; Number of symbols: 20000; Red curve: inverse of dual polarization matrix; Blue curve: estimated channel using the likelihood functions of 16-QAM and 32-QAM; Black curve: estimated channel using the likelihood functions of 16-QAM.

Another comparison is shown in Figures 4.5 and 4.6 for the likelihood-based BSS algorithm. In these two figures, case 1 is when we employed the likelihood functions based on the exact modulation types, which are 16-QAM and 32-QAM. Case 2 used 16-QAM-based likelihood functions for both input signals regardless of the modulation types.

We can also observe that cost functions based on the actual modulation type of the signals exhibited similar performance of tracking the coefficients as the cost functions based on single modulation type, which indicates that the modulation types used in the cost function will not affect the performance of the separation. As a result, in all of our simulations, the modulation types in the likelihood functions are assumed to be 16-QAM regardless of the modulation types of the source signals.

4.2.2 Comparison of the Source Signals and the Separated Signals

Figure 4.7 shows the comparison of the constellation maps of the received signals and the signals after separation. The simulation results in this section assume that the rate of change in a dual-polarized channel is 1.3 ms.

The constellation maps are obtained by demodulating the signals using the known carrier frequency, pulse shaping filter and baud rate. The two source signals were 16-QAM and 32-QAM signals. The SNR in the channel was 20 dB in this example. The number of symbols was 20000.

We can see that the corresponding 16 and 32 symbol clusters cannot be detected from the constellation maps of the received signals. The correct symbol patterns can be observed from the constellation maps of the estimated signals after applying the likelihood-based BSS algorithm.

In addition, Figure 4.8 presents the results when the two source signals were 16-QAM and 64-QAM. The separation performance for source signals with different modulation types is similar.

Figures 4.7 and 4.8 also present the comparisons between the results obtained by applying the likelihood-based BSS algorithm and the natural gradient-based algorithm. From these figures, the estimated signals using the likelihood-based BSS algorithm and the natural gradient-based algorithm show the corresponding symbol patterns as the source signals under different time-varying channels.

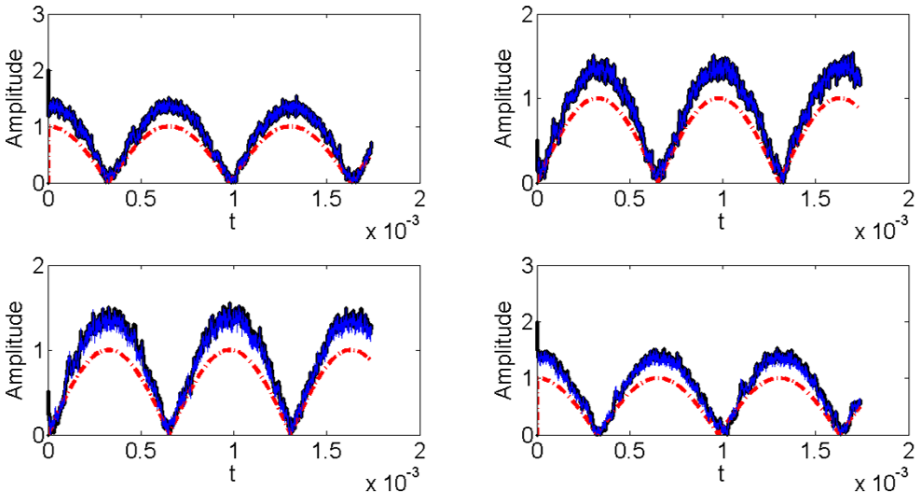

(a) Amplitudes of the coefficients at each time.

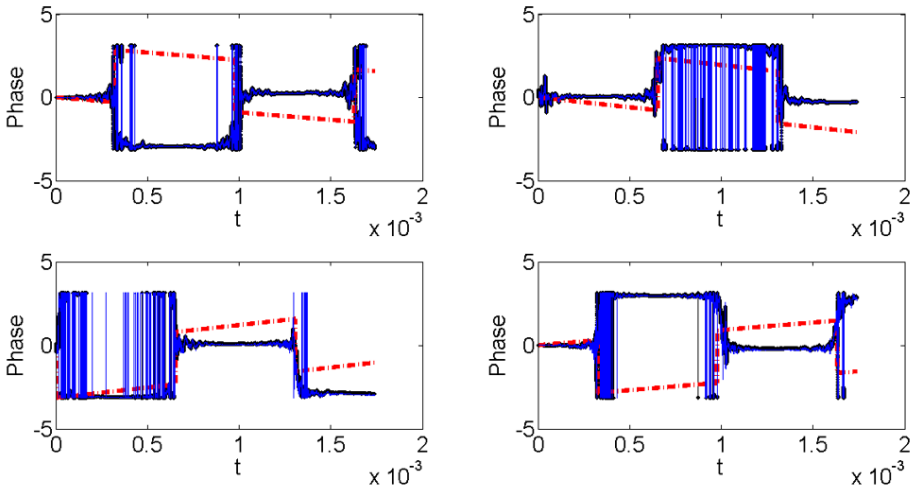

(b) Phase of the coefficients at each time.

Figure 4.5: Comparison of estimated coefficients with actual coefficients at each time using different modulation types in the likelihood functions: 16-QAM and 32-QAM; Rate of the change of dual-polarized channel: 1.3 ms; SNR=20 dB; Number of symbols: 20000; Blue curve: product of the estimated channel matrix and the dual polarization matrix using the likelihood functions of 16-QAM and 32-QAM; Black curve: product of the estimated channel matrix and the dual polarization matrix using the likelihood functions of 16-QAM.

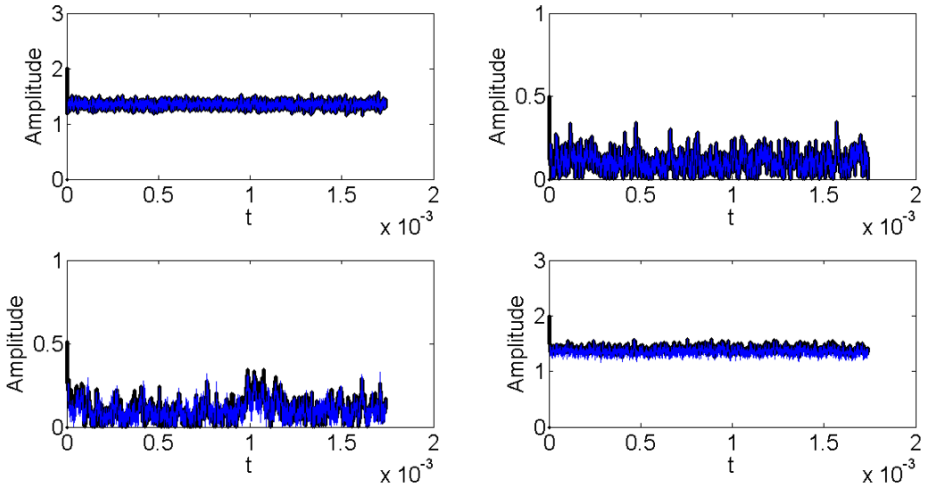

(a) Amplitudes of the product at each time.

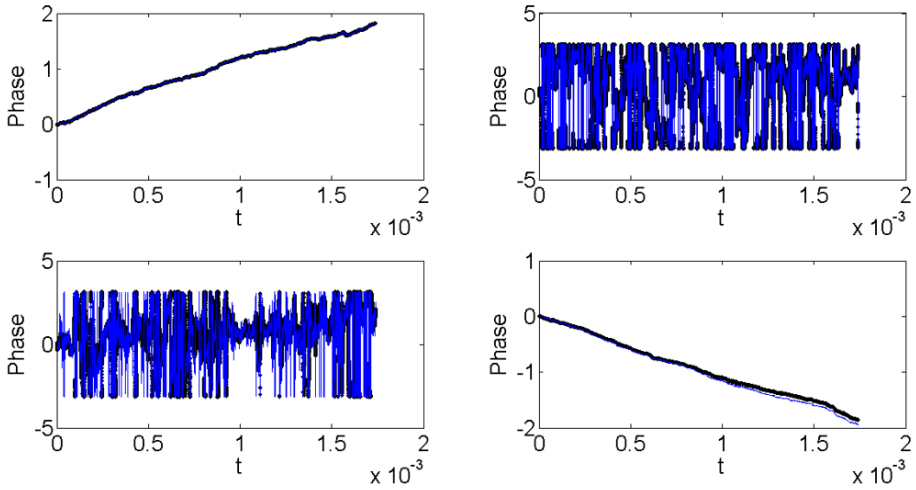

(b) Phase of the product at each time.

Figure 4.6: Product of the dual polarization and estimated coefficients at each time using different modulation types in the likelihood functions: 16-QAM and 32-QAM; Rate of the change of dual-polarized channel: 1.3 ms; SNR=20 dB; Number of symbols: 20000; Blue curve: product of the estimated channel matrix and the dual polarization matrix using the likelihood functions of 16-QAM and 32-QAM; Black curve: product of the estimated channel matrix and the dual polarization matrix using the likelihood functions of 16-QAM.

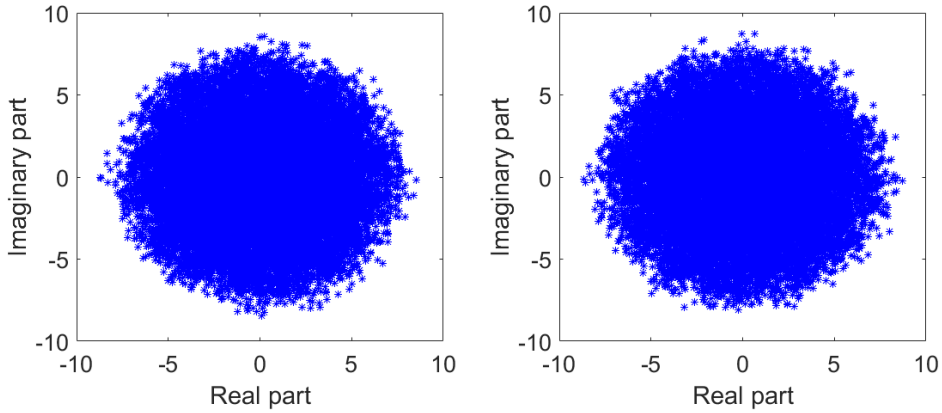

(a) Received signals in dual-polarized channel

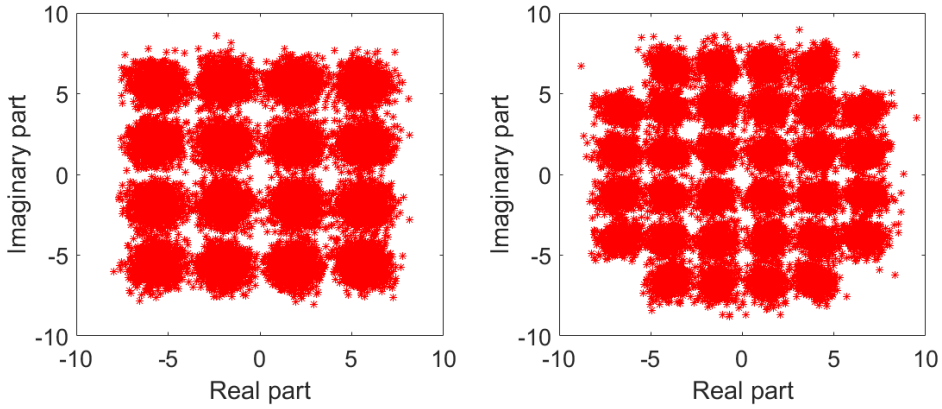

(b) Estimated signals using the likelihood-based BSS algorithm

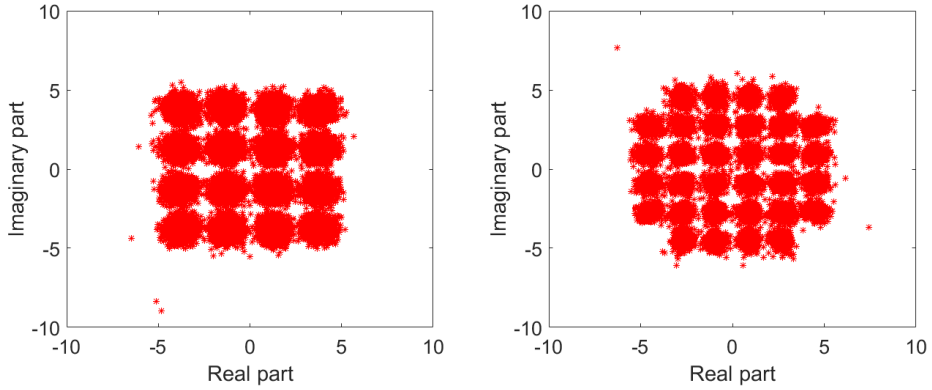

(c) Estimated signals using the natural gradient-based BSS algorithm

Figure 4.7: Comparison of the constellation maps of the received signals, the estimated signals using likelihood-based BSS algorithm and the estimated signals using natural gradient-based BSS algorithm: 16-QAM and 32-QAM; Rate of the change of the dual-polarized channel: 1.3 ms; SNR = 20 dB; Number of symbols: 20000.

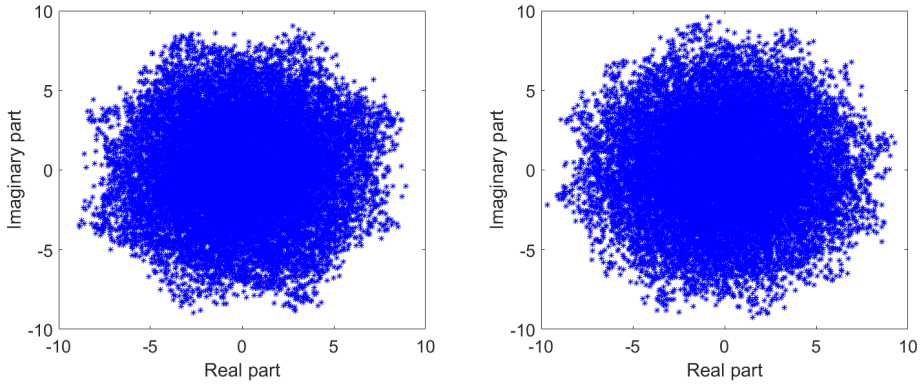

(a) Received signals in dual-polarized channel

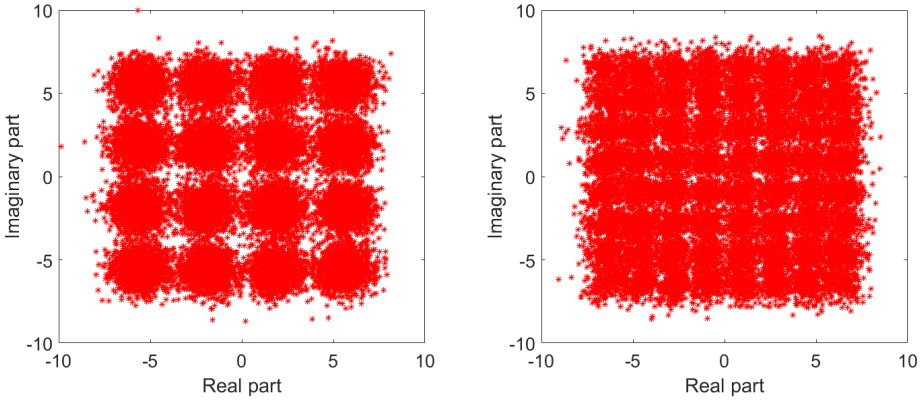

(b) Estimated signals using the likelihood-based BSS algorithm

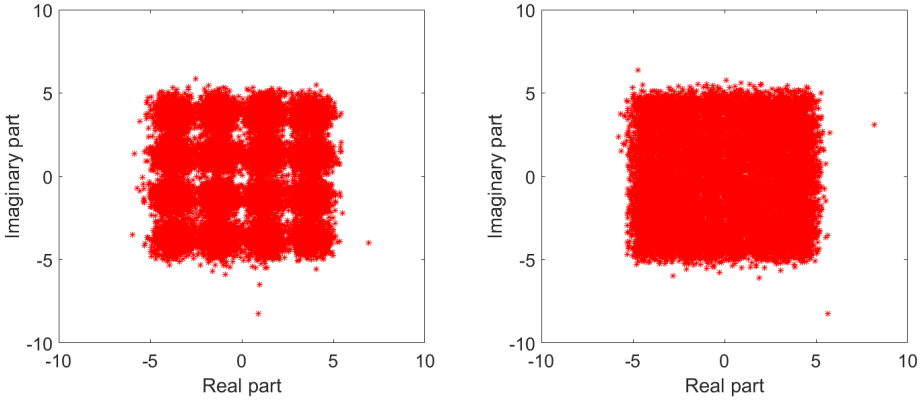

(c) Estimated signals using the natural gradient-based BSS algorithm

Figure 4.8: Comparison of the constellation maps of the received signals, the estimated signals using likelihood-based BSS algorithm and the estimated signals using natural gradient-based BSS algorithm: 16-QAM and 64-QAM; Rate of the change of the dual-polarized channel: 1.3 ms; SNR = 20 dB; Number of symbols: 20000.

Figure 4.9 and 4.10 show the comparison of the real and imaginary parts of a short segment of the separated signals and the source signals. The two source signals in Figure 4.9 were 16-QAM and 32-QAM signals and the two source signals in Figure 4.10 were 16-QAM and 64-QAM signals. The signals are normalized by their signal powers. The separated signals also assumes the compensation of the phase from the estimated channel coefficients. The effect of this phase has been shown in Section 4.2.1. We can observe that the separated signals match well with the source signals at both channels. The figures also show that the separated signals using the likelihood-based BSS algorithm and the natural gradient-based BSS algorithm match well with the source signals.

4.2.3 Symbol Error Rate

The symbol error rate was calculated as the number of errors between the source symbols and the separated symbols. The estimated symbols were obtained by demodulating the separated signals using known signal parameters. The SER can be expressed as

$$SER = \frac{N_{ser}}{N_s} \tag{4.20}$$

where N_{ser} is the number of symbols when the estimated symbol after demodulation is different from the source symbol and N_s is the number of symbols of the signal.

The choice of the step size in the adaptive BSS algorithms is critical to the performance of the symbol error rate of the signals transmitted in time-varying dual-polarized channels. Figure 4.11 and 4.12 show the symbol error rates as a function of the step size of the adaptive BSS algorithm for different time-varying dual-polarized channels. The SERs in these figures are obtained by averaging over the 100 independent runs at each step size. In this example, the number of symbols in the signal in each run was 20000. The parameter values of different channels used in the simulations are displayed in Table 4.3. The SNR in the channel was 20 dB. The two source signals were 16-QAM and 32-QAM signals.

From these figures, we can see that there exists an optimum step size which results in the smallest symbol error rate for the separated signals resulting from the adaptive BSS algorithms. The optimum step size increases when the period of the time-varying dual-polarized channels decreases, i.e., the rate of the change of the time-varying polarized channel is faster. Furthermore, the faster the time-varying dual-polarized channels are, the higher the symbol error rates of the separated signals.

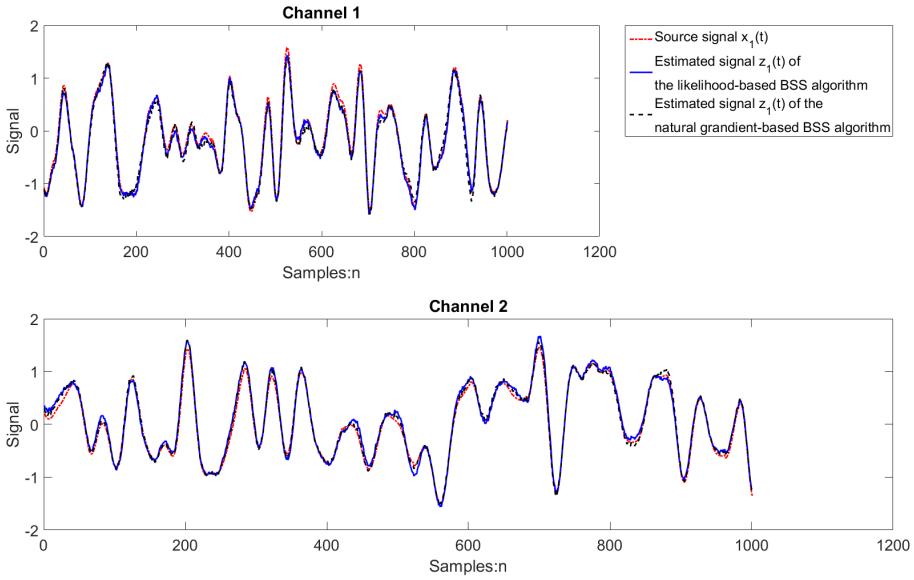

(a) Real part of the signals

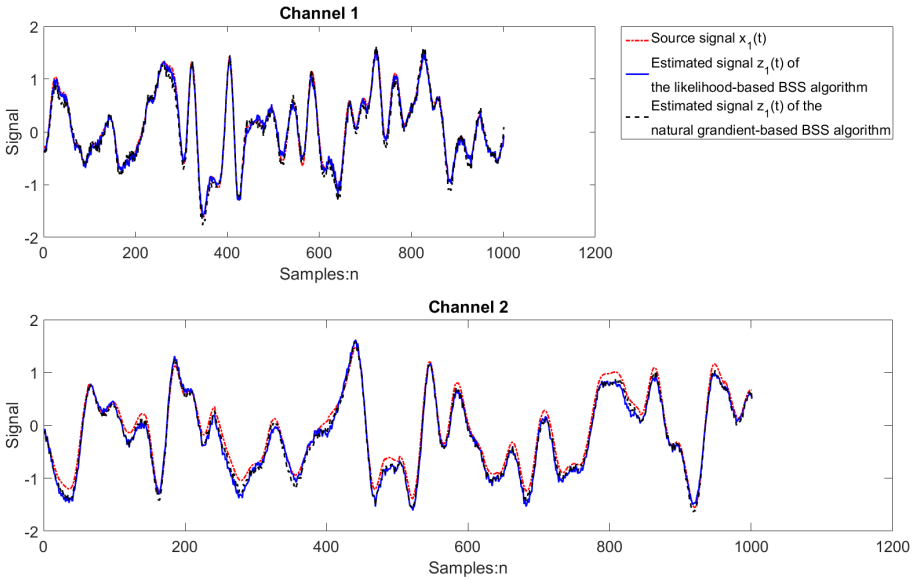

(b) Imaginary part of the signals

Figure 4.9: Comparison of real and imaginary parts of the source signals, the estimated signals using likelihood-based BSS algorithm and the estimated signals using natural gradient-based BSS algorithm: 16-QAM and 32-QAM; Rate of the change of the dual-polarized channel: 1.3 ms; SNR = 20 dB; Number of symbols: 20000.

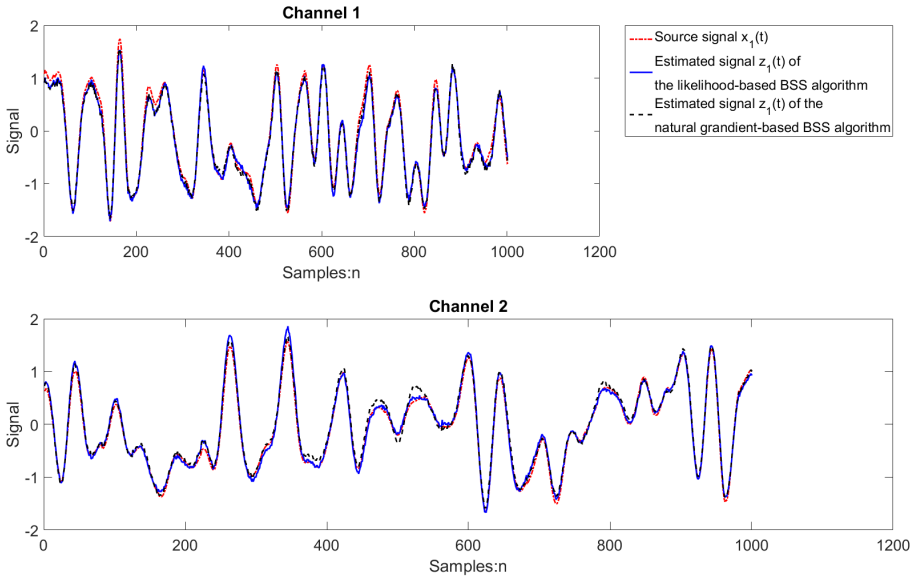

(a) Real part of the signals

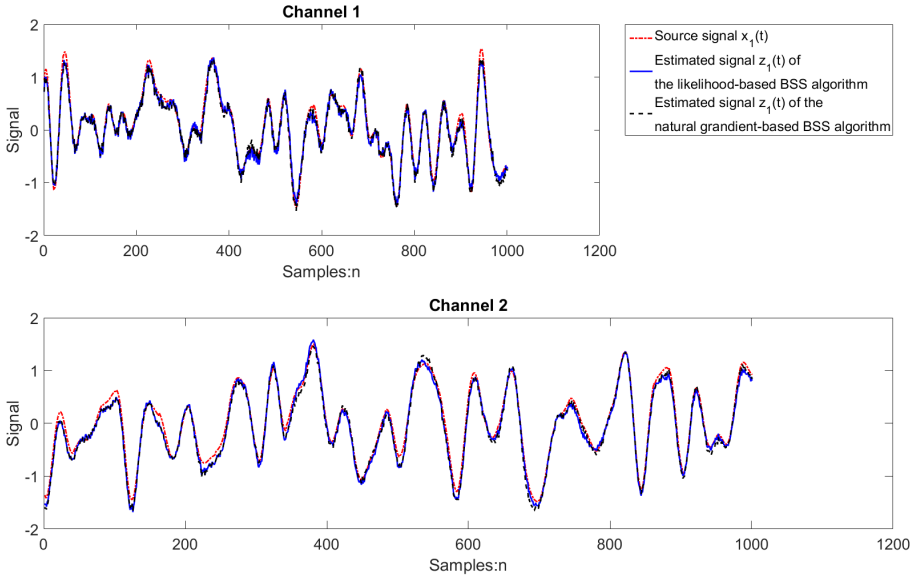

(b) Imaginary part of the signals

Figure 4.10: Comparison of real and imaginary parts of the source signals, the estimated signals using likelihood-based BSS algorithm and the estimated signals using natural gradient-based BSS algorithm: 16-QAM and 64-QAM; Rate of the change of the dual-polarized channel: 1.3 ms; SNR = 20 dB ; Number of symbols: 20000.

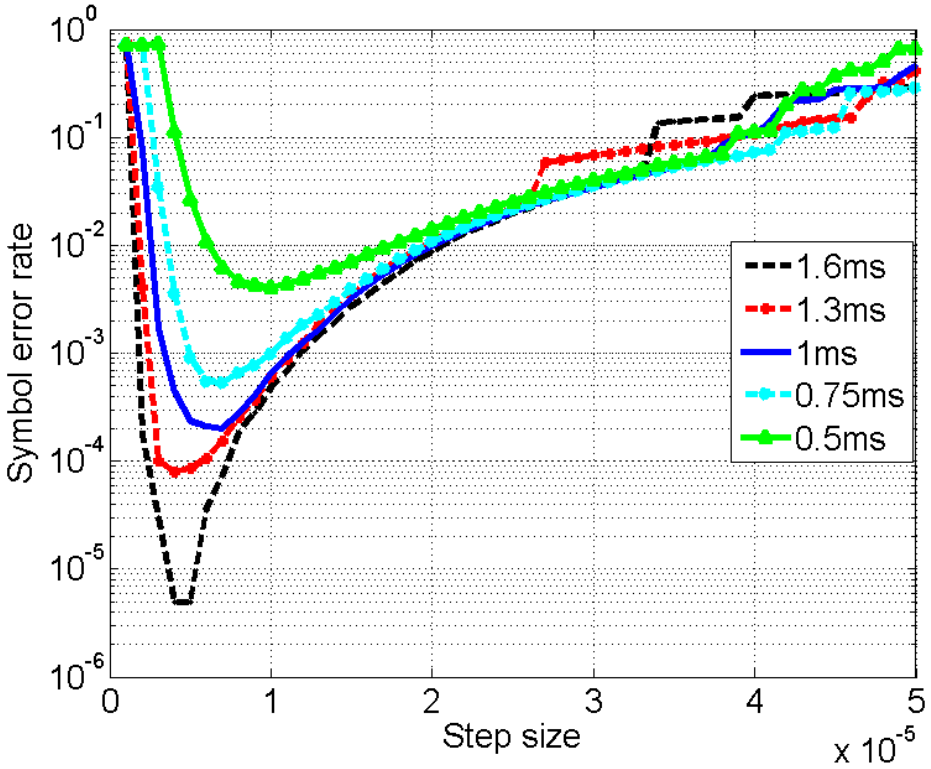

(a) The likelihood-based BSS algorithm.

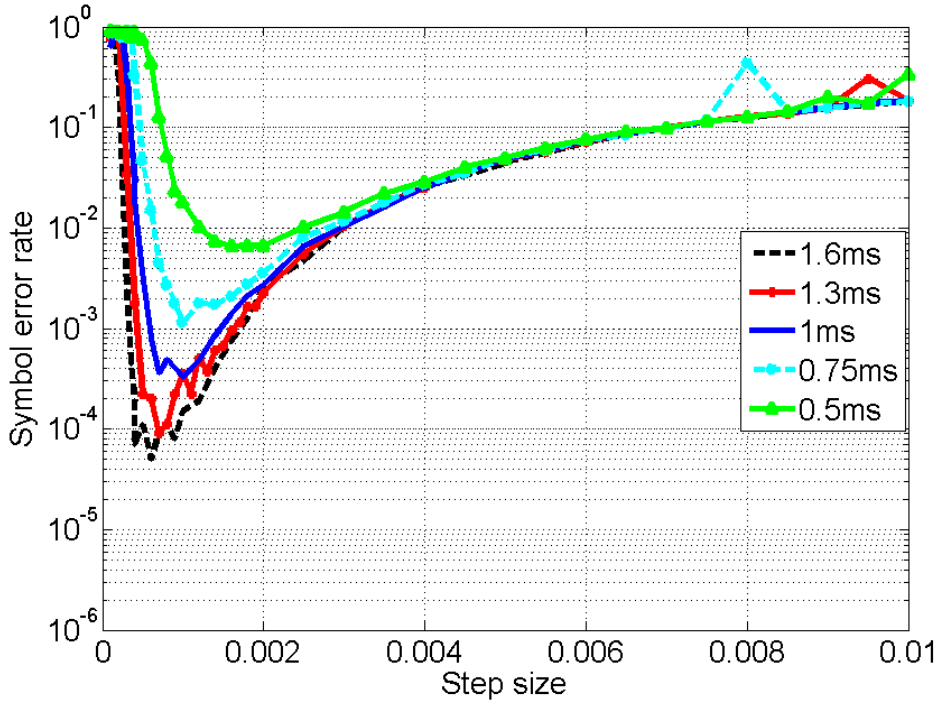

(b) The natural gradient-based BSS algorithm.

Figure 4.11: Symbol error rate with different step size in the adaptive BSS algorithms under different time-varying dual-polarized channels: 16-QAM and 32-QAM signals; Channel 1: 16-QAM signals; SNR = 20 dB; Number of symbols: 20000.

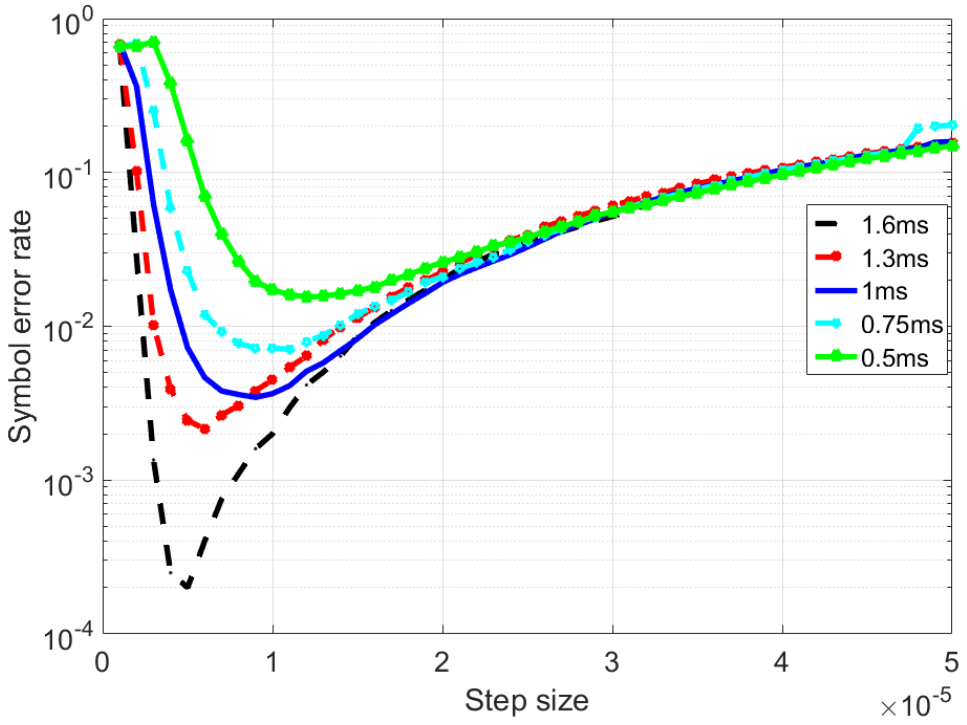

(a) The likelihood-based BSS algorithm.

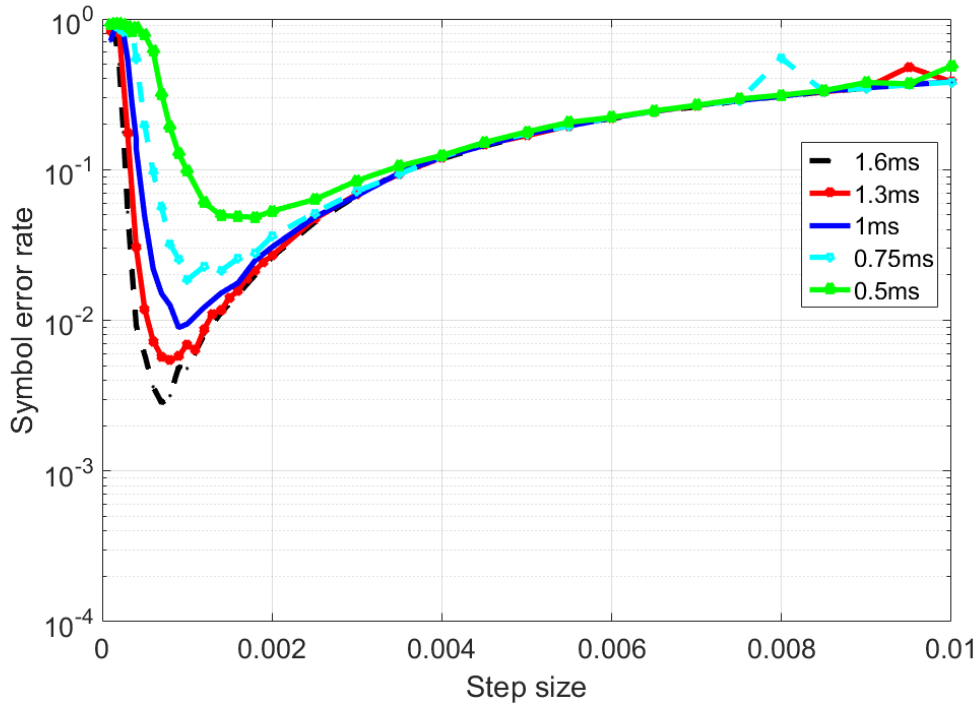

(b) The natural gradient-based BSS algorithm.

Figure 4.12: Symbol error rate with different step size in the adaptive BSS algorithms under different time-varying dual-polarized channels: 16-QAM and 32-QAM signals; Channel 2: 32-QAM signals; SNR = 20 dB; Number of symbols: 20000.

We can also conclude that the smallest error of the likelihood-based BSS algorithm is substantially smaller than the corresponding values for the natural gradient-based BSS algorithm. This indicates that the likelihood-based BSS algorithm is a more efficient estimator than the natural gradient-based BSS algorithm for the time-varying dual-polarized channels.

Figure 4.13, 4.14, 4.15 and 4.16 present the comparison between SERs for different modulation types by applying the likelihood-based BSS algorithm and the natural gradient-based BSS algorithm for the received signals. The results shown in the figures use the step size that resulted in the smallest error based on the results in Figure 4.11 for each method at different SNRs. Figure 4.13 and 4.15 show the results when the two input signals were 16-QAM with 32-QAM signals and Figure 4.14 and 4.16 display the results for 16-QAM with 64-QAM signals. The SNR value is ranged from 0 to 30 dB. The rates of the change of the dual polarization were 1.3 ms and 1ms.

From the comparisons in these figures, we see that the SERs of the separated signals of the likelihood-based BSS algorithm are higher than those of the natural gradient-based BSS algorithm at lower SNRs. When SNR increases, the SERs of the separated signals of the likelihood-based BSS algorithm are smaller than that of the natural gradient-based BSS algorithm. This indicates that the likelihood-based BSS algorithm can outperform the natural gradient-based BSS algorithm for the separation above a specific SNR.

We also notice from the results that the SERs of the estimated signals decrease when SNR increases. At high SNRs, the SERs are dominated by the source separation errors. This results in essentially no reduction in SERs with increasing SNR after some threshold.

This happens because the BSS algorithm introduces a residual error into the separated signals during the blind separation process. At higher SNRs, the effect of this error on SERs will dominate the error compared with the effect of channel noise. The residual error power will depend on the rate of time variations in the dual-polarized channel and the step size of the adaptive separation system. Thus, the performance of the receiver or other types of processors of the separated signals is limited by these separation errors. Performance analysis of BSS algorithms and similar behavior at high SNRs can be found in [42] and [43].

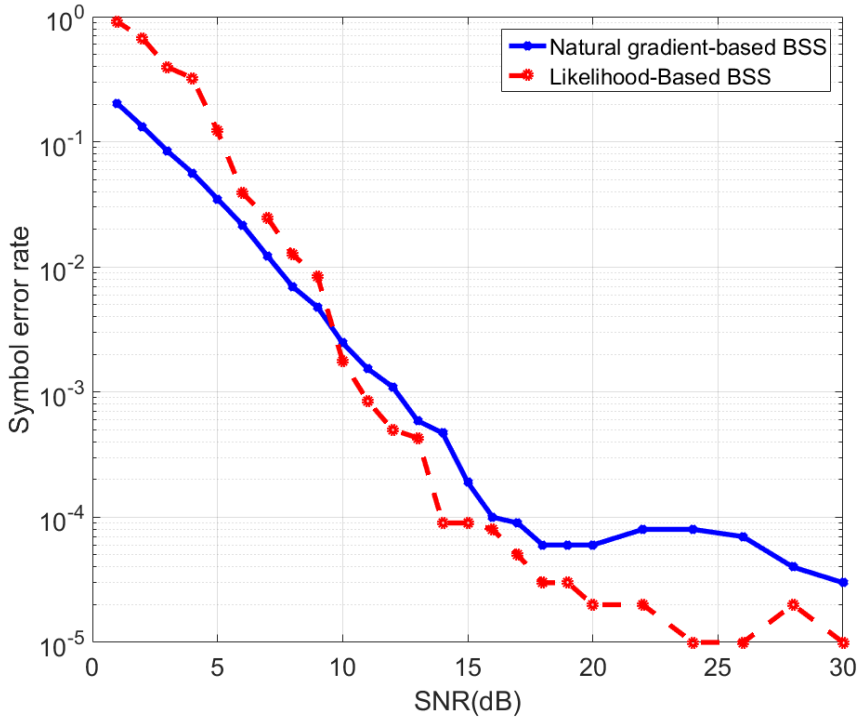

(a) 16-QAM

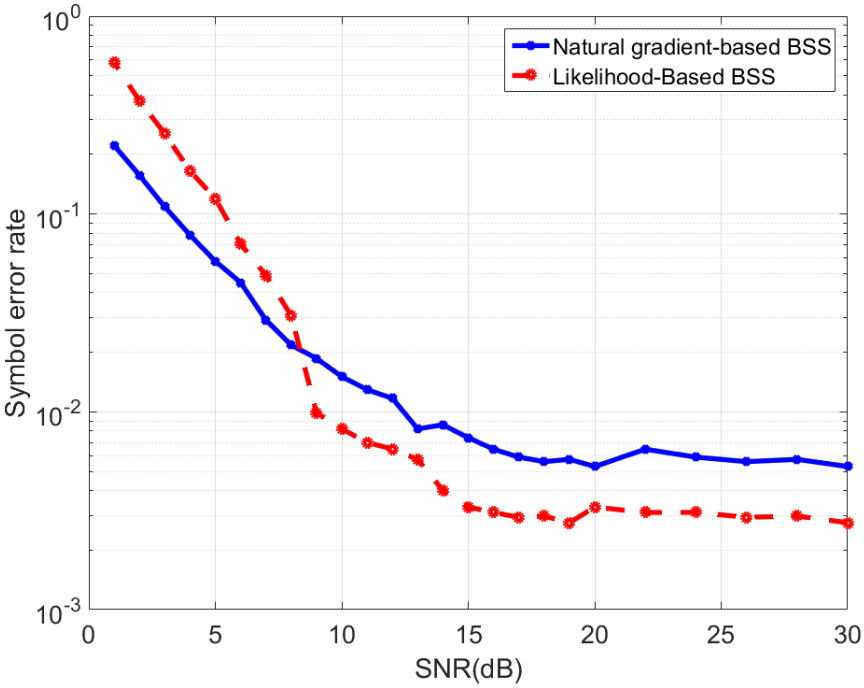

(b) 32-QAM

Figure 4.13: Comparison between SERs of separated signals after the likelihood-based BSS and the natural gradient-based BSS and the theoretical SERs at different SNRs: 16-QAM and 32-QAM; Rate of the change of dual-polarized channel: 1.3 ms; SNR=20 dB; Number of symbols: 20000.

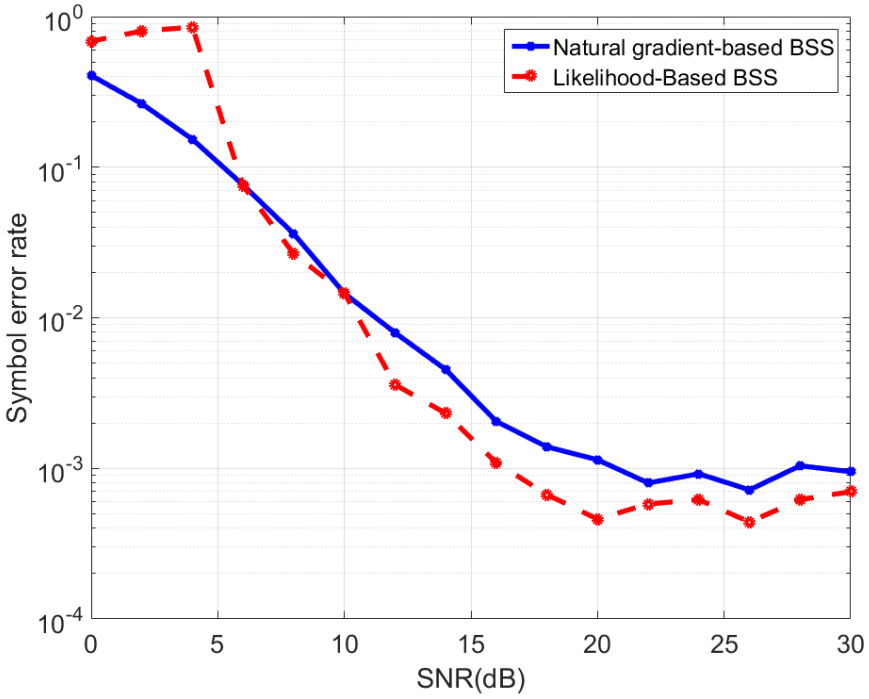

(a) 16-QAM

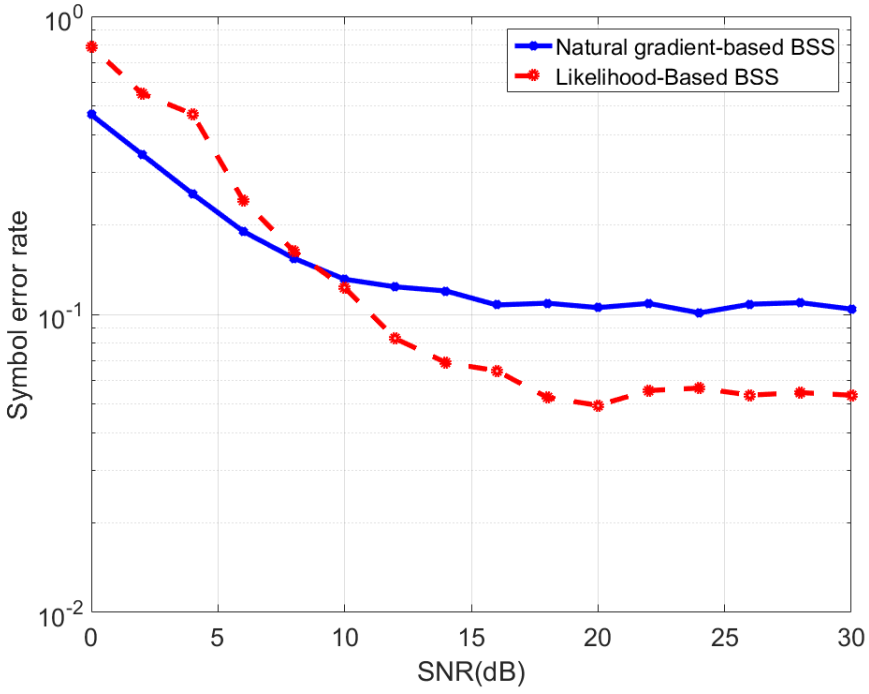

(b) 64-QAM

Figure 4.14: Comparison between SERs of separated signals after the likelihood-based BSS and the natural gradient-based BSS and the theoretical SERs at different SNRs: 16-QAM and 64-QAM; Rate of the change of the dual-polarized channel: 1.3 ms; SNR=20 dB; Number of symbols: 20000.

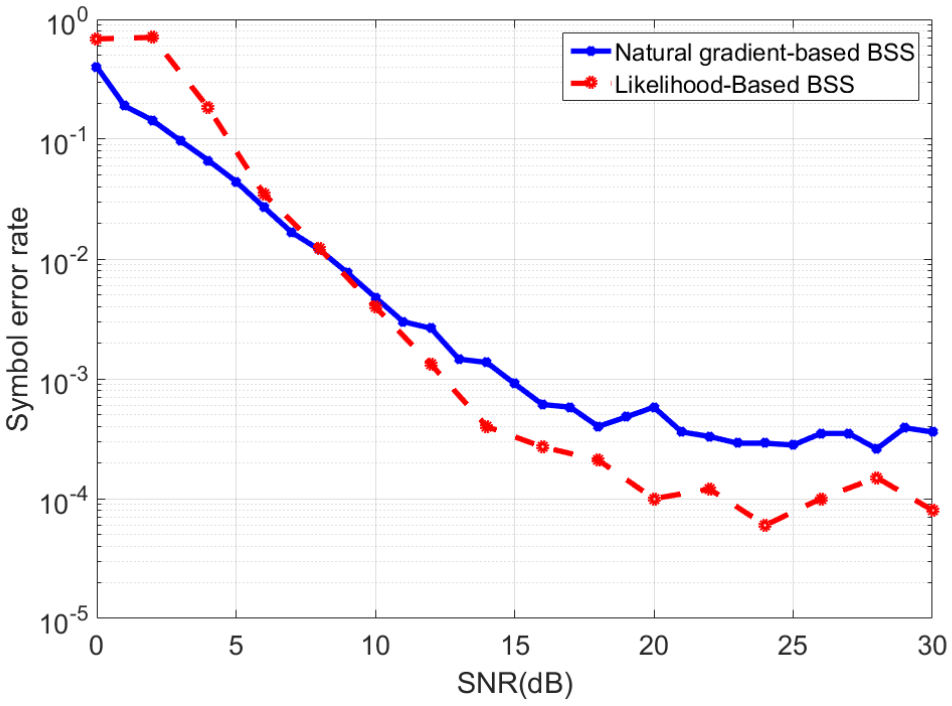

(a) 16-QAM

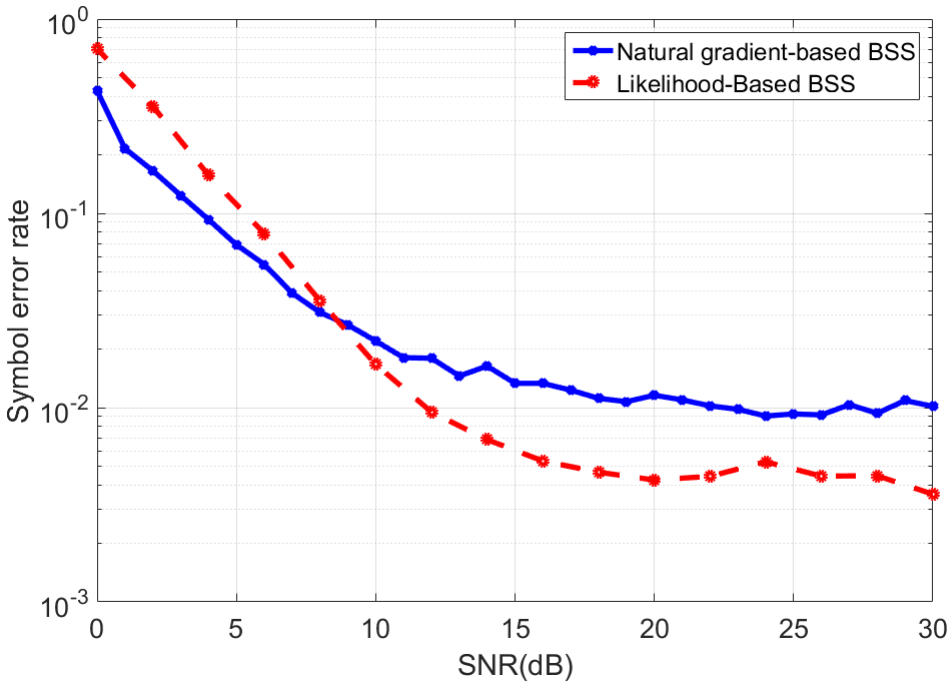

(b) 32-QAM

Figure 4.15: Comparison between SERs of separated signals after the likelihood-based BSS and the natural gradient-based BSS and the theoretical SERs at different SNRs: 16-QAM and 32-QAM; Rate of the change of the dual-polarized channel: 1 ms; SNR=20 dB; Number of symbols: 20000.

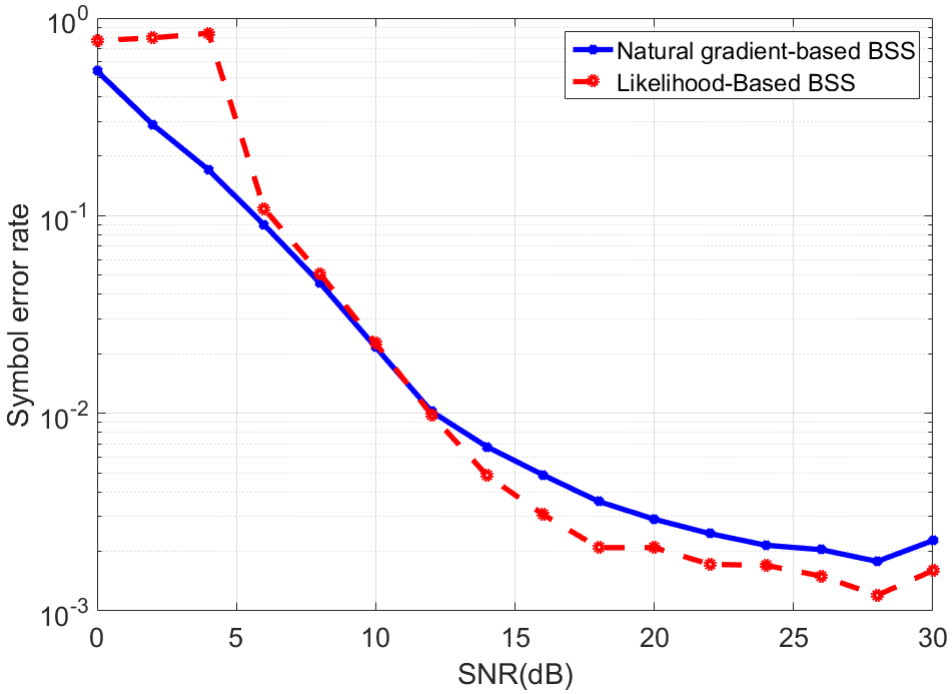

(a) 16-QAM

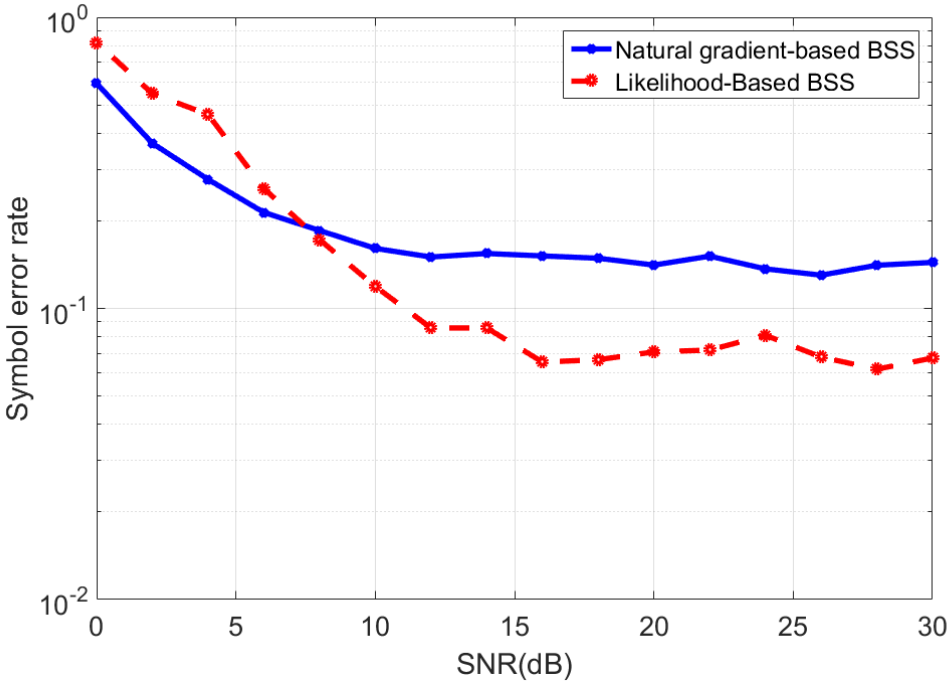

(b) 64-QAM

Figure 4.16: Comparison between SERs of separated signals after the likelihood-based BSS and the natural gradient-based BSS and the theoretical SERs at different SNRs: 16-QAM and 64-QAM; Rate of the change of the dual-polarized channel: 1 ms; SNR=20 dB; Number of symbols: 20000.

4.3 Modulation Identification

In this section, the probability of correct modulation identification of the signals in time-varying dual-polarized channels when combining the likelihood-based BSS algorithm with the likelihood-based modulation identification algorithm is presented. The results for the signals in the dual-polarized channel with different SNRs are presented first. Next, the probability of correct modulation for the signals in different dual-polarized channels is shown. Finally, the probability of correct modulation identification for the signals with different signal length is demonstrated. In this section, 100 independent runs were used to calculate the probability of correct modulation identification.

4.3.1 Probability of Correct Modulation Identification of Signals with Different SNRs

Figure 4.17 presents the probability of correct modulation identification of the signals in time-varying dual-polarized channels with different SNRs. The number of symbols was 20000. The rate of the change of the dual-polarized channel was 1.3 ms.

The results indicate that the system can identify the signals with different modulation types accurately at sufficient low SNRs. For example, the system can identify 16-QAM and 32-QAM signal with 99% accuracy at SNR above 8 dB. When the orders of the modulation type of the signals increase, the higher SNRs are needed in order to obtain accurate identification results.

Comparing with the identification results for the signal in a single noisy environment shown in Chapter 3, the probability of correct identification for the signal in the dual-polarized channel needs higher SNRs and longer signal length to obtain accurate results. For example, the likelihood-based modulation identification algorithm can identify 16-QAM with 99% accuracy at SNR above -1 dB with 10,000 symbols for the signals in single AWGN channels.

This is expected because the source separation brings more errors to the signals in the process. Due to these errors, the estimation errors when applying the likelihood-based modulation identification algorithm increase. As a result, the system needs higher SNRs and longer signal length in order to achieve accurate results.

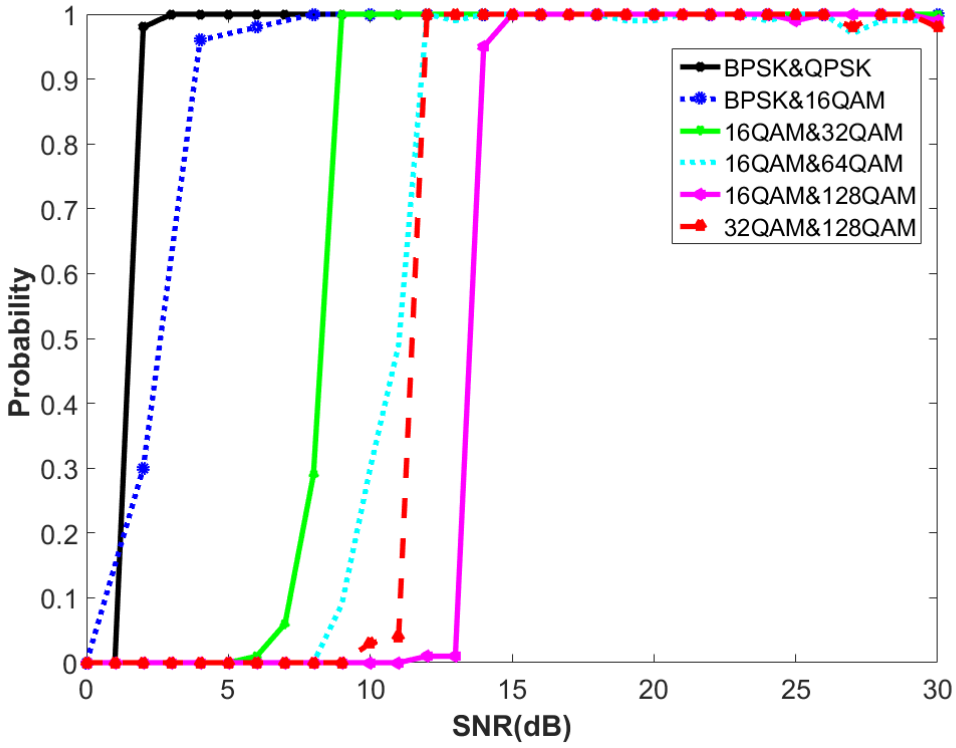

Figure 4.17: Probability of correct modulation identification of the signals in dual-polarized channel at different SNRs: Number of symbols: 20000; Rate of the change of the dual-polarized channel: 1.3 ms.

4.3.2 Probability of Correct Modulation Identification of Signals in Different Time-varying Dual-polarized Channels

Figure 4.18 presents the probability of successful modulation identification of the signals in different time-varying dual-polarized channels. The periods of the change of the channels included in this figure were 0.5 ms, 0.75 ms, 1 ms, 1.3 ms and 1.6 ms. The modulation types of the two input signals are 16-QAM and 32-QAM. The number of symbols was 20000.

We can observe from the figure that the system identifies the modulation types accurately with slightly lower SNRs when the period of the change of the channel is larger (change of the channels is slower). This is due to the separation error of the likelihood-based blind source separation algorithm in the process. From the results shown in Section 4.2.3, the separation error increases when the change of the channel is faster.

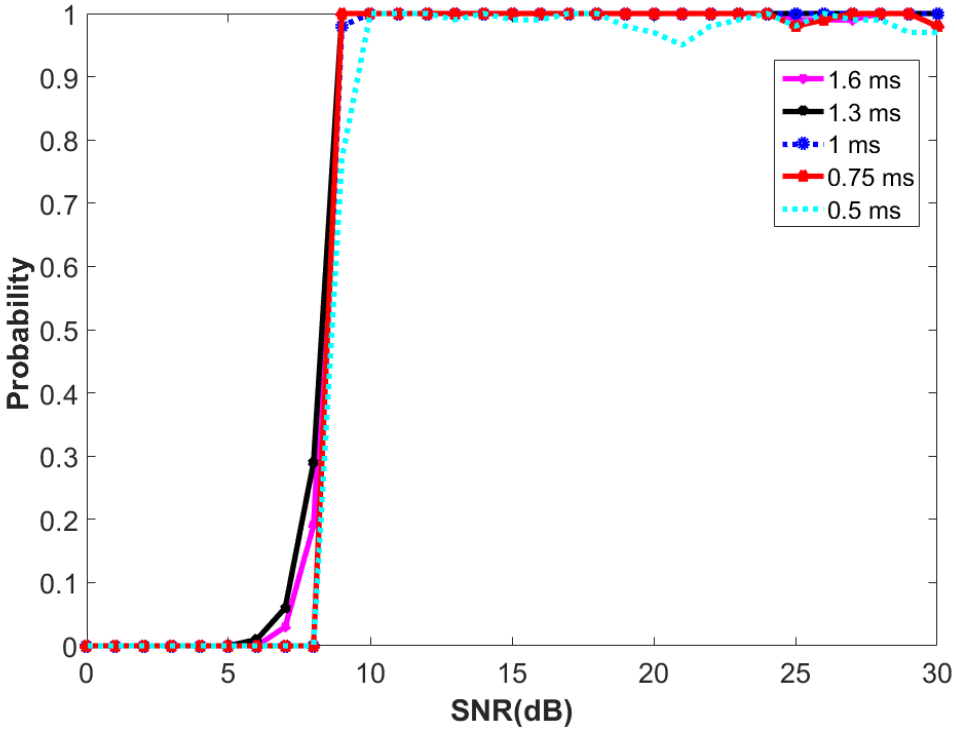

Figure 4.18: Probability of correct modulation identification of the signals in different dual-polarized channel: 16-QAM and 32-QAM signals; Number of symbols: 20000.

4.3.3 Probability of Correct Modulation Identification of Signals with Different Signal Length

Figure 4.19 presents the probability of correct modulation identification of the signals with different signal length. The rate of change in the channel was 1.3 ms. SNR in this example was 20 dB.

The results show that the system can identify the modulation types with 99% accuracy with shorter signal length at sufficient high SNRs. For example, the system is able to identify BPSK and 16-QAM signals above 99% accuracy with 10,000 symbols. When the order of the modulation type increases, the system needs longer signal length in order to achieve accurate identification results.

Comparing with the performance of the modulation identification of the signal in single AWGN channels, the system needs more symbols in order to get accurate modulation identification for the signal in dual-polarized channels.

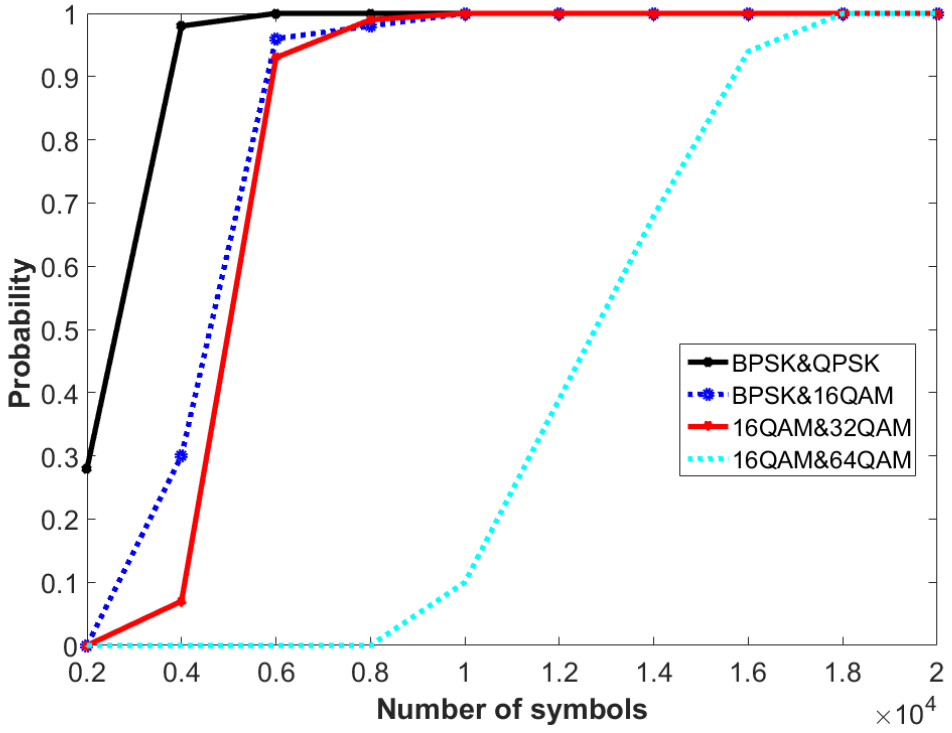

Figure 4.19: Probability of correct modulation identification of the signals in dual-polarized channel with different signal length: SNR=20 dB; Rate of the change of the dual-polarized channel: 1.3 ms.

4.4 Conclusions

This chapter presented a likelihood-based blind separation method for QAM and PSK signals in time-varying dual-polarized channels. The performance indicated that the likelihood-based adaptive blind source separation in this paper can recover the signals from the dual-polarized channels. The system recovered the signal with small symbol error rates in a wide range of different SNR values. This algorithm also tracks the coefficients well. In addition, the smaller symbol error rate of applying the likelihood-based BSS algorithm suggests that the likelihood-based BSS algorithm can outperform the natural gradient-based BSS algorithm for separating the signals in dual-polarized channels.

Furthermore, combining the likelihood-based BSS algorithm with the likelihood-based modulation identification algorithm demonstrated accurate identification results for the signals in dual-polarized channels with relatively high symbol length and sufficient high SNRs. For example, the system can identify 16-QAM and 32-QAM signal with 99% ac-

curacy at SNR above 8 dB with 20,000 symbols. When the orders of the modulation type of the signals increase, higher SNRs in the system are needed in order to obtain accurate identification results. Comparing with the identification results for the signal in a single noisy environment in Chapter 3, the probability of correct identification for the signal in the dual-polarized channels needs higher SNRs and longer signal length to obtain accurate results.

The algorithm needs to be improved in order to identify the modulation types of the signals in dual-polarized channels with lower number of symbols and at lower SNRs. More performance evaluation of the algorithm such as the sensitivity of the likelihood-based BSS algorithm to the rate of the change of the dual-polarized channels and the capacity of the modulation identification combining the likelihood-based BSS algorithm and the modulation identification also needs to be studied.

CHAPTER 5

SUMMARY AND FUTURE WORK

This chapter includes two parts. Section 5.1 presents the summary of this dissertation. Then, the future work is introduced in Section 5.2.

5.1 Summary

This dissertation described the algorithms for blind modulation identification of the PSK and QAM signals in three different environments: single AWGN channel, dual-polarized channel with noise and multipath channel with noise.

First of all, the algorithms utilized the likelihood functions of the amplitude and phase for the PSK and QAM signals, which is a new method for blind modulation identification for PSK and QAM signals. This method does not need any information from the transmitter and is able to identify the PSK and QAM types with high accuracy under relatively lower SNRs compared with other existing methods.

Second, this dissertation included the likelihood-based blind source separation algorithm for the signals in the dual-polarized channels. This algorithm focused on tracking the time-varying dual polarization and on separating the mixed signals at the receiver. This algorithm is able to track the time-varying dual-polarized channels with a different speed of rotation. Furthermore, combining the likelihood-based BSS algorithm and the likelihood-based modulation identification algorithm demonstrates accurate identification results for the QAM and PSK signals in dual-polarized channels.

Furthermore, the combination of the CMA equalizer and likelihood-based modulation identification algorithm demonstrated good performance of identifying the modulation types of the signals in multipath channels. Further modification and performance evaluation is worth studying in the future.

5.2 Future Work

There are several aspects that need to be improved based on the algorithms developed in this dissertation.

First, the likelihood-based modulation identification algorithm for PSK and QAM signals in AWGN channels needs to be improved for the signals with shorter symbol durations. The modification of this algorithm may be done by decreasing the estimation errors on the signal parameters such as baud rate, noise variance and so on. The theoretical analysis also suggested that if the effect of the estimation errors on the model can be counted into the likelihood functions, the performance of the modulation identification may be improved. In addition, the joint PDF considering both the amplitude and phase of the signals can be studied for the likelihood functions.

Second, for the signals in time-varying dual-polarized channels, the performance capabilities of the receiver may be limited by fast variations in the dual-polarized channels and residual separation errors in the separation process. More modifications of the BSS algorithm to faster variations in the channels need to be developed. This can be improved in two ways. On one hand, the optimization of the step size in the likelihood-based BSS algorithm needs to be developed in order to track the change of the channel coefficients better. Section 5.2.1 presents a combinational method for the adaptive BSS algorithm. However, the preliminary results indicate that the combinational method can achieve the better one among the two BSS algorithms. A better optimization scheme considering the step size may be designed. On the other hand, in order to increase the accuracy of the system, the adaptive BSS method that can track the phase of the coefficients in the dual-polarized channels may be developed.

Finally, more accurate modulation identification algorithms for the signals in multipath channels need to be developed. In one aspect, the modification of the blind equalizer can be done to decrease the errors of the estimated signals. Also, the modification of the likelihood functions considering the effect of the multipath in the channels can increase the accuracy of modulation identification. Section 5.2.2 presents a modified likelihood-based modulation algorithm considering the change of the amplitude distribution of PSK signals in two-path channels. What's more, the signal in multipath channels has the feature of sparsity. The methods such as dictionary learning for equalizing the signals in multipath

channels can be explored. Section 5.2.3 introduces the basic idea of applying the dictionary algorithm for estimating the symbols and channel coefficients for the signal in multipath channels. More studies need to be done for the application of the dictionary algorithm.

5.2.1 Convex Combination Method for Adaptive BSS Algorithm

The speed of the time-varying dual polarization of the transmission is unknown. In this case, the capability of tracking of the time-varying channel coefficients with fast convergence and high accuracy is necessary in order to achieve better performance of separation and identification of the input signals. As shown in Chapter 4, the step size of the adaptive BSS algorithm determines the performance of separation.

To achieve better performance of the adaptive BSS algorithm, the combinational step size method is designed to find the optimum step size and achieve lower mean square errors (MSEs) after convergence. The combination method for the adaptive BSS is demonstrated in Figure 5.1.

In the first stage, two adaptive BSS algorithms with two step sizes will be utilized. One step size is larger in order to achieve faster convergence speed; another one is smaller to decrease the MSEs after convergence. In the second stage, the combination of the two adaptive system will be applied. The combination is implemented in such way that the final estimated signal will be a scaled summation of the two initial estimated signals in the

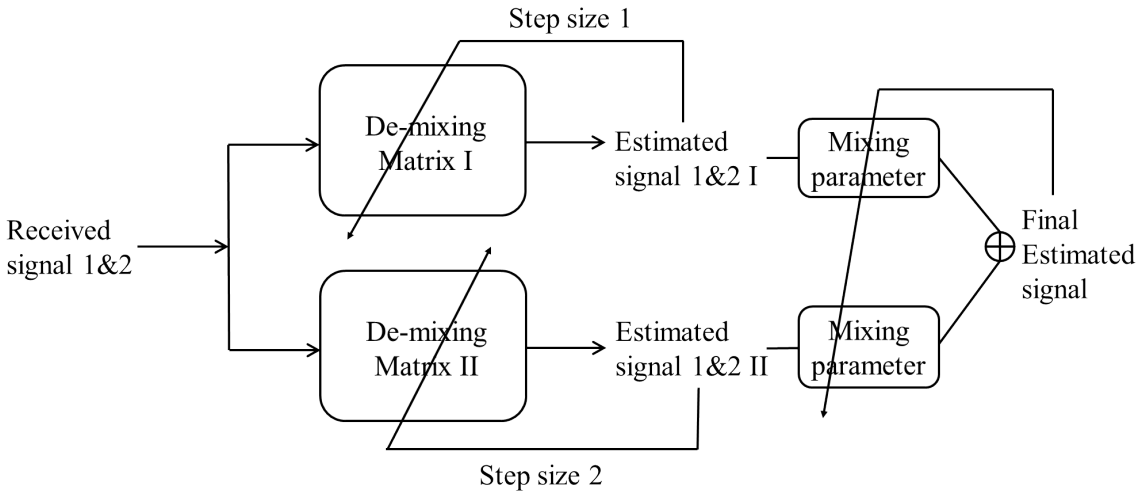

Figure 5.1: Block diagram of adaptive BSS algorithm implementing combination step size method.

first stage. The scaling factor is updated using the final estimated signals so that the fast convergence and small errors can be achieved at the same time.

The algorithm is described in Table 5.1.

The cost function for updating the mixing parameter $\lambda(t)$ is the likelihood function for $\tilde{Z}(t)$ as described in (4.5). In order to distinguish between the likelihood functions for different signals, here $\tilde{C}(t)$ is represented as the cost function for $\tilde{Z}(t)$. The update equation for $\lambda(t)$ will be

$$\lambda(t+1) = \lambda(t) + \mu_\lambda \frac{d\tilde{C}(t)}{d\lambda(t)} \tag{5.1}$$

where μ_λ is a constant step size.

The gradient can be expressed as

$$\frac{d\tilde{C}(t)}{d\lambda(t)} = \frac{d\tilde{C}(t)}{d|\tilde{Z}(t)|}\frac{d|\tilde{Z}(t)|}{d\lambda(t)} \tag{5.2}$$

The first part in the gradient $\frac{d\tilde{C}(t)}{d|\tilde{Z}(t)|}$ is the same as in (4.9). The second part is derived as

$$\frac{d|\tilde{Z}(t)|}{d\lambda(t)} = \frac{d\sqrt{\Re^2\{\tilde{Z}(t)\} + \Im^2\{\tilde{Z}(t)\}}}{d\lambda(t)}$$

$$= \frac{1}{|\tilde{Z}(t)|}(2\Re\{\tilde{Z}(t)\}\frac{d\Re\{\tilde{Z}(t)\}}{d\lambda(t)} + 2\Im\{\tilde{Z}(t)\}\frac{d\Im\{\tilde{Z}(t)\}}{d\lambda(t)}) \tag{5.3}$$

The real and imaginary parts of $\tilde{Z}(t)$ are written as

$$\Re\{\tilde{Z}(t)\} = \lambda(t)\Re\{Z_1(t)\} + (1-\lambda(t))\Re\{Z_2(t)\} \tag{5.4}$$

$$\Im\{\tilde{Z}(t)\} = \lambda(t)\Im\{Z_1(t)\} + (1-\lambda(t))\Im\{Z_2(t)\} \tag{5.5}$$

Then, the gradient in (5.3) is

$$\frac{d|\tilde{Z}(t)|}{d\lambda(t)} = \frac{1}{|\tilde{Z}(t)|}[2\Re\{\tilde{Z}(t)\}(\Re\{Z_1(t)\} - \Re\{Z_2(t)\}) + 2\Im\{\tilde{Z}(t)\}(\Im\{Z_1(t)\} - \Im\{Z_2(t)\})] \tag{5.6}$$

Table 5.1: The convex combination method of the adaptive BSS algorithm

First stage:
$Z_1(t) = Q_1(t)Y(t)$
$Q_1(t+1) = Q_1(t) + \mu_1 \frac{dC_1(t)}{dQ_1(t)}$
$Z_2(t) = Q_2(t)Y(t)$
$Q_2(t+1) = Q_2(t) + \mu_2 \frac{dC_2(t)}{dQ_2(t)}$
Second stage:
$\tilde{Z}(t) = \lambda(t)Z_1(t) + (1-\lambda(t))Z_2(t)$

Figure 5.2 shows the constellation maps of separated signals after applying two likelihood-based BSS algorithms with different step size and after implementing the combination of these two likelihood-based BSS algorithms. In this example, the two input source signals were 16-QAM and 32-QAM signals. The number of symbols were 20000. The SNR was 20dB. The number of samples per symbol was 20. The rate of the change of the dual-polarized channel was 1.3 ms. We can see that using different step size in the BSS algorithm changes the performance of the separation of the signals in time-varying dual-polarized channels. The combination of the two likelihood-based BSS algorithms with different step sizes can achieve the better separation among these two BSS algorithms.

5.2.2 A Modified Amplitude Likelihood-based Modulation Identification Algorithm for PSK Signals in Two-path Channels

The amplitude or phase distributions of the PSK and QAM signals in the multipath channels do not have distinct features as clean as the PSK and QAM symbols. The symbol patterns will be more complex when there exists more paths in the channels. When there are a smaller number of paths in the channel, the signal still shows some distinct features for the amplitude distributions of different modulation types. Thus, direct application of the likelihood-based modulation identification by changing the PDF of the amplitude to the corresponding distribution for the signals in the multipath channels may be able to identify the modulation types. This section provides a derivation of the modified likelihood functions of the PSK signals in a two-path channel. The goal is to show feasibility of such an approach. Further explorations are left for future work.

Figure 5.3 shows the detailed block diagram of the modified likelihood-based modulation identification algorithm for signals in multipath channels. The system estimates the baud rate first in order to subsample the received signal. Then, the method using the correlation coefficients of subsampled signals is applied to estimate the amplitude and time-delay for the multipath channels. Finally, the likelihood functions including the effect of the multipath are implemented to identify the modulation type.

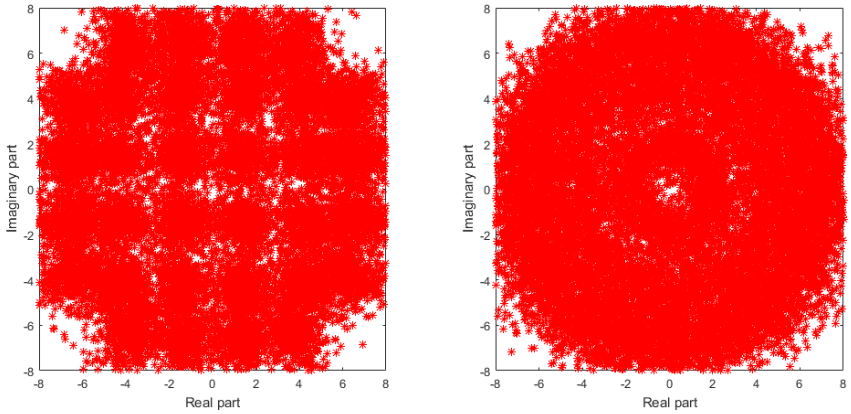

(a) Step size 1

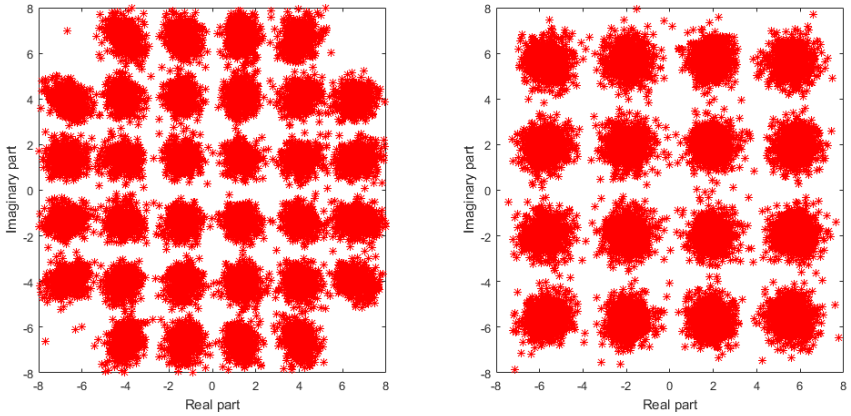

(b) Step size 2

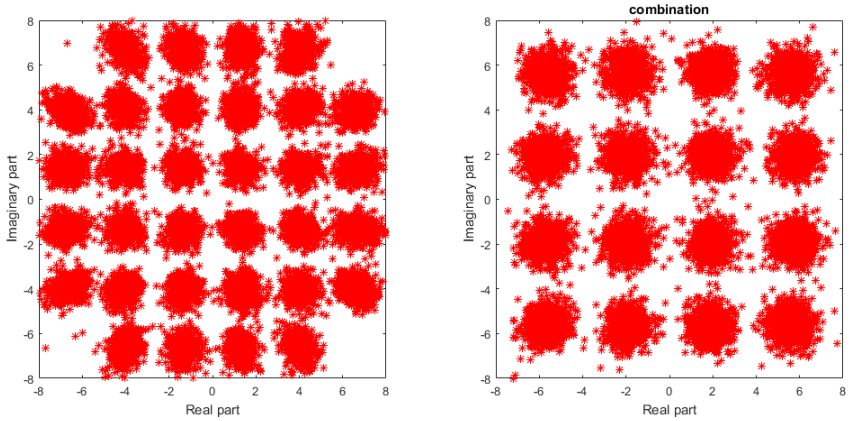

(b) Combination of the two step sizes

Figure 5.2: Comparison of the constellation maps of the separated signals before and after applying the combination of the BSS algorithm: 16-QAM and 32-QAM; Number of symbols: 20000; SNR: 20dB; Number of samples per symbol: 20; Rate of the change of the dual-polarized channel: 1.3 ms.

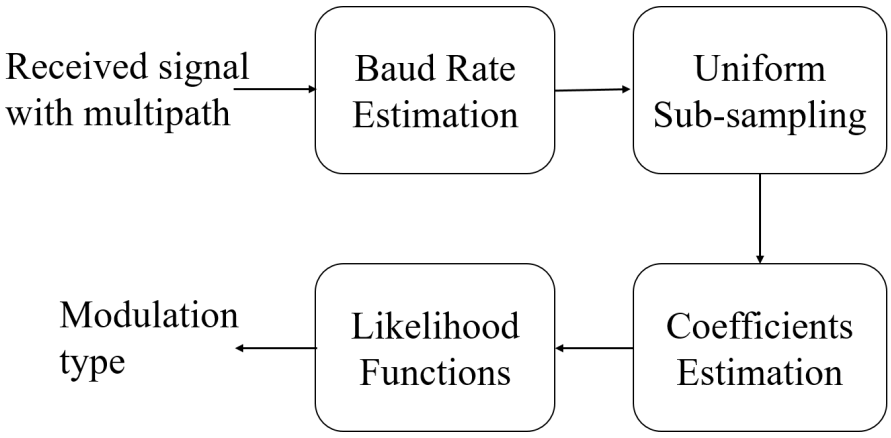

Figure 5.3: Block diagram of the modified likelihood-based modulation identification for the signals in multipath channels.

5.2.2.1 PDF of the Amplitude of the Signals in Multipath Channels

In order to derive the likelihood functions of the signals in multipath channels, the PDF of amplitude of the signals is derived first.

Based on the sampled version of the signals with noise in Chapter 3, the sampled version of the signal in multipath channels with noise can be described as

$$y_c(n) = \sum_i a_m \sum_k (s_k g_T(nT_s - kT_b - mT_s)) e^{j2\pi f_c (nT_s - mT_s)} + N_0(nT_s) \tag{5.7}$$

where a_m is the power of each path and m is the coefficients of the time delay.

When the signal is in a two-path channel, the signal model can be written as

$$\begin{aligned} y_c(n) = a_0 \sum_k (s_k g_T(nT_s - kT_b)) e^{j2\pi f_c nT_s} \\ + a_m \sum_k (s_k g_T(nT_s - kT_b - mT_s)) e^{j2\pi f_c (nT_s - mT_s)} + N_0(nT_s) \end{aligned} \tag{5.8}$$

Let $y_m(l)$ represent the subsampled signals at l_{th} baud, which can be modeled as

$$y_c(l) = a_0 s_l g_T(0) e^{j2\pi f_c l T_b} + a_m s_{l-m} g_T(mT_s) e^{j2\pi f_c l T_b} e^{-j2\pi f_c m T_s} + N_0(l) \tag{5.9}$$

This signal model is also a sinusoidal signal with a Gaussian noise, where the symbols for the sinusoid signal are

$$s_c = a_0 s_l g_T(0) + a_m s_{l-m} g_T(mT_s) e^{-j2\pi f_c m T_s} \tag{5.10}$$

The PDF of the amplitude for this signal $y_c(l)$ will be the same as (3.27) in Chapter 3 by changing the amplitude values in the PDF into the corresponding values created by the multipath.

In order to obtain the amplitude for the symbols s_c in (5.10), a constant is defined as

$$a = \frac{a_m g_T(mT_s)e^{-j2\pi f_c mT_s}}{a_0 g_T(0)} \tag{5.11}$$

The symbols are now simplified as

$$\hat{s}_c = s_l + as_{l-m} \tag{5.12}$$

If $m < T_b/T_s$, the symbols of the signals in two-path channels after subsampling is a scaled version of the source symbols. If $m > T_b/T_s$, then the symbols of the signals in the two-path channels after subsampling will be a scaled combination of the symbols of the source signals. For example, for a QPSK signal, it has four symbols. After it is transmitted through a two-path channel, the symbols contained in the signal will have 16 symbols as shown in Table 5.2.

Figure 5.4 shows the constellation maps and histograms of the amplitude of different PSK signals in a two-path channel after subsampling. In this example, the number of samples per symbol T_b/T_s is 20. The time delay in this simulation was 35 samples. The multipath amplitudes were $a_0 = 1, a_m = 0.5$. The number of symbols was 20000.

From these figures, we can see that the constellation maps and histograms of the PSK signals with multipath will be different from those of the PSK signals in AWGN channels.

The number of distinct amplitudes for each modulation type for a PSK signal in a two-path channel is listed in Table 5.3.

When the order of the modulation types increases, the number of symbols and the amplitude values increase rapidly. From this, directly applying the amplitude groups of signals with multipath into the likelihood-based ID algorithm is useful for low-order modulation types. Table 5.4 lists the amplitudes distributions of the symbols for PSK signals in two-path channels after subsampling.

Table 5.2: QPSK symbols after transmitting through a two-path channel

Symbols of QPSK signals	1+1j	1-1j	-1-1j	-1+1j
	(1-a)+(1-a)j	(1+a)+(1-a)j	(1+a)+(1+a)j	(1-a)+(1+a)j
Symbols of	-(1-a)-(1-a)j	-(1-a)-(1-a)j	-(1-a)-(1-a)j	-(1-a)-(1-a)j
QPSK signals	(a-1)+(1-a)j	-(1+a)+(1-a)j	-(1+a)+(1+a)j	-(1-a)+(1+a)j
with one reflection	(1-a)-(1-a)j	(1+a)-(1-a)j	(1+a)-(1+a)j	(1-a)-(1+a)j

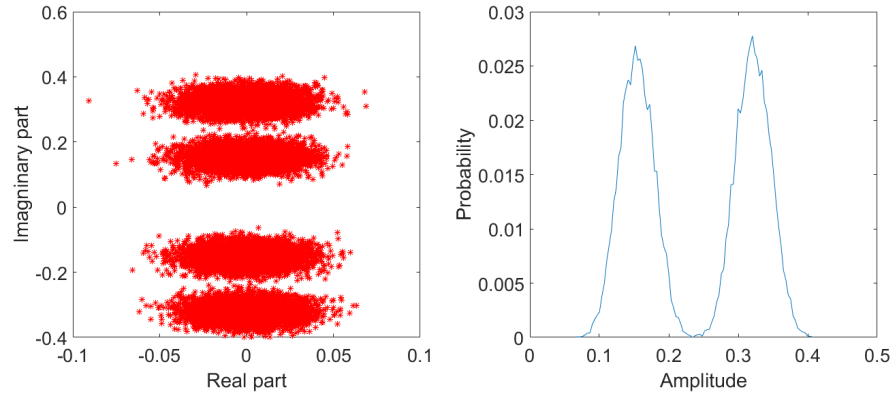

(a) BPSK

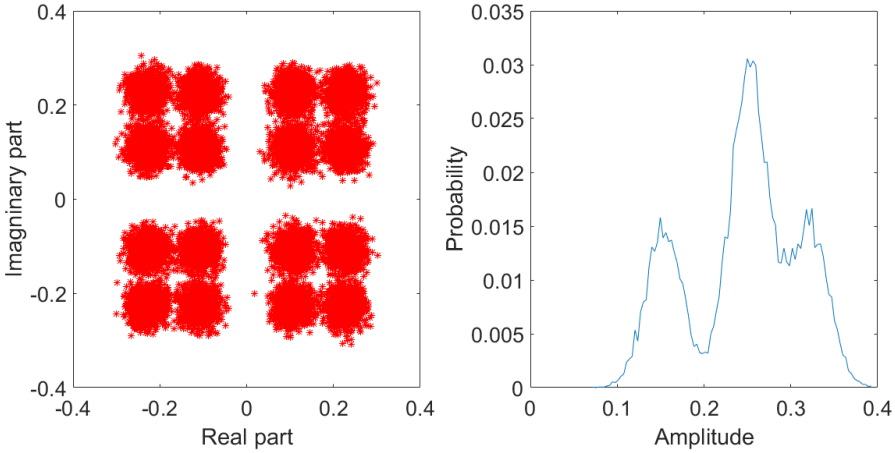

(b) QPSK

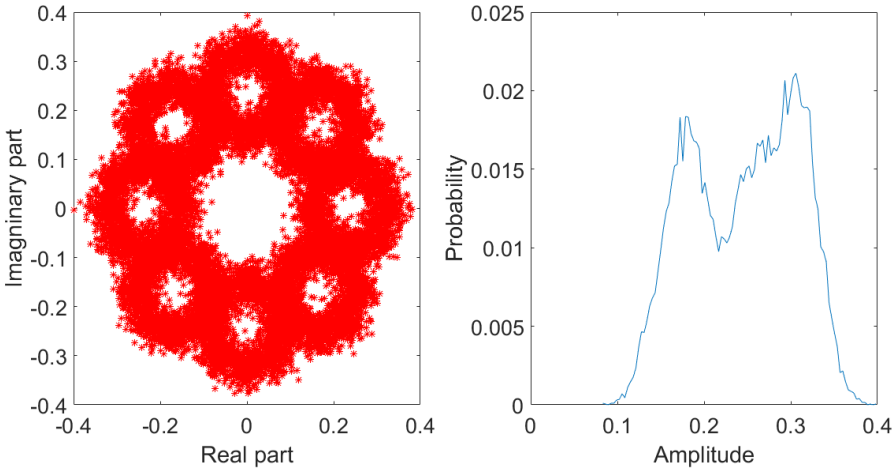

(b) 8PSK

Figure 5.4: Constellation maps and histograms of the amplitude of PSK signals in a two-path channel: $a_0 = 1, a_m = 0.5, m = 35$; Number of symbols: 20000; Number of samples per symbol: 20; SNR = 20 dB.

Table 5.3: Number of symbols and amplitudes of signals with two path

Type	Number of Symbols	Number of Amplitudes
BPSK	4	2
QPSK	16	3
8PSK	64	5

Table 5.4: Amplitudes of the PSK signals in two-path channels

Type	Amplitudes	Probability
BPSK	[1-a, 1+a]	$[\frac{1}{2}, \frac{1}{2}]$
QPSK	[1-a, $\sqrt{(1+a^2)}$, 1+a]	$[\frac{1}{4}, \frac{1}{2}, \frac{1}{4}]$
8PSK	[1-a,1+a, $\sqrt{(1+a^2)}$, $\sqrt{(1+\sqrt{2}a+a^2)}$, $\sqrt{(1-\sqrt{2}a+a^2)}$]	$[\frac{1}{8}, \frac{1}{8}, \frac{1}{4}, \frac{1}{4}, \frac{1}{4}]$

5.2.2.2 Estimation of Channel Coefficients for Signals in Two-path Channels

In order to obtain the corresponding amplitude values for different PSK signals in two-path channels, the constant scaled factor a must be estimated. In this section, an algorithm for estimating this parameter implementing the auto-correlation coefficients of the signals after subsampling is introduced.

From (5.9), the auto-correlation coefficients of $y_c(l)$ with different time lags can be derived as

$$\begin{aligned}
&\rho_{y_c}(p) = E\{y_c(l)y_c^*(l+p)\} \\
&= E\{[a_0 s_l g_T(0)e^{j2\pi f_c l T_b} + a_1 s_{l-m} g_T(mT_s)e^{j2\pi f_c l T_b}e^{-j2\pi f_c m T_s} + N_0(l)] \\
&[a_0 s_{l+p}^* g_T(0)e^{-j2\pi f_c(lT_b+pT_s)} + a_1 s_{l+p-m}^* g_T(mT_s)e^{-j2\pi f_c(lT_b+pT_s)}e^{j2\pi f_c m T_s} + N_0(l+p)]\} \\
&= \sigma^2 + E\{a_0^2 s_l s_{l+p}^* g_T^2(0)e^{-j2\pi f_c p T_s} + a_1^2 g_T^2(mT_s)s_{l-m}s_{l+p-m}^* e^{-j2\pi f_c p T_s} + \\
&g_T(0)a_0 a_1 g_T(mT_s)s_{l-m}s_{l+p}^* e^{j2\pi f_c(m-p)T_s} + g_T(0)a_0 a_1 g_T(mT_s)s_l s_{l+p-m}^* e^{-j2\pi f_c(m+p)T_s}\}
\end{aligned} \tag{5.13}$$

where p is the time lag.

Since the input symbols are i.i.d., there exists three peaks in ρ_{y_m} which are listed in Table 5.5. In this table, P_s is the symbol power. We observe that the two peaks when time lag is not equal to 0 have the same amplitude. Thus by finding the two different peaks after calculating the auto-correlation coefficients, the scaled factor a can be estimated.

Figure 5.5 shows one example of the normalized auto-correlation coefficients (normal-

Table 5.5: The peak value of the auto-correlation coefficients for the signals after subsampling

Time Lag	Peak Value
$p = 0$	$(a_0^2 g_T^2(0) + a_1^2 g_T^2(mT_b))P_s$
$p = m$	$a_0 g_T(0) a_1 g_T(mT_b) P_s$
$p = -m$	$a_0 g_T(0) a_1 g_T(mT_b) P_s$

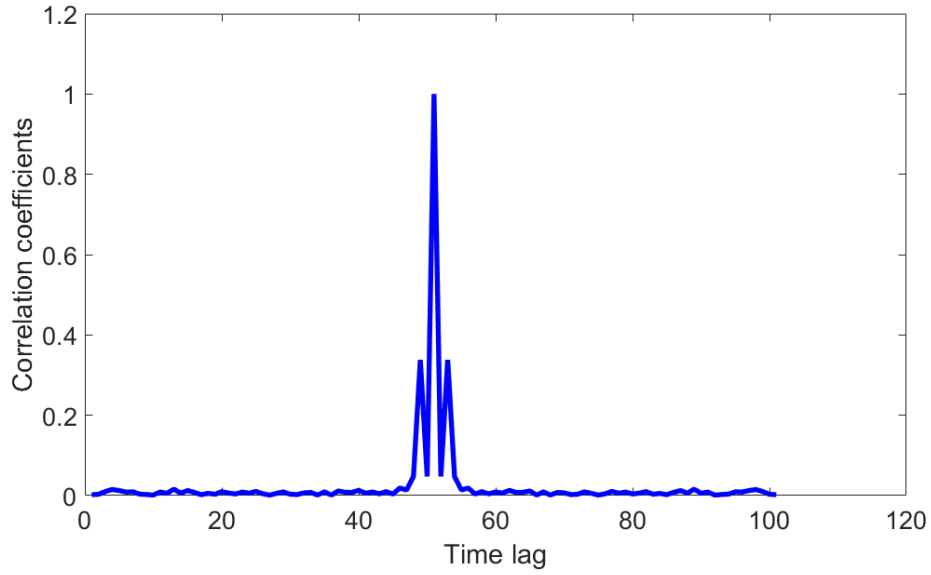

Figure 5.5: The normalized auto-correlation coefficients of the signals in a two-path channel around middle point: $a_0 = 1, a_m = 0.5, m = 35$; Number of symbols: 10000; Number of samples per symbol: 20; SNR = 20 dB.

ized by the signal power of $y_c(l)$). The three distinct peaks can be observed around the middle points in Figure 5.5. As we derived in (5.10), $a = \frac{a_1 g_T(mT_s)}{a_0 g_T(0)}$ when there is no carrier. Let $a_m g_T(mT_s) = x$ and $a_0 g_T(0) = y$. Let the amplitude of two different peaks be c and d. Their relationship are

$$x^2 + y^2 = c; \tag{5.14}$$

$$xy = d; \tag{5.15}$$

The solution is given by

$$\begin{aligned} a &= \frac{x}{y} \\ &= \frac{c - \sqrt{(c^2 - 4d^2)}}{2d} \end{aligned} \tag{5.16}$$

5.2.2.3 Preliminary Performance Evaluation

In this section, the preliminary results of the probability of correct identification for the PSK signals in a two-path channel is presented. Number of symbols in the signals was 10,000. Number of samples per symbol was 20. Fifty independent runs were used to calculate the probability of correct identification in this section.

Figure 5.6 shows the probability of correct identification for PSK signals under different SNRs. We can see that the modified amplitude likelihood-based identification algorithm identifies BPSK, QPSK and 8PSK above 99% accuracy at SNR = 2 dB. The identification between QPSK and 8PSK needs higher SNRs in order to get accurate results.

5.2.3 Dictionary Learning for the Signals in Multipath Channels

For the signal model described in Chapter 3, a discrete signal model for the signals in multipath channels can be written as

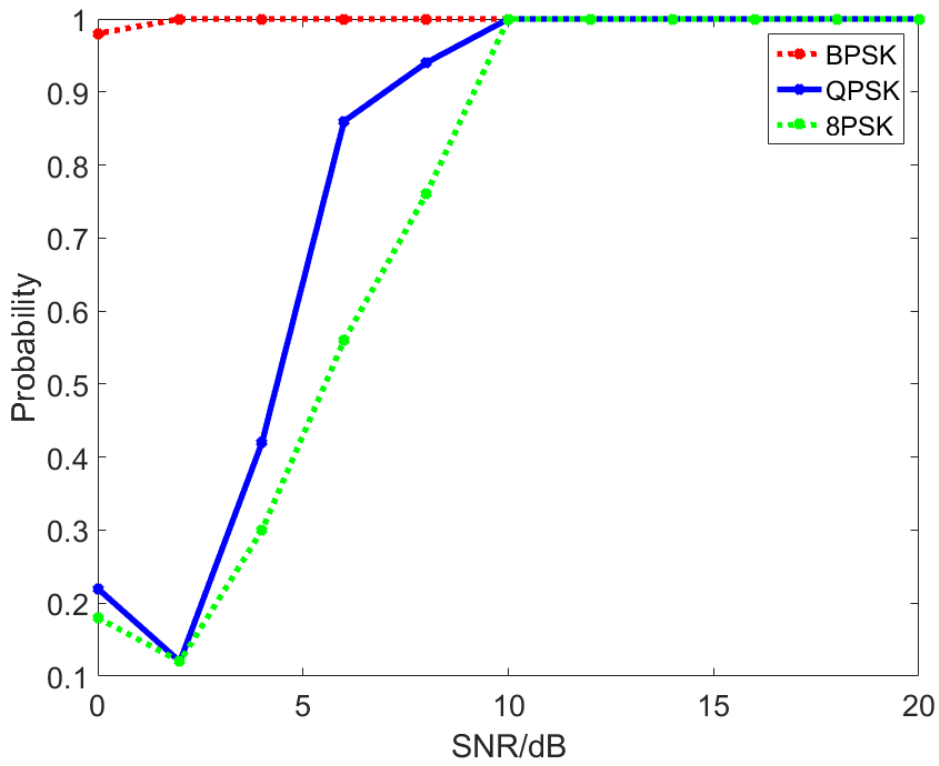

Figure 5.6: Probability of successful identification of different PSK signals in a two-path channel under different SNRs: $a_0 = 1, a_m = 0.5, m = 35$; Number of symbols: 10000; Number of samples per symbol: 20.

$$y_c(n) = \sum_k s_k c(n - kT) + N_0(n) \tag{5.17}$$

where $T = \frac{T_b}{T_s}$ is the number of samples per baud and $c(n)$ is the channel coefficients including the pulse shaping filter and the multipath.

Assuming that $c(n)$ has finite length as mT, where m is an integer, the signal can be reconstructed as

$$\begin{bmatrix} y_c(0) \\ y_c(1) \\ . \\ . \\ . \\ y_c(T-1) \\ y_c(T) \\ . \\ . \\ . \\ y_c(2T-1) \\ . \\ . \\ . \\ y_c(NT-1) \end{bmatrix} = \tag{5.18}$$

$$\begin{bmatrix} s(0) & 0 & ... & s(1) & 0 & ... & s(m-1) & 0 & ... \\ 0 & s(0) & ... & 0 & s(1) & ... & 0 & s(m-1) & ... \\ & & & & . & . & . & & \\ & & & & . & . & . & & \\ & & & & . & . & . & & \\ 0 & ... & s(0) & 0 & ... & s(m-2) & ... & 0 & ... \\ s(1) & 0 & ... & s(2) & 0 & ... & s(m) & 0 & ... \\ & & & & . & . & . & & \\ & & & & . & . & . & & \\ & & & & . & . & . & & \\ 0 & ... & s(1) & 0 & ... & s(m-1) & ... & 0 & ... \\ & & & & . & . & . & & \\ & & & & . & . & . & & \\ & & & & . & . & . & & \\ 0 & ... & ... & s(N) & 0 & ... & s(N+1) & ... & s(N+m-1) \end{bmatrix} \begin{bmatrix} c(0) \\ c(1) \\ . \\ . \\ . \\ c(T-1) \\ c(T) \\ . \\ . \\ . \\ c(2T-1) \\ . \\ . \\ . \\ c(mT-1) \end{bmatrix}$$

Rearranging the signal vector to a matrix, the model can be then written as

$$\begin{bmatrix} y_c(0) & y_c(T) & ...y_c((N-1)T) \\ y_c(1) & y_c(T+1) & ...y_c((N-1)T+1) \\ . & & \\ . & & \\ . & & \\ y_c(T-1) & y_c(2T-1) & ...y_c(NT-1) \end{bmatrix} = \tag{5.19}$$

$$\begin{bmatrix} s(0) & ... & s(1) & ... & s(N+m-1) & ... & ... \\ 0 & s(0) & ... & ... & 0 & s(N+m-1) & ... \\ & & & & . & . & . \\ & & & & . & . & . \\ & & & & . & . & . \\ 0 & s(0) & ... & s(1)) & & ... & s(N+m-1) \end{bmatrix} \times$$

$$\begin{bmatrix} c(0) & 0 & ... & 0 \\ c(1) & c(0) & ... & ... \\ . & . & . & c(0) \\ . & . & . & c(1) \\ . & . & . & . \\ c(mT-1) & c(mT-2) & ... & . \\ 0 & c(mT-1) & ... & . \\ ... & 0 & ... & c(mT-1) \\ ... & ... & ... & c(mT-1) \\ & & & \end{bmatrix}$$

Let Y be the $T \times N$ matrix for the received signal on the left, S be the $T \times (N+m)T$ matrix for the symbols on the right and P be the $NT \times (N+m)T$ matrix for the coefficients.

We can see that S is a sparse matrix and the coefficients matrix P satisfies that the elements at each column are the same (with a shift). This is a similar problem as that of dictionary learning, where P is the dictionary that we want to learn without knowing the sparse code matrix S. The problem can be formalized as

$$\min_{S,P} ||Y - SP||^2 \tag{5.20}$$

$$\text{s.t.} ||P(:,j)^2|| = A, \text{for} j = 1, 2, ...(N+m)T$$

where A is a constant. This turns out to be a convex optimization problems. A typical dictionary learning algorithm is shown in the block diagram in Figure 5.7.

The system first estimates a sparse matrix S with a initial P by solving the optimization problems in (5.20). Then, the dictionary is updated using the estimated sparse matrix $\hat{S}$. The process is iterated until convergence.

This potential algorithm gives a new direction of blind equalization for the signals in multipath channels.

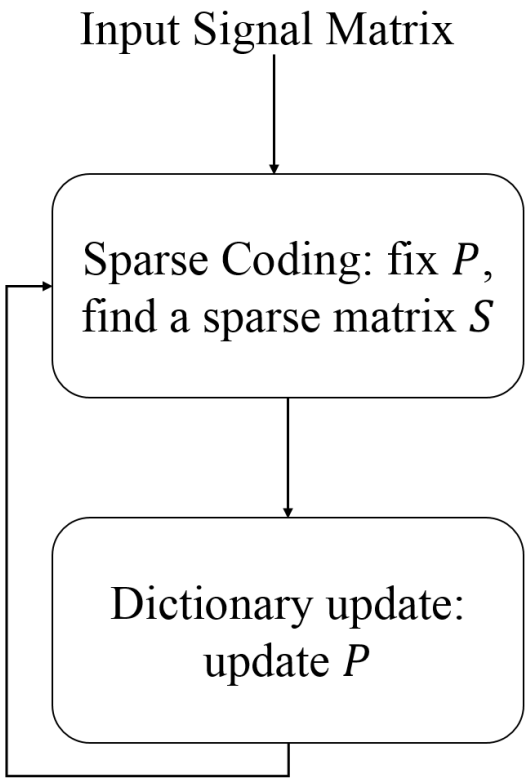

Figure 5.7: Block diagram of dictionary learning process.

APPENDIX

THE DERIVATION OF MEAN AND VARIANCE FOR THE VARIABLE OF THE DIFFERENCE BETWEEN THE LIKELIHOOD FUNCTIONS

The mean of $\Delta_{l_{Mm}}$ can be derived as:

$$\begin{aligned}
\mu_{l_{Mm}} &= \int_{s_1}\int_{s_2}\ldots\int_{s_{N_s}}\left[\Delta_{l_{Mm}} p(s_1, s_2, \ldots, s_{N_s}|H_M)\right] ds_1 ds_2 \ldots ds_{N_s} \\
&= \int_{s_1}\int_{s_2}\ldots\int_{s_{N_s}}\left[\sum_i \Delta_{L_{p_{Mm}}}(s_i) p(s_1, s_2, \ldots, s_{N_s}|H_M)\right] ds_1 ds_2 \ldots ds_{N_s} \\
&= \sum_i \left\{ \int_{s_1}\int_{s_2}\ldots\int_{s_{N_s}}\left[\Delta_{L_{p_{Mm}}}(s_i) p(s_1, s_2, \ldots, s_{N_s}|H_M)\right] ds_1 ds_2 \ldots ds_{N_s}\right\}
\end{aligned}$$

When the signal samples are independent from each other,

$$\begin{aligned}
&\mu_{l_{Mm}} = \int_{s_2}\ldots\int_{s_{N_s}}[P(s_2|H_M)\ldots P(s_{N_s}|H_M)] ds_2 \ldots ds_{N_s}] \int_{s_1}\Delta_{L_{p_{Mm}}}(s_1) P(s_1|H_M) ds_1 \\
&+ \sum_{i>1}\{\int_{s_1}\int_{s_2}\ldots\int_{s_{N_s}}[\Delta_{L_{p_{Mm}}}(s_i) p(s_1, s_2, \ldots, s_{N_s}|H_M)] ds_1 ds_2 \ldots ds_{N_s}\} \\
&= \int_{s_1}\Delta_{L_{p_{Mm}}}(s_1) P(s_1|H_M) ds_1 + \\
&\sum_{i>1}\{\int_{s_1}\int_{s_2}\ldots\int_{s_{N_s}}[\Delta_{L_{p_{Mm}}}(s_i) p(s_1, s_2, \ldots, s_{N_s}|H_M)] ds_1 ds_2 \ldots ds_{N_s}\} \\
&= N_s \int_s \Delta_{L_{p_{Mm}}}(s) P(s|H_M) ds
\end{aligned}$$

where N_s is the number of signal samples used in the calculation.

Using the same procedure, we can obtain the variance of $\Delta_{l_{Mm}}$ as

$$\Omega_{l_{Mm}} = \int_{s_1}\int_{s_2}...\int_{s_{N_s}}[(\sum_i \Delta_{L_{p_{Mm}}}(s_i) - \mu_{l_{Mm}})^2 p(s_1, s_2, ..., s_{N_s}|H_M)]ds_1 ds_2 ...ds_{N_s}$$

$$= \int_{s_1}\int_{s_2}...\int_{s_{N_s}}(\sum_i \Delta_{L_{p_{Mm}}}(s_i))^2 - 2\mu_{l_{Mm}}\sum_i \Delta_{L_{p_{Mm}}}(s_i) + \mu_{l_{Mm}}^2)$$

$$p(s_1, s_2, ..., s_{N_s}|H_M)ds_1 ds_2 ...ds_{N_s}$$

$$= \int_{s_1}\int_{s_2}...\int_{s_{N_s}}(\sum_i \Delta_{L_{p_{Mm}}}(s_i))^2 p(s_1, s_2, ..., s_{N_s}|H_M)]ds_1 ds_2 ...ds_{N_s} - \mu_{l_{Mm}}^2$$

$$= \sum_i\sum_j \int_{s_1}\int_{s_2}...\int_{s_{N_s}} \Delta_{L_{p_{Mm}}}(s_i)\Delta_{L_{p_{Mm}}}(s_j) p(s_1, s_2, ..., s_{N_s}|H_M)ds_1 ds_2 ...ds_{N_s} - \mu_{l_{Mm}}^2$$

$$= \sum_j \int_{s_1}\int_{s_2}...\int_{s_{N_s}} \Delta_{L_{p_{Mm}}}(s_1)\Delta_{L_{p_{Mm}}}(s_j) p(s_1, s_2, ..., s_{N_s}|H_M)]ds_1 ds_2 ...ds_{N_s} +$$

$$\sum_{i>2}\sum_j \int_{s_1}\int_{s_2}...\int_{s_{N_s}} \Delta_{L_{p_{Mm}}}(s_i)\Delta_{L_{p_{Mm}}}(s_j) p(s_1, s_2, ..., s_{N_s}|H_M)ds_1 ds_2 ...ds_{N_s} - \mu_{l_{Mm}}^2$$

$$= \int_{s_1}[(\Delta_{L_{p_{Mm}}}(s_1))^2 P(s_1|H_M)]ds_1$$

$$+ \int_{s_1}[\Delta_{L_{p_{Mm}}}(s_1)P(s_1|H_M)]ds_1 \sum_{j>2}\int_{s_2}...\int_{s_{N_s}} \Delta_{L_{p_{Mm}}}(s_j) p(s_2, ..., s_{N_s}|H_M)ds_1 ds_2 ...ds_{N_s}$$

$$+ \sum_{i>2}\sum_j \int_{s_1}\int_{s_2}...\int_{s_{N_s}} \Delta_{L_{p_{Mm}}}(s_i)\Delta_{L_{p_{Mm}}}(s_j) p(s_1, s_2, ..., s_{N_s}|H_M)ds_1 ds_2 ...ds_N - \mu_{l_{Mm}}^2$$

$$= \int_{s_1}[(\Delta_{L_{p_{Mm}}}(s_1))^2 P(s_1|H_M)]ds_1 + \frac{N_s - 1}{{N_s}^2}\mu_{l_{Mm}}^2 +$$

$$\sum_{i>2}\sum_j \int_{s_1}\int_{s_2}...\int_{s_{N_s}} \Delta_{L_{p_{Mm}}}(s_i)\Delta_{L_{p_{Mm}}}(s_j) p(s_1, s_2, ..., s_{N_s}|H_M)ds_1 ds_2 ...ds_{N_s} - \mu_{l_{Mm}}^2$$

$$= N_s\Big(\int_s [(\Delta_{L_{p_{Mm}}}(s))^2 P(s|H_M)]ds + \frac{N_s - 1}{{N_s}^2}\mu_{l_{Mm}}^2\Big) - \mu_{l_{Mm}}^2$$

$$= N_s \int_s [(\Delta_{L_{p_{Mm}}}(s))^2 P(s|H_M)]ds - \frac{\mu_{l_{Mm}}^2}{N_s}$$

REFERENCES

[1] S. O. Rice , "Mathematical Analysis of Random Noise", *Bell System Technical Journal*, vol. 24, No. 1, pp. 46-156, Jan. 1945.

[2] J. T. Fleck and E. A. Trabka, "Error Probabilities of Multiple-state Differentially Coherent Phase-shift Keyed Systems in the Presence of White, Gaussian Noise," in *Investigation of Digital Data Communication Systems*, Rep. UA-1420-S-1, J. G. Lawton, Ed., Cornell Aeronaut. Lab., Inc., Buffalo, NY, Jan. 1961, Detect Memo 2A; available as NTIS Doc. AD256584.

[3] P. D. Welch, "The Use of Fast Fourier Transform for the Estimation of Power Spectra: A Method Based on Time Averaging Over Short, Modified Periodograms," *IEEE Transactions on Audio Electroacoustics*, vol. AU-15, No. 2, pp. 70-73, June 1967.

[4] R. F. Pawula, S. O. Rice and J. H. Roberts, "Distribution of the Phase Angle between Two Vectors Perturbed by Gaussian Noise," *IEEE Transactions on Communications*, vol. COM-30, No. 8, pp. 1828-1841, Aug. 1982.

[5] Y. Bar-Ness, J. W. Carlin and M. L. Steinberger, "Bootstrapping Adaptive Cross-Pol Canceller for Satellite Communications," *1982 International Conference on Communications*, vol. 2, pp. 4F.5.1-4F.5.5, Philadelphia, PA, USA, June 1982.

[6] N. Amitay and J. Salz, "Linear Equalization Theory in Digital Data Transmission over Dually Polarized Fading Radio Channels," *AT & T Bell Laboratories Technical Journal*, vol. 63, No. 10, pp. 2215-2259, Dec. 1984.

[7] K. Kim and A. Polydoros, "Digital Modulation Classification: the BPSK versus QPSK Case", *1988 Military Communications Conference*, vol. 2, pp. 431-436, San Diego, CA, USA, 1988.

[8] S. Krenk and H. Gluwer, "An Algorithm for Moments of Response from Non-normal Excitation of Linear Systems", *Stochastic Structural Dynamics*, pp. 181-195, London, Elsevier Applied Science, 1988.

[9] A. Dinc and Y. Bar-Ness, "Performance Comparison of LMS, Diagonalizer and Bootstrapped Adaptive Cross-pol Cancellers for M-ary QAM," *1990 Military Communications Conference*, vol. 1, pp. 101-105, Monterey, CA, USA, 1990.

[10] Y. Yang and S. S. Soliman, "Statistical Moments Based Classifier for MPSK Signals", *1991 Global Telecommunications Conference*, vol. 1, pp. 72-76, Phoenix, AZ, USA, 1991.

[11] J. Reichert, "Automatic Classification of Communication Signals Using Higher Order Statistics", *1992 IEEE International Conference on Acoustics, Speech, and Signal Processing*, vol. 5, pp. 221-224, San Francisco, CA, USA, 1992.

[12] A. Genz, "Numerical Computation of Multivariate Normal Probabilities," *Journal of Computational and Graphical Statistics*, vol. 1, No. 2, pp. 141-149, 1992.

[13] C. Long, K. Chugg and A. Polydoros, "Further Results in Likelihood Classification of QAM Signals", *1994 Military Communications Conference*, vol. 1, pp. 57-61, Fort Monmouth, NJ, USA, 1994.

[14] M. Takahashi, H. Takahashi and T. Tanaka, "Cross Polarization Interference Canceler for Microcellular Mobile Communication Systems," *1995 IEEE International Conference on Communications, 'Gateway to Globalization',*, vol. 2, pp. 910-914, Seattle, WA, USA, June 1995.

[15] C. Y. Huang and A. Polydoros, "Likelihood Methods for MPSK Modulation Classification", *IEEE Transactions on Communications*, pp. 1493-1504, 1995.

[16] K. M. Chugg, C. S. Long and A. Polydoros, "Combined Likelihood Power Estimation and Multiple Hypothesis Modulation Classification", *The Twenty-Ninth Asilomar Conference on Signals, Systems and Computers*, vol. 2, pp. 1137-1141, Pacific Grove, CA, USA, 1995.

[17] P. C. Sapiano and J. D. Martin, "Maximum Likelihood PSK Classifier", *1996 Military Communications Conference*, vol. 3, pp. 1010-1014, McLean, VA, 1996.

[18] H. Ge, Y. Bar-Ness and M. Visser, "Combined Adaptive Interference Cancellation and Bootstrap Separation of Dual Polarized Signals," *The Thirtieth Asilomar Conference on Signals, Systems and Computers* , vol. 1, pp. 694-698, Pacific Grove, CA, USA, 1996.

[19] S.-I. Amari and J.-F. Cardoso, "Blind Source Separation – Semiparametric Statistical Approach," *IEEE Transaction on Signal Processing*, vol. 45, pp. 2692-2700, Nov. 1997.

[20] S.-I. Amari, T.-P. Chen and A. Cichocki, "Stability Analysis of Learning Algorithms for Blind Source Separation," *Neural Networks*, vol. 10, Issue 8, pp. 1345-1351, Nov. 1997.

[21] L. Yiin and G. L. Stuber,"MLSE and Soft-output Equalization for Trellis-coded Continuous Phase Modulation," *IEEE Transactions on Communications*, vol. 45, No. 6, pp. 651-659, June 1997.

[22] C. Martret and D. M. Boiteau, "Modulation Classification by Means of Different Order Statistical Moments", *1997 Military Communications Conference*, vol. 3, pp. 1387-1391, Monterey, CA, USA, 1997.

[23] P. Marchand, J. L. Lacoume and C. L. Martret, "Classification of Linear Modulations by A Combination of Different Orders Cyclic Cumulants", *1997 IEEE Signal Processing Workshop on Higher-Order Statistics*, pp. 47-51, Banff, Atalanta, USA, 1997.

[24] P. Marchand, J. L. Lacoume and C. L. Martret, "Multiple Hypothesis Classification Based on Cyclic Cumulants of Different Orders", *1998 IEEE International Conference on Acoustics, Speech and Signal Processing*, pp. 2157-2160, Seattle, WA, USA, 1998.

[25] A. O. Hero and H. H. Mahram, "Digital Modulation Classification Using Power Moment Matrices", *1998 IEEE International Conference on Acoustics, Speech and Signal Processing*, vol. 4, pp. 3285-3288, Seattle, WA, USA, 1998.

[26] Y. Yang, C.-H. Liu and T.-W. Soong, "A Log-likelihood Function-based Algorithm for QAM Signal Classification," *Signal Processing*, vol. 70, No. 1, pp. 61-71, Oct. 1998.

[27] J.-F. Cardoso, "Blind Signal Separation: Statistical Principles," *Proceedings of the IEEE*, vol. 86, No. 10, pp. 2009-2025, Oct. 1998.

[28] J. A. Sills, "Maximum-likelihood Modulation Classification for PSK/QAM", *1999 Military Communications Conference*, vol. 1, pp. 57-61, Atlantic City, NJ, USA, 1999.

[29] L. Hong and K. C. Ho, "Identification of Digital Modulation Types Using the Wavelet Transform", *1999 Military Communications Conference*, vol. 1, pp. 427-431, Atlantic City, NJ, USA, 1999.

[30] W. Wei and J. M. Mendel, "Maximum-likelihood Classification for Digital Amplitude-phase Modulations", *IEEE Transactions on Communications*, vol. 48, pp. 189-193, 2000.

[31] P. Panagiotou, A. Anastasoupoulos and A. Polydoros, "Likelihood Ratio Tests for Modulation Classification", *2000 Military Communications Conference*, vol. 1, pp. 670-674, Los Angeles, CA, USA, 2000.

[32] L. Hong and K. C. Ho, "BPSK and QPSK Modulation Classification with Unknown Signal Level", *2000 Military Communications Conference*, vol. 1, pp. 976-980, Los Angeles, CA, USA, 2000.

[33] H. H. Mahram and A. O. Hero, "Robust QAM Modulation Classification via Moment Matrices", *1th IEEE International Symposium on Personal Indoor and Mobile Radio Communications*, vol. 1, pp. 133-137, London, UK, 2000.

[34] A. Swami and B. M. Sadler, "Hierarchical Digital Modulation Classification Using Cumulants," *IEEE Transactions on Communications*, vol. 48, No. 3, pp. 416-429, Mar. 2000.

[35] G. Hatzichristos and M. P. Fargues, "A Hierarchical Approach to the Classification of Digital Modulation Types in Multipath Environments", *The Thirty-Fifth Asilomar Conference on Signals, Systems and Computers*, vol. 2, pp. 1494-1498, Pacific Grove, CA, USA, 2001.

[36] C. M. Spooner, "On the Utility of Sixth-order Cyclic Cumulants for RF Signal Classification", *The Thirty-Fifth Asilomar Conference on Signals, Systems and Computers*, vol. 1, pp. 890-897, Pacific Grove, CA, USA, 2001.

[37] S. C. Douglas, "Blind Signal Separation and Blind Deconvolution," *Handbook of Neural Network Signal Processing*, 2001.

[38] W. Dai, Y. Wang and J. Wang, "Joint Power and Modulation Classification Using Second and Higher Statistics", *2002 IEEE Wireless Communications and Networking Conference Record*, vol. 1, pp. 155-158, Orlando, Florida, USA, 2002.

[39] L. Hong and K. C. Ho, "Classification of BPSK and QPSK Signals with Unknown Signal Level Using the Bayes Technique", *2003 International Symposium on Circuits and Systems*, vol. 4, pp. IV.1-IV.4, Bangkok, Thailand, 2003.

[40] O. A. Dobre, Y. Bar-Ness and W. Su, "Higher-order Cyclic Cumulants for High Order Modulation Classification", *2003 IEEE Military Communications Conference*, vol. 1, pp. 112-117, Monterey, CA, USA, 2003.

[41] O. A. Dobre, Y. Bar-Ness and W. Su, "Robust QAM Modulation Classification Algorithm Using Cyclic Cumulants," *2004 IEEE Wireless Communications and Networking Conference*, vol. 2, pp. 745-748, Atlanta, USA, USA, 2004.

[42] P. Chevalier, L. Albera, P. Comon and A. Ferreol, "Comparative Performance Analysis of Eight Blind Source Separation Methods on Radio Communications Signals," *2004 IEEE International Joint Conference on Neural Networks*, vol. 1, pp. 273-278, Budapest, Hungary, July 2004.

[43] V. Zarzoso and P. Comon, "How Fast is FastICA?", *2006 European Signal Processing Conference*, pp. 1-5, Florence, Italy, Sept. 2006.

[44] S. G. Kim and C. D. Yoo, "Underdetermined Blind Source Separation Based on Generalized Gaussian Distribution," *The 16th IEEE Signal Processing Society Workshop on Machine Learning for Signal Processing*, pp. 103-108, Maynooth, Ireland, Sept. 2006.

[45] J. Arenas-Garcia and A. R. Figueiras-Vidal, "Improved Blind Equalization via Adaptive Combination of Constant Modulus Algorithms," *2006 IEEE International Conference on Acoustics, Speech and Signal Processing*, vol. 3, pp. 14-19, Toulouse, France, May 2006.

[46] K.-T. Woo and C.-W. Kok, "Clustering Based Distribution Fitting Algorithm for Automatic Modulation Recognition," *2007 IEEE Symposium on Computers and Communications*, pp. 13-18, Averio, Portugal, July 2007.

[47] O. A. Dobre, A. Abdi, Y. Bar-Ness and W. Su, "Survey of Automatic Modulation Classification Techniques: Classical Approaches and New Trends", *Communications, IET*, vol. 1, No. 2, pp. 137-156, Apr. 2007.

[48] J. Xi and Z. Wang, "MQAM Modulation Scheme Recognition Using Hilbert Transform," *Journal on Communications*, vol. 28, No. 6, June 2007.

[49] E. Ip, A. P. T. Lau, D. J. F. Barros and J. M. Kahn, "Coherent Detection in Optical Fiber Systems," *Optics Express*, vol. 16, Issue 2, pp. 753-791, 2008.

[50] H. C. Wu, M. Saquib and Z. Yun, "Novel Automatic Modulation Classification Using Cumulant Features for Communications via Multipath Channels," *IEEE Transactions on Wireless Communications,* vol. 7, No. 8, pp. 3098-3105, Aug. 2008.

[51] T. Pfau, *Real-time Coherent Optical Receivers*, Sdwestdeutscher Verlag fr Hochschulschriften, Germany, 2009.

[52] Z. Xu and W. Bai, "A Novel Blind Recognition Algorithm for Modulated M-QAM Signals," *2009 International Conference on Communications and Mobile Computing*, vol. 1, pp. 461-465, Kunming, Yunnan, China, Jan. 2009.

[53] D. Zhang and X. Wang, "MPSK Signal Modulation Recognition Based on Wavelet Transformation," *2009 International Conference on Networking and Digital Society*, pp. 203-205, Guiyang, Guizhou, China, May 2009.

[54] G. Wan, J. Liang, Y. Li and Q.Wu, "An Improved Estimation Algorithm of Symbol Synchronization for QAM Signal," *International Conference on Innovation Management*, pp. 67-70, Wuhan, China, Dec. 2009.

[55] O. A. Dobre, A. Abdi, Y. Bar-Ness and W. Su, "Cyclostationarity-based Modulation Classification of Linear Digital Modulations in Flat Fading Channels." *Wireless Personal Communications*, No. 2, pp. 699-717, 2010.

[56] X. Tan, H. Zhang, Y. Shen and W. Lu, "Blind Modulation Recognition of PSK Signals Based on Constellation Reconstruction," *2010 International Conference on Wireless Communications and Signal Processing*, pp. 1-6, Suzhou, China, Oct. 2010.

[57] B. Farhang-Boroujeny, *Signal Processing Techniques for Software Radios*, LuLu Publishing House, 2010.

[58] H. R. Nikoofar and A. R. Sharafat, " Modulation Classification for Burst-mode QAM Signals in Multipath Fading Channels," *Iranian Journal Science Technology Transaction B: Engineering*, vol. 34, No. B3, pp. 257-274, June 2010.

[59] C.-J. Liu, H. Peng, D. Wu and G.-Q. Zhao, "Modulation Recognition Algorithm Of Burst Adaptive Modulation Signal," *Signal Processing*, vol. 28, No. 3, Mar. 2012.

[60] L. Cui, S. Li, X. Zhu, L. Liu and Z. Shao,"Research on Cross-Polarization Interference Canceller with Blind Adaptive Algorithm," *2012 International Conference on Computational Problem-Solving*, pp. 202-204, Leshan, China, 2012.

[61] D. Zhu and V J. Mathews, "Likelihood-based Algorithms for Blind Identification of QAM Signals," *2013 Digital Signal Processing and Signal Processing Education Workshop*, pp. 158-163, Napa, CA, USA, Aug. 2013.

[62] D. Zhu, V J. Mathews and D. H. Detienne, "A Phase Likelihood-based Algorithm for Blind Identification of PSK Signals," *2014 IEEE International Conference on Acoustics, Speech and Signal Processing*, pp. 5730-5734, Florida, Italy, May 2014.

[63] D. Wei and J. Zhu,"Baseband Cross-polarization Interference Cancellation Based On SCS Algorithm," *12th IEEE International Conference on Electronic Measurement and Instruments (ICEMI)*, pp. 336-340, Qingdao, China, 2015.

[64] D. Zhu, V J. Mathews and D. H. Detienne, "Likelihood-based Blind Separation of QAM Signal in Time-varying Dual-polarized Channels," *23rd European Signal Processing Conference*, pp. 894-898, Nice, France, Aug. 2015.

[65] D. Zhu, V J. Mathews and D. H. Detienne, "A Likelihood-based Algorithm for Blind Identification of QAM and PSK Signals," Submitted to *IEEE Transactions on Wireless Communications*, Dec. 2016.